RESIDUAL CURRENTS AND MIXING IN THE WADDEN SEA

HERMAN RIDDERINKHOF

RESIDUAL CURRENTS AND MIXING IN THE WADDEN SEA

RESIDUAL CURRENTS AND MIXING IN THE WADDEN SEA

RESTSTROMEN EN MENGING IN DE WADDENZEE

(met een samenvatting in het Nederlands)

Proefschrift ter verkrijging van de graad van doctor
aan de Rijksuniversiteit te Utrecht,
op gezag van de Rector Magnificus, Prof. dr. J.A. van Ginkel,
ingevolge het besluit van het College van Dekanen
in het openbaar te verdedigen
op 2 mei 1990 des namiddags te 3.45 uur

door

HERMAN RIDDERINKHOF

geboren op 6 februari 1959 te Zwartsluis

Promotor: Prof. dr. J.T.F. Zimmerman
Faculteit Natuur- en Sterrenkunde Rijksuniversiteit Utrecht

Dit proefschrift werd mede mogelijk gemaakt met financiele steun van Rijkswaterstaat (projekt WAWAMO)

Publikatie nr. 12 van het projekt Beleidsgericht Wetenschappelijk Onderzoek NIOZ (BEWON)

aan mijn ouders
aan Ria, Wim en Anna

CONTENTS

STELLINGEN

I

De zoetwaterinhoud en de verblijftijd van het zoete water in de Waddenzee worden onderschat wanneer een reststroom vanuit het Vlie bekken naar het Marsdiep bekken niet in rekening wordt gebracht.

(H. POSTMA, 1954, proefschrift RUG
J.T.F. ZIMMERMAN, 1976, proefschrift RUU
dit proefschrift)

II

Ongeveer 6% van de watermassa in de westelijke Waddenzee is via de Noordzee afkomstig uit de Rijn en ongeveer 8% is afkomstig uit het IJsselmeer.

III

Een theorie, die de verschillende mechanismen voor horizontale menging in een getijdegebied zoals de Waddenzee alle omvat, bestaat niet.

IV

Laterale wrijvingslagen zijn in natuurlijke bekkens van ondergeschikt belang voor de generatie van vorticiteit.

(K.T. TEE, 1976, J. Mar. Res. **34:** 603
H.E. DE SWART & J.T.F.ZIMMERMAN, 1987, J. Fluid Mech. **184:** 381)

V

De suggestie dat wervels in de buitendelta van het Zeegat van Texel worden veroorzaakt door de interactie tussen Noordzee-getijdestromen en de bodemvorm van de delta, is onjuist.

(SHA, 1989, Mar. Geol. **89:** 11)

VI

De grootte van de dispersiecoefficient in een transportmodel is omgekeerd evenredig met de nauwkeurigheid van het gebruikte snelheidsveld.

VII

Het gedrag van veel natuurlijke systemen is intrinsiek onvoorspelbaar.

VIII

Gezien de effekten van de visserij op het ecosysteem in de Noordzee is het beleid gericht op een schone, maar lege Noordzee.

IX

De gesuggereerde grote belasting van de continentale kust met rivierwater uit Engeland, aannemelijk gemaakt met sterk contrasterende kleuren in een computersimulatie van de verspreiding van rivierwater in de Noordzee, is volksverlakkerij.
(NOS journaal, 5–3–1990)

X

De enige reden om op dit moment het broeikaseffect serieus te nemen is de hierdoor vrijkomende geldstroom voor onderzoek.

XI

Wanneer de verspreiding van kraakbeendeeltjes in de knie van Ruud Gullit chaotisch is, kan Nederland het WK wel vergeten.

XII

Bij de opvoeding van kinderen is het raadzaam de overstelpende hoeveelheid lectuur over dit onderwerp te negeren.

Texel, maart 1990

H. Ridderinkhof

VOORWOORD

Zoals bij bijna al onze bezigheden zijn ook bij de vervaardiging van een proefschrift veel mensen direct of indirect onmisbaar. Dit voorwoord is een goede gelegenheid een aantal van hen met name te bedanken.

Mijn promotor, Sjef Zimmerman, was tevens initiator en begeleider van dit onderzoek. Van zijn kennis en vermogen om een probleem te reduceren tot de essentie, heb ik veel geleerd. Ik realiseer me terdege dat dit proefschrift grotendeels een uitwerking is van door hem aangeleverde ideeën.

Bij de voormalige Deltadienst van Rijkswaterstaat kreeg ik via ir. J. Voogt de mogelijkheid om een hydrodynamisch model van de Waddenzee op te zetten. Johan Dijkzeul leerde mij 'spelen' met het hiervoor gebruikte WAQUA-software pakket. Via dit model kwam ik in contact met het Nederlands Instituut voor Onderzoek der Zee (NIOZ). Het als eenling op het NIOZ werken met het WAQUA-pakket was praktisch onuitvoerbaar geweest zonder de ondersteuning van de (ook) voormalige Dienst Informatieverwerking van Rijkswaterstaat. Of het nu het inbouwen van speciale opties in de software of gewoon 'domme vragen' betrof, de geleverde hulp was altijd snel en efficient. Aan NIOZ-zijde zorgden Frans Eigenraam en Rob Dapper ervoor dat problemen met de lijnverbinding tussen den Haag en Texel snel opgelost werden.

Han Lindeboom liet mij in grote mate vrij bij de invulling van het onderzoek dat aanvankelijk uitgevoerd werd bij de projektgroep Ecologisch Onderzoek Noordzee en Waddenzee (EON) en later bij haar opvolgster, de groep Beleidsgericht Wetenschappelijk Onderzoek NIOZ (BEWON). Uit de eerste naam van deze groep blijkt al dat ik met mijn direkte collega's vaak discussieerde over de consequenties van mijn resultaten voor andere disciplines. Dit was voor mij erg stimulerend. Bovendien bood dit de mogelijkheid de Waddenzee niet alleen vanaf een beeldscherm te zien. Een paar keer als opstapper (garnalenteller) op de Navicula meevaren was niet alleen leerzaam maar ook gezellig.

De belangstelling van Leo Maas en zijn hulp bij het oplossen van een analytisch probleem was aanmoedigend. Marc Philippart werkte als student aan de bepaling van tijdschalen. Vooral in de laatste fase besprak ik met Hans van Haren bijna dagelijks de vele beslommeringen die nu eenmaal aan een promotie verbonden zijn.

Dr. J. Dronkers (Rijkswaterstaat, Dienst Getijdewateren) en Prof. dr. J. van de Kreeke (University of Miami, USA) becommentarieerden met veel aandacht de manuscripten van de artikelen die in dit proefschrift zijn opgenomen.

In tegenstelling tot de zetmachine liepen Joke Mulder en Nelleke Krijgsman niet stuk op de grote hoeveelheid te zetten formules. Bob Verschuur verzorgde het tekenwerk en merkte dat computerplaatjes nog veel nabewerking behoeven. Overige NIOZ'ers verzorgden een prettige werksfeer. Vooral het zaalvoetbalteam dat mij de gelegenheid bood om, als het in het werk niet lukte, toch nog regelmatig te scoren.

Mijn ouders bedank ik voor de geboden vrijheid en hun immer positieve belangstelling. Vrienden maakten het gemakkelijk om het werk af en toe naar de achtergrond te verplaatsen of zelfs helemaal te vergeten. Het vertrouwen van Ria en haar begrip voor mijn regelmatige 'afwezigheid' in deze periode was onmisbaar. De geboorte en het zien opgroeien van onze kinderen, Wim en Anna, deden het belang van dit proefschrift gelukkig geregeld verbleken.

INLEIDING EN SAMENVATTING

Voor het functioneren van het ecosysteem in de Waddenzee is het van groot belang dat het water in dit gebied regelmatig wordt ververst. Deze verversing vindt plaats met zoet water dat direct vanaf het continent op de getijdebekkens wordt geloosd en met Noordzee water dat via uitwisseling door de zeegaten het gebied binnenkomt. Beide fracties brengen allerlei opgeloste stoffen en (passief) met het water meebewegende organismen naar de Waddenzee. Voorbeelden zijn nutrienten die onmisbaar zijn voor de groei van fytoplankton, en microverontreinigingen die een serieuze bedreiging vormen voor delen van het ecosysteem. Het belang van de uitwisseling door de zeegaten wordt geillustreerd door de passieve intrek van schollarven in het voorjaar die de Waddenzee haar karakteristieke functie als kinderkamer voor deze vissoort geeft.

In het verleden is reeds veel onderzoek verricht naar de snelheid waarmee (enkele) Waddenzee bekkens worden ververst. In bekkens waarin relatief veel zoet water direct wordt geloosd werden gemeten zoutgehalteverdelingen gebruikt om de zoetwaterinhoud te bepalen. Deze is relatief groot (klein) bij een langzame (snelle) verversing. POSTMA (1954) gebruikte deze methode voor het Marsdiep bekken, o.a. om de gemiddelde tijdsduur te bepalen waarin zoet water gespuid bij den Oever de Noordzee bereikt. Het berekenen van verschillende mengingstijdschalen om de verversing te kwantificeren met behulp van een zgn. 'doos' model werd toegepast door ZIMMERMAN (1976) voor de gehele westelijke Waddenzee, het Marsdiep en Vlie bekken. In zo'n model wordt het bekken in een aantal compartimenten opgedeeld. Het verversings proces wordt geschematiseerd als een combinatie van een 'advectief' gedeelte dat wordt veroorzaakt door de continue doorstroming van het bekken met lozingen vanaf het continent, en een 'dispersief' gedeelte dat een uitwisseling van watermassa's tussen aangrenzende compartimenten beschrijft. Gemeten zoutgehalteverdelingen worden gebruikt om uitwisselingscoefficienten te bepalen. In dit proefschrift ligt het accent op de mechanismen die de verversing van Waddenzee bekkens veroorzaken.

Verversing kan alleen plaatsvinden wanneer waterdeeltjes niet op een vaste positie in een bekken blijven. De verplaatsing van waterdeeltjes wordt veroorzaakt door een continue, doorgaande stroming en/of door een verwisseling van de positie van verschillende waterdeeltjes. Het eerste proces, advectie, veroorzaakt een netto horizontale verplaatsing van het zwaartepunt van een watermassa, en het tweede, dispersie of menging, een uitwisseling van watermassa's tussen verschillende gebieden.

Vanwege massabehoud moet de continu doorgaande stroming in een omsloten bekken gelijk zijn aan de externe toevoer van water, meestal vanuit een sluis of een rivier. Echter, wanneer een bekken in open verbinding staat met andere bekkens en zeegaten kan er een doorgaande stroming ontstaan vanuit het ene zeegat naar het andere. Een dergelijke stroming kan veroorzaakt worden door het getij, de wind en/of door dichtheidsverschillen.

Menging kan slechts optreden wanneer de getijdestromingen niet uniform zijn. Immers, uniform heen en weergaande stromingen veroorzaken geen netto verplaatsing van een waterdeeltje. Turbulentie, het kleinschalige en willekeurige gedeelte van de onregelmatigheden in de stroming, is op zichzelf bij lange na niet voldoende om de men-

ging in de Waddenzee te verklaren. Daarom moet het niet-willekeurige gedeelte van de onregelmatigheden in het snelheidsveld, zoals de afname in stroomsnelheid naar de ondiepere gedeelten van de getijdegeulen, van groot belang zijn voor de menging in dit gebied. In de Waddenzee worden deze onregelmatigheden veroorzaakt door de interaktie van getijstromingen met de grillige vorm van de bodem.

Beide aspekten die van belang zijn voor de verversing van bekkens, de continue doorstroming en de onregelmatigheden in het snelheidsveld, kunnen worden onderzocht m.b.v. een numeriek hydrodynamisch model. In een dergelijk model worden de zgn. twee-dimensionale ondiep water vergelijkingen numeriek opgelost, resulterend in berekende waterstanden en snelheidsvectoren in elk roosterpunt van het model. Hiervoor is gebruik gemaakt van het in Nederland wijd verspreide WAQUA-software pakket dat ontwikkeld werd door STELLING (1980). Het gebruikte model heeft een roosterafstand van 500 m en bestrijkt de vier meest westelijke Waddenzee bekkens en de aangrenzende kuststrook van de Noordzee. Het model wordt gestuurd door het verticaal oscillerende getij (met als basisperiode 12,5 uur) langs de Noordzee randen. De effekten van winden/of dichtheidsgedreven stromingen worden buiten beschouwing gelaten.

In het eerste gedeelte van deze studie staan de 'Eulerse' getijgedreven reststromingen centraal; d.w.z. het snelheidsveld dat overblijft wanneer in elk roosterpunt van het model de fluctuerende snelheidsvectoren worden gemiddeld over een getijperiode. Deze reststromingen blijken te kunnen worden opgevat als een combinatie van een grootschalige doorgaande stroming tussen aangrenzende bekkens met snelheden van $O(10^{-2}$ $ms^{-1})$ en van relatief kleinschalige restwervels met snelheden van $O(10^{-1}$ $ms^{-1})$.

De getijgedreven doorgaande stroming, van groot belang voor het advectieve transport, wordt nader onderzocht m.b.v. een analytisch model. In dit model worden het Marsdiep en Vlie gebied geschematiseerd tot twee onderling verbonden rechthoekige bekkens. De beinvloeding van de doorgaande stroming door geometrische verschillen tussen beide bekkens en door verschillen in het verticale getij tussen beide zeegaten, kunnen zo relatief eenvoudig worden onderzocht. De grotere amplitude van het getij in het Zeegat van het Vlie blijkt veruit de belangrijkste oorzaak te zijn van de zuidwaarts gerichte continue doorstroming vanuit het Zeegat van het Vlie in het Vlie bekken naar het Zeegat van Texel in het Marsdiep bekken.

De getijgedreven restwervels, met afmetingen van 3–10 km, zijn belangrijk voor de menging in het gebied omdat deze wervels een uitdrukking zijn van de onregelmatigheden in het snelheidsveld. De mechanismen die deze restwervels veroorzaken zijn nader bestudeerd m.b.v. een vorticiteitsbalans voor een karakteristiek gedeelte van het numerieke model. Vorticiteit of wervelsterkte, blijkt voornamelijk te worden opgewekt langs de dwarshelling van getijdegeulen. Deze getij-vorticiteit wordt stroomafwaarts meegevoerd naar aangrenzende gebieden waar bodemwrijving zorgt voor een snelle demping (binnen enkele uren). In gebieden die alleen 'gevoed' worden met vorticiteit tijdens de vloed- of ebstroming ontstaan restwervels wanneer het snelheidsveld over een getijperiode wordt gemiddeld. De benaming restwervels kan overigens tot verwarring leiden omdat deze 'restwervels' het resultaat zijn van een mathematische bewerking: de middeling van een kortdurend fenomeen, nl. de vorticiteit die gedurende enkele uren aanwezig is, over een gehele getijperiode.

In het tweede gedeelte van dit proefschrift wordt het numeriek model gebruikt om banen van waterdeeltjes te berekenen en te analyseren. Deze zgn. 'Lagrangeaanse' methode wordt eerst gebruikt om de uitwisseling van Noordzee- en Waddenzee water door de zeegaten te bestuderen. Het uitgewisselde volume blijkt sterk af te hangen van de getijfase waarop de berekening wordt gestart. Voor alle zeegaten is het uitgewisselde volume maximaal wanneer de aanvangssituatie zo gekozen wordt dat de grens tussen zee- en bekkenwater tijdens een getijperiode zo ver mogelijk zeewaarts wordt verplaatst. Noordzee water blijkt de Waddenzee voornamelijk binnen te komen vanuit het gebied ten zuiden van de zeegaten, Waddenzee water verdwijnt voornamelijk naar het gebied ten noorden van de zeegaten.

De berekende uitgewisselde volumina zijn gebruikt om verversings tijdschalen van de verschillende bekkens in de Waddenzee te schatten. Door het in rekening brengen van de getijgedreven doorstroming van het Vlie bekken naar het Marsdiep bekken blijken deze tijdschalen voor de westelijke Waddenzee groter te zijn dan eerdere schattingen deden vermoeden. Deze doorstroming heeft namelijk tot gevolg dat de berekende zoetwaterinhoud groter wordt omdat het gemiddelde zoutgehalte van zeewater, dat wordt gebruikt als referentie om de zoetwaterfractie te bepalen, toeneemt.

In het laatste gedeelte van dit proefschrift wordt in meer detail het mengingsproces in Waddenzee bestudeerd door de Lagrangeaanse banen van groepen deeltjes met verschillende initiele posities en afmetingen te analyseren. Aangetoond wordt dat de onregelmatigheden in het niet-willekeurige, deterministische, snelheidsveld zeer belangrijk zijn voor de verspreiding van een watermassa. Het klassieke scherings-dispersie concept, dat de verspreiding verklaard door de interactie tussen (deterministische) snelheids-schering en willekeurig in ruimte- en tijd verdeelde turbulentie, is als enig mechanisme onvoldoende omdat ook zonder willekeurige bewegingen de verspreiding groot is. Eerste analyses suggereren dat de deeltjesverspreiding t.g.v. het deterministische snelheidsveld chaotisch kan zijn, o.a. vanwege de extreme gevoeligheid van een deeltjesbaan voor de initiele positie. Het voorkomen van deterministische chaos is een karakteristieke eigenschap van sommige niet-lineaire dynamische systemen. De verplaatsing van deeljes in twee-dimensionaal oscilllerend snelheidsveld, waarin de deeltjessnelheid zowel plaats- als tijdsafhankelijk is, is een dergelijk systeem. Het is daarom zinvol om methoden die ontwikkeld zijn in (theoretische) studies naar het voorkomen van deterministische chaos in dergelijke systemen, toe te passen in toekomstig onderzoek naar mengingsprocessen in getijdegebieden zoals de Waddenzee.

REFERENTIES

POSTMA, H., 1954. Hydrography of the Dutch Wadden Sea.—Archs. Néerl. Zool. **10:** 405–511.

STELLING, G.S., 1984. On the construction of computational methods for shallow water flow problems. Communications no. 35. Rijkswaterstaat, The Netherlands: 1–226.

ZIMMERMAN, J.T.F., 1976. Mixing and flushing of tidal embayments in the western Dutch Wadden Sea, I: Distribution of salinity and calculation of mixing time scales.—Neth. J. Sea Res. **10:** 149–191.

The following chapters have been published elsewhere or submitted for publication:

Chapter 2: Neth. J. Sea Res. **22:** 1-22

Chapter 3: Neth. J. Sea Res. **22:** 185-198

Chapter 4: Neth. J. Sea Res. **24:** 9-26

Chapter 5: Co-authors: J.T.F. ZIMMERMAN & M.E. PHILIPPART.,1990. Submitted to Neth. J. Sea Res.

Chapter 6: Co-author: J.T.F. ZIMMERMAN., 1990. Accepted for publication in: R.T. CHENG (ed.) Lecture notes on Coastal and Estuarine studies. Springer-Verlag.

CHAPTER 1

INTRODUCTION, OVERVIEW AND CONCLUSIONS

1. INTRODUCTION

The Dutch Wadden Sea is a shallow tidal area in front of the Dutch coast, that is enclosed by a chain of Wadden islands. This tidal area consists of more or less separated tidal basins, each drained by an inlet. The shape of most of these basins is roughly identical in that the inlets between two islands connect a system of tidal channels with the adjacent North Sea. These tidal channels end up in relatively narrow tidal creeks surrounded by tidal flats which dry during part of the tidal cycle and form a watershed between adjacent basins.

North Sea water flushes continuously all basins. This North Sea water is mainly a mixture of relatively salt ocean water entering the North Sea from the English Channel and of fresh river water, particularly from the river Rhine. Some of the basins have a direct supply of fresh water from the continent and can be regarded as estuaries. Thus, in general Wadden Sea water is a mixture of North Sea water and fresh water supplied directly by a river or through sluices from the adjacent coastal area. Mutual differences in fresh water content between different tidal basins depend largely on the presence of a fresh water source in the basins considered.

For the functioning of the Wadden Sea ecosystem the flushing of tidal basins with North Sea and fresh water is of great importance. Both water fractions carry many substances that are essential to biological and chemical processes. Examples of chemical substances are nutrients which are indispensable for primary production, the basis of the food chain, and micropollutants which may form a serious threat for parts of the ecosystem. The importance of the flushing with North Sea water can be illustrated by the more or less passive inflow of flathfish eggs through the inlets during spring, giving the Wadden Sea basins its characteristic function as a nursery area for these organisms.

For basins with a substantial fresh water input this flushing can be quantified by means of measurements of the salinity distribution, which is subsequently used to determine the fresh water content. The fresh water fraction is a measure of the flushing of a basin because its value is relatively low (high) if the flushing intensity is high (low). For the Marsdiep basin POSTMA (1954) used this method in his study on the hydrography of this area in which, among other things, the residence time of fresh water supplied from the sluice at den Oever was calculated. The use of mixing time scales to quantify the flushing in a basin has been applied to the Ems Dollart estuary by DORRESTEIN & OTTO (1960) and to the western Wadden Sea, the Marsdiep and Vlie basin, by ZIMMERMAN (1976a). In both studies box models are used to calculate mixing time scales. In these box models the basin is subdivided in a number of compartments and the flux of a dissolvent is parametrized in an 'advective' part that is caused by the continuous throughflow, the external supply from the sluices or from a river, and a 'dispersive' part that causes an exchange of watermasses between different compartments. The exchange coefficients between the compartments are chosen in such a way that computed and observed salinity distributions agree reasonably well. The use of a box model gives the possibility to calculate a variety of mixing time scales that depend on the position of the waterfraction in the basin and on its source as has been shown by ZIMMERMAN (1976a). In the present study the focus lies on the mechanisms that cause the flushing or displacement of water masses in the Wadden Sea basins.

2. BASIC MECHANISMS FOR THE FLUSHING OF TIDAL BASINS

The displacement of waterparcels is caused by currents which prevent that a waterparcel remains on a fixed position. The forces that cause these currents can be used for a classification in tidally driven, wind driven and density driven currents. From these, tidal currents are energetically the most dominant in the the Wadden Sea basins. Only in regions close to relatively large fresh water sources, like the sluices in the Afsluitdijk or the river mouths in the Ems-Dollart, the magnitude of density driven currents may be comparable to the magnitude of tidal currents. The fact that tidal currents energetically dominate does not mean automatically that these currents are the most important agency for the flushing of the basins. For, in a uniform periodic tidal current field waterparcels are carried only backwards and forwards without having any net displacement. Such a net displacement of water parcels after a tidal period can only exist if there is a continuous throughflow through the basin considered and/or if different waterparcels exchange their position.

Because of mass conservation, the continuous throughflow, which causes the so called 'advective' part of the displacement of a watermass (and the aforementioned advective flux in box models) must be equal to the external supply from a river or sluice in a semi-enclosed basin. However, if a basin has open connections with adjacent basins a continuous flow can exist from one inlet to another through the tidal basins. Such a throughflow can be driven by the tide itself as has been shown by VAN DE KREEKE & DEAN (1975). In an analytical study they showed that asymmetries in the fluctuating tidal waterlevels at both inlets of a single tidal channel induce a continuous flow through the system.

The exchange of the position of waterparcels, or mixing, must be caused by the non-uniformity of the current field. The random part of the current field (turbulence) that is generated by the tidal currents, is in itself by far not strong enough to explain the relatively large mixing intensity in the Wadden Sea basins. Therefore the non-random part of the irregularities in the current field must be of great importance for mixing in this area.

An example of such an irregularity is the higher magnitude of the currents in the center of tidal channels as compared with the shallower parts. Combining this so called 'shear' in a current field with random movements by turbulence gives the classical shear dispersion concept as the basic mechanism for mixing. For oscillating current fields this concept was developed by OKUBO (1967).

Another type of irregularities arises if the fluctuating current field is averaged over the basic tidal period, giving the residual current field. Residual eddies with a length scale which is comparable to the tidal excursion length are present all over the Wadden Sea area. ZIMMERMAN (1976b) showed that a current field that consists of these residual eddies combined with a uniform periodic current field, causes a 'tidal random walk' of waterparcels. This 'tidal random walk' can be responsible for a relatively large mixing intensity.

Recently AREF (1984), in a numerical study, and OTTINO *et al.* (1988), in laboratory experiments, studied the chaotic aspects of mixing of fluids in simple two-dimensional time- periodic current fields which have much in common with the current field in the Wadden Sea. Without the presence of random components in the underlying velocity field the trajectories of fluid parcels appear to be quasi-random. In this concept methods from non-linear dynamical systems theory are used to explain the spreading of waterparcels.

Thus, random components in the underlying velocity field need to be present only in the shear-dispersion concept. This random part of the the current field is indispensable because it is assumed that the deterministic velocity field is in essence one-dimensional; it has no components in a lateral direction. In both other concepts the spreading of water parcels is quasi-random although the underlying velocity field has no random components. Here the interaction of longitudinal and lateral velocity varia-

tions gives rise to a complex behavior of water parcels. Most fascinating is that non- random, Eulerian, currents can cause random, Lagrangean, displacements.

In a tidal area like the Wadden Sea the non-uniformity of the current field which is a necessary ingredient in all concepts mentioned, is caused by the interaction of the tidal currents with the complicated bathymetry.

3. OVERVIEW OF THE FOLLOWING CHAPTERS

Both aspects that are of importance for the flushing of tidal basins, *viz.* the continuous throughflow between connected tidal basins and the irregularity of the currents, can be examined by means of a numerical hydrodynamical model. For the western Wadden Sea the WAQUA software system has been applied, This software package, originally developed by LEENDERTSE (1967) and later revised by STELLING (1984), solves the two-dimensional depth-integrated shallow water equations numerically and can be applied for an arbitrary bathymetry. The model application that is used here covers the four westernmost basins of the Dutch Wadden Sea and a part of the adjacent coastal zone of the North Sea. In this study only the effect of the ever present and most dominating forcing mechanism, the tide, is considered. The gridsize of the model is 500 m. Along the open boundaries in the North Sea periodic tidal waterlevels with a basic period of 12.5 hours are prescribed.

Chapters 2, 3 and 4 describe mainly the magnitude and origin of the residual current field in the western Wadden Sea, which remains if in all grid points of the model the currents are averaged over the basic period. First, in chapter 2, the outcome of numerical model simulations are discussed. Modelresults, tidal waterlevels in some stations and transport rates through the inlets, are compared with measurements. Also the influence of different terms in the tidal momentum equations is discussed. Averaging the computed, fluctuating waterlevels and velocities over a tidal period gives the tidal mean or residual field for these variables. The drop in residual waterlevels in the inlets, which is caused by a Bernoulli accelleration, and the rise in the tidal basins are phenomena characteristic for all tidal basins. The tidally driven residual current field appears to be a combination of a constant throughflow between connected tidal basins causing residual velocities of $O(10^{-2}\ ms^{-1})$ and of isolated residual eddies with velocities of $O(10^{-1}\ ms^{-1})$ and a typical length scale of 3 to 10 km. With respect to the influence of the different terms in the equation governing residudual currents an important shift takes place in that compared with the tidal equations the influence of the nonlinear advective terms increases substantially.

In chapter 3 the origin of the large scale throughflow between connected tidal basins is examined by means of an analytical model, which is similar to the model applied by VAN DE KREEKE & DEAN (1975) in their study on tide-induced throughflow in a single tidal channel. In this model the Marsdiep and Vlie basin are schematized in rectangular basins each with a constant width and depth. After deducing analytically solvable equations for the residual transport, the effect of asymmetries in the fluctuating tidal waterlevels at both boundaries, the inlets, and the effect of large scale geometrical differences are studied. The influence of tidal asymmetries appears to be much larger than the influence of geometrical differences. The asymmetry in the amplitude of the fluctuating waterlevels with a larger amplitude at the northern boundary, causes a southward directed throughflow from one inlet (in the Vlie basin) to the other (in the Marsdiep basin). The magnitude of this flow is suppressed by the phase difference in the waterlevel fluctuations, which, acting alone, would drive the flow in the opposite direction.

In chapter 4 results of the numerical model are used to study the origin of the small scale residual eddies which express a part of the irregularity in the current field. The origin of these eddies is examined with a vorticity-dynamics approach which eludicates the mechanisms that produce and damp vorticity, as shown by ZIMMERMAN (1980) in an

analytical study on the origin of tidally driven residual eddies in the open sea. Terms in the vorticity balance equations are determined on the basis of the outcome of the numerical model. The torque from bottom friction along the side walls of the inlets and tidal channels appears to be the dominating mechanism in generating tidal vorticity, the magnitude of which is much larger than that of planetary vorticity. Residual vorticity or residual eddies arise mainly outside the production regions of tidal vorticity. The transfer of vorticity from its source regions to adjacent regions is most effective near a transition from straight to curved isobaths. This is illustrated by showing the vorticity possessed by a fluid column during its tidal excursion. This Lagrangean approach also clearly shows that residual eddies are the result of averaging a transient phenomenon, the vorticity which is present during a short period (some hours), over a complete tidal cycle.

In chapter 5 and 6 the Lagrangean approach is followed by analyzing trajectories of marked, free flowing, particles in the numerical model. In the first part of chapter 5 the tidal exchange of watermasses through the inlets between the islands is discussed. It is shown that after a tidal period the exchanged volume across a fixed boundary in an inlet, as calculated from the final position of labeled particles, depends strongly on the initial phase of the computation. For all four inlets the largest exchange occurs if the calculation is started around slack tide before ebb. Then the boundary between 'sea' water and 'basin' water reaches its maximimum seaward displacement. The largest net inflow of North Sea water takes place along the southern coast and the largest net outflow of Wadden Sea water along the northern coast of the inlets. Relating the exchanged volume to the tidal prism entering a basin during a full flood period shows that the ratio between both is about equal for three inlets. Only the Eierlandse Gat deviates in that this ratio is substantially larger for this inlet.

The second part of chapter 5 disusses mixing time scales in Dutch Wadden Sea basins. For the connected Marsdiep and Vlie basin the residence time of fresh water from both sluices and the turn over time of each basin separately are calculated. The consequence of the southward directed tidally driven throughflow is that in general these mixing time scales increase as compared with previous estimates by POSTMA (1954) and ZIMMERMAN (1976a). For other Dutch Wadden Sea basins the turn over time is estimated from the tidal mean basin volume and the tidally exchange volume through the inlets. The latter is assumed to be a fixed percentage of the tidal prism, which is deduced from calculations for some inlets that are covered by the numerical model.

Chapter 6 focusses in more detail on the mixing processes that cause watermasses to be exchanged between different regions in a tidal basin. For this the Lagrangean trajectories of particle groups with different initial position and initial size in the numerical model are analyzed. It is shown that random motion, or small scale turbulence, does not have to be present for an effective dispersion of a watermass which is in conflict with the classical shear-dispersion concept. In the Wadden Sea the irregularity of the non-random Eulerian current field on length scales that are comparable to the tidal excursion length makes that a watermass deforms or disperses. The Lagrangean particle trajectories appear to have much in common with the outcome of studies on chaotic mixing in relatively simple two- dimensional periodic current fields (OTTINO *et al.*, 1988).

4. CONCLUSIONS

The tidally driven residual current field in the western Dutch Wadden Sea is composed of a large scale part, the throughflow between connected tidal basins, and a small scale part, the residual eddies. The former, which is of importance for the advective part of the displacement of watermasses, is caused by the difference in amplitude of the vertical tide at the sea boundary of the connected Marsdiep and Vlie basin. Between both basins this flow is directed southwards from the Vlie basin towards the Marsdiep basin. Residual eddies are the most dominant part of the residual current field by the magnitude of the associated residual velocities, as well as by their presence all over the

area. The origin of these eddies, which express part of the irregularity in the current field, can be explained by means of a vorticity balance. The torque from bottom friction is most dominant in producing tidal vorticity, the advective terms cause the transfer to the mean field.

The exchange by the tide of North Sea and Wadden Sea water through the tidal inlets is caused by the irregularity of the tidal current field in the inlet region. For three of four western Wadden Sea basins the tidally exchanged volume is about 8 percent of the tidal prism entering a basin. The flushing of the Marsdiep and Vlie basin is less intense than previous estimates suggested because of the throughflow between both basins, which makes that the 'observed' fresh water content increases. Regarding the displacement of watermasses in more detail shows that the irregularity of the non- random, deterministic, current field is very important for the spreading of watermasses. In a tidal area like the Wadden Sea the classical shear dispersion concept cannot be applied to quantify the mixing intensity. A preliminary analysis of Lagrangean particle trajectories suggests the occurence of deterministic chaos in this area, which is a characteristic feature of certain nonlinear dynamical systems. Therefore it is useful to apply concepts and methods that have been developed in studies on deterministic chaos in nonlinear dynamical systems in future research on mixing in tidal basins like the Wadden Sea.

REFERENCES

AREF, H., 1984. Stirring by chaotic advection.—J. Fluid. Mech. **143:** 1–21.

DORRESTEIN, R. & L. OTTO, 1960. On the mixing and flushing of the water in the Ems-estuary.—Verh. K. ned. geol.-mijnb. Genoot. **19:** 83–102.

KREEKE, J. VAN DE & R.G. DEAN, 1975. Tide induced mass transport in lagoons.—J. Waterw. Harb. Coast. Eng. Div. ASCE Vol 101, no WW4, 393–403.

LEENDERTSE, J.J., 1967. Aspects of a computational model for long period water wave propagation. Memorandum RM–5294-PR, Rand Corporation, Santa Monica, 1967.

OKUBO, A., 1967. The effect of shear in an oscillatory current on horizontal diffusion from an instantancous source.—Int. J. Oceanol. Limnol. **1:** 194–204.

OTTINO, J.M., C.W. LEONG, H. RISING & P.D. SWANSON, 1988. Morphological structures produced by mixing in chaotic flows.—Nature **333:** 419–425.

POSTMA, H., 1954. Hydrography of the Dutch Wadden Sea.—Archs. Néerl. Zool. **10:** 405–511.

STELLING, G.S., 1984. On the construction of computational methods for shallow water flow problems. Communications no. 35. Rijkswaterstaat, The Netherlands: 1–226.

ZIMMERMAN, J.T.F., 1976a. Mixing and flushing of tidal embayments in the western Dutch Wadden Sea, **I:** Distribution of salinity and calculation of mixing time scales.—Neth. J. Sea Res. **10:** 149–191.

——, 1976b. Mixing and flushing of tidal embayments in the western Dutch Wadden Sea, II: Analysis of mixing processes.—Neth. J. Sea Res. **10:** 397–439.

——, 1980. Vorticity transfer by tidal currents over an irregular topography.—J. Mar. Res. **38:** 601–630.

CHAPTER 2

TIDAL AND RESIDUAL FLOWS IN THE WESTERN DUTCH WADDEN SEA I: NUMERICAL MODEL RESULTS*

H. RIDDERINKHOF

Netherlands Institute for Sea Research, P.O. Box 59, 1790 AB Den Burg, Texel, The Netherlands

ABSTRACT

A two-dimensional numerical model, which includes tidal basins in the western Dutch Wadden Sea and a part of the adjacent North Sea, is used to study tidal and tidally-driven residual flows and elevations. The model is verified by comparing observed and computed water elevations in some stations and transport rates through the tidal inlets. The consequence of topographical and geometrical differences for the terms in the governing equations is discussed by comparing the magnitude of these terms in some characteristic grid points, *viz.* the open sea, inlet and basin channel, in which all terms are decomposed along and perpendicular to the dominant current direction. Averaging over a tidal period shows that compared to the time-dependent equations an important shift takes place in the relative influence of the different terms, mainly caused by the increased influence of the advective term. The resulting tidally-driven residual flow field is interpreted as a combination of a constant volume transport (1 to 2% of the tidal transport in the tidal inlets) between connected tidal basins and isolated residual eddies (with velocities of 10 to 15% of the tidal velocity amplitude and a typical length scale of between 3 and 10 km). Observations confirm that the drop in residual elevations in tidal inlets and the rise in tidal basins are phenomena characteristic of all tidal basins.

1. INTRODUCTION

The western Dutch Wadden Sea consists of four more or less separated tidal basins drained by inlets between the islands. Global characteristics of tide and topography were described by POSTMA (1954) and ZIMMERMAN (1976) in their studies on the chemistry (POSTMA) and mixing processes (ZIMMERMAN) of this area. Observed salinity distributions and measurements of tidal velocities formed the basis of their studies on mixing time scales in the western Wadden Sea.

In the present study a detailed two-dimensional numerical model is used to study tidal and tidally-driven flows. In a later phase of the project the same numerical model will be used to study exchanges between the Wadden Sea and adjacent North Sea and mixing processes in the interior of the tidal basins. This first paper in a series presents the results of research on tidal and residual flows of the numerical model. In separate papers both the origin of the computed tidally-driven residual volume transport between two tidal basins and the isolated residual eddies will be discussed, as the residual current velocity field plays an important role in the displacement of dissolved matter.

Comparable modelling studies of tidal and/or residual flows in shallow seas and estuaries were performed by MADDOCK & PINGREE (1978), PRANDLE (1978), TEE (1976) and OEY *et al.* (1986). The present model is different in that its open boundaries are selected outside the sphere of influence of the tidal inlets. This makes it a model of large geographical coverage suitable for the study of internal tidally-driven residual volume transports between different basins.

Acknowledgements.—The author is much indebted to Rijkswaterstaat, Dienst Informatieverwerking, for the use of their computer

*Publication no. 21 of the project "Ecological Reseach of the North Sea and Wadden Sea" (EON).

and the support in employing the extended system of computer programmes. The close cooperation with especially J. Dijkzeul of Rijkswaterstaat, Dienst Getijdewateren, was of great importance during the setting up and calibration of the numerical model.

2. NUMERICAL MODEL

2.1. INTRODUCTION

An extended system of computer programmes, the WAQUA system, developed and supported by the Dutch Ministry of Transport and Public Works, was used for two-dimensional simulation of tidal movements in the Wadden Sea. In the simulation programme the well-known shallow-water equations are solved numerically. These equations read:

$$\frac{\partial u}{\partial t} + u\frac{\partial u}{\partial x} + v\frac{\partial u}{\partial y} - fv =$$

$$= -g\frac{\partial \zeta}{\partial x} - g\frac{u\sqrt{(u^2+v^2)}}{C^2(H+\zeta)} + \nu\left(\frac{\partial^2 u}{\partial x^2} + \frac{\partial^2 u}{\partial y^2}\right) \quad (1)$$

$$\frac{\partial v}{\partial t} + u\frac{\partial v}{\partial x} + v\frac{\partial v}{\partial y} + fu =$$

$$= -g\frac{\partial \zeta}{\partial y} - g\frac{v\sqrt{(u^2+v^2)}}{C^2(H+\zeta)} + \nu\left(\frac{\partial^2 v}{\partial x^2} + \frac{\partial^2 v}{\partial y^2}\right) \quad (2)$$

$$\frac{\partial \zeta}{\partial t} + \frac{\partial (H+\zeta)u}{\partial x} + \frac{\partial (H+\zeta)v}{\partial y} = 0 \quad (3)$$

in which:

- u, v vertically averaged velocity components
- ζ water elevation relative to a reference plane
- H depth relative to a reference plane
- f coriolis parameter
- g acceleration of gravity
- ν horizontal eddy viscosity coefficient
- C bottom friction coefficient (Chezy coefficient)

These equations are solved numerically by employing a so-called ADI (Alternating Direction Implicit) method on a staggered grid. This method was developed by LEENDERTSE (1967) and has been applied successfully for tidal computations in several shallow seas and estuaries (LEENDERTSE *et al.*, 1981). STELLING (1984) recently revised the numerical approximations of the different terms in the shallow-water equations, changing the discretisations of the advective terms in the interior as well as along the boundaries into discretisations proved to be unconditionally stable. This version of the WAQUA system has been used for the computations discussed in this article. Earlier applications can be found in VOOGT, (1984) and KLATTER *et al.*, (1986).

2.2. MODEL DESCRIPTION

Boundary conditions for the small-scale model of the western Wadden Sea have been derived from a model which describes the tidal movement in the North Sea area to the north of the Wadden Sea (Fig. 1a). The latter model (grid size 3200 m) was constructed on the basis of data gathered during an extensive measurement campaign in May-June 1971 (STUDIEDIENST HOORN & DELFZIJL, 1973). During this campaign water-levels along the sea boundary were observed, from which boundary conditions were constructed for the 3200-m model. Filtering of the observed data showed that during the chosen simulation period (8 to 9 June 1971) the tidal water-levels along these boundaries could be described in three basic periodic bands (12.5, 6.25 and 4.16 h). The amplitude of the daily component, with a period of 25 h, was very small (less than 0.01 m) during these days. This simulation period, representative of average conditions during the neap-springtide cycle, was also chosen because of the simultaneous measurement of transport rates in the tidal inlets of the Wadden Sea basin. Furthermore, the influence of the wind could be neglected in this period (Dijkzeul, personal communication).

The aforementioned three basic periods are subsequently used in describing the water-levels along the open sea boundary of the smaller-scale model. The amplitude of the 12.5 h component increases from 0.67 m along the southern boundary to 0.90 m along the northern boundary, while the phase difference is about 4.0 h. The less important tidal components (overtides) with periods of 6.25 and 4.16 h are described with amplitudes of about 0.14 m and 0.08 m, respectively.

The location of the boundaries in the smaller-scale model (grid size 500 m), together with some

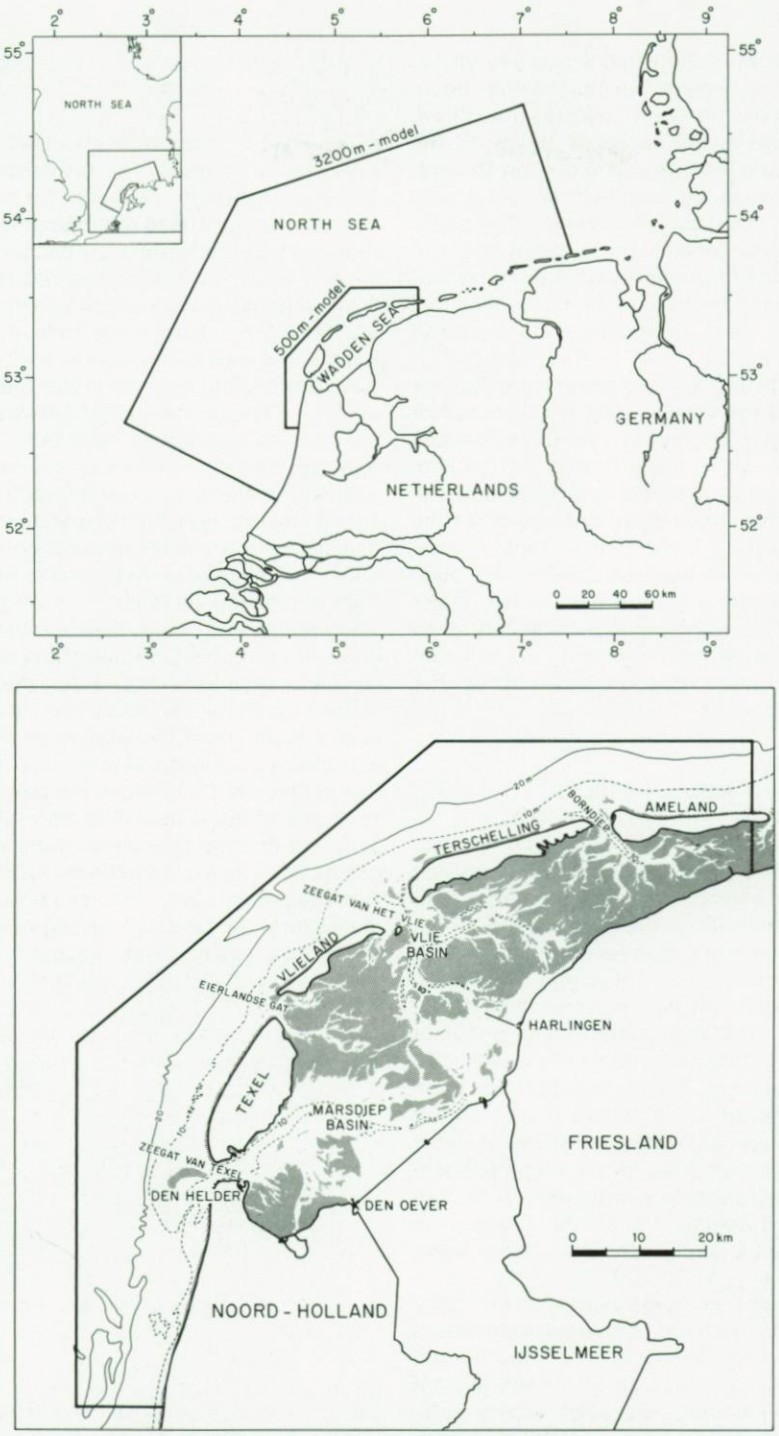

Fig. 1. (a) Location of the boundaries of the models with 3200 m and 500 m grid size. Results of the 500 m model are discussed in this article.

(b) Map showing the boundaries and some isobaths (10 m, 20 m) of the 500 m model. Shaded areas represent tidal flats.

isobaths is shown in more detail in an overall picture of the model area in Fig. 1b. The open boundaries at which water-levels are prescribed from the larger-scale model lie about 15 km off the coast, where the the inflow and outflow through the inlets between the islands have a negligible influence on the tidal movement. The north-eastern boundary between the island of Ameland and the mainland coincides with a tidal flat that separates two tidal basins. In the model this boundary has been schematized as a closed boundary.

The isobaths in Fig. 1b clearly show that the model area of the Wadden Sea is composed of four tidal basins drained by the inlets between the islands. Each of these basins can be subdivided into tidal channels and tidal flats, of which the latter are emersed during part of the tidal cycle. Most of these tidal flats form a separation between adjacent basins. An open connection exists only between the two major basins, the Marsdiep basin in the south, drained through the Zeegat van Texel, and the Vlie basin in the middle, drained through the Zeegat van het Vlie.

2.3. MODEL RESULTS

When a grid size of 500 m is used to schematize the area, sufficient resolution of the bottom topography is only expected for the larger tidal channels. Especially in the parts of the model where the water enters and leaves the tidal flats by way of narrow gullies, this grid size is too coarse to simulate the tidal movements in detail. So, although special procedures can simulate the emersion of tidal flats, no locally meaningful results in these areas can be expected. The main function of the tidal flats in this model is their capacity to store water. Model results are only compared with prototype measurements insensitive to such small-scale variations in bottom topography as volume transports through the deeper channels and water elevations along such channels.

Calibration of the model has been achieved by comparing observed and computed water-levels in different computations in which the bottom friction coefficient, being an important, but not well-known parameter, has been varied. Sufficiently accurate results were achieved by varying the Chezy coefficient, computed via the depth-dependent Manning's formulation,

$$C = \frac{1}{n} H^{\frac{1}{6}}$$

in which $n = 0.023$, from about 40 $m^{0.5}s^{-1}$ on tidal flats to 75 $m^{0.5}s^{-1}$ in the deeper channels. The less important coefficient for horizontal eddy viscosity, ν, is used to parametrize the lateral exchange of momentum on subgrid scale. The chosen value, $\nu = 7$ m^2s^{-1}, is based on modelling experience in the Eastern Scheldt (LEENDERTSE, 1984). The order of magnitude of this value is in agreement with dimensions and velocities of turbulent eddies observed in the Zeegat van Texel (VETH & ZIMMERMAN, 1981). This parameter has not been varied because the lateral stress term is only of minor importance to the computed volume transports and water-levels. Results of a sensitivity analysis for the parameter ν will be discussed in a subsequent paper, whose main subject will be the generation and dissipation of tidal and residual eddies.

In Figs 3a to d computed and observed water-levels are compared in some of the stations used for calibration (see Fig. 2 for their location). These Figs show that the agreement between the two is fairly good. The amplitude amplification and phase difference between the water elevation at the inlet (Den Helder, Fig. 3a) and the landward end of the Marsdiep basin (Harlingen, Fig. 3c) show that the tidal wave in the Wadden Sea can be seen as a combination of a standing and a propagating wave. This combined character stems from the relatively strong bottom friction in the tidal basin, which reduces the energy in

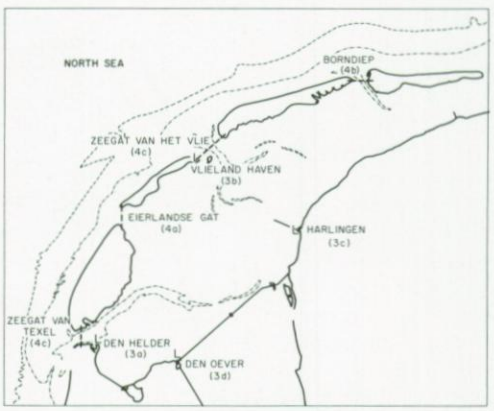

Fig. 2. Position of water-level stations (L) and transport crossections (----) used for calibration of the 500 m model.

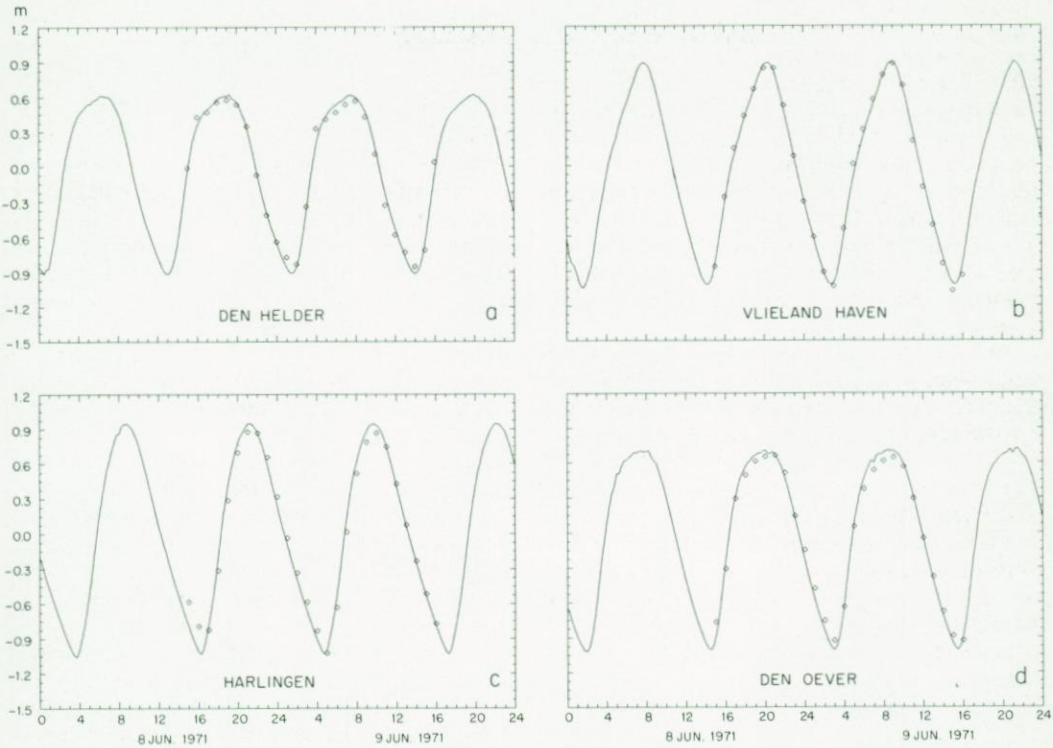

Fig. 3. Comparison of computed (——) and observed (□ □) water-levels. a) Den Helder; b) Vlieland Haven; c) Harlingen; d) Den Oever.

the incoming and reflected tidal wave. By this the amplitude of the reflected wave is very small near the tidal inlet. In this area the tidal wave can be characterized as a propagating wave, reflected in the phase difference between Figs 3a and c, while at the landward end near Harlingen it can be characterized as a standing wave. Figs 4a to d show a validation of the transport rates through the tidal inlets measured during the extensive campaign in 1971 (STUDIEDIENST HOORN & DELFZIJL, 1973). The differences in the dimensions of the tidal basins are clearly reflected in the amplitude of these transport rates. For the smaller inlets, Eierlandse Gat (Fig. 4a) and Borndiep (Fig. 4b), deviations can be recognized between observations and computations which can be explained by the use of rather too coarse a grid. For the greater part, these two basins are covered with tidal flats, poorly presented in the model, which causes perturbations in the transport rates. Model results and observations of the major inlets, the Zeegat van het Vlie (Fig. 4c), which drains the Vlie basin, and the Zeegat van Texel (Fig. 4d), which drains the Marsdiep basin, show that the tidal transport amplitudes through these inlets are nearly equal. The slightly better agreement of the transport rates through the Zeegat van Texel than of those of the Zeegat van het Vlie stems from the morphological differences between the two basins, the percentage of the tidal flats in the Vlie basin (40%) being much larger than in the Marsdiep basin (17%). However, small deviations can also be ascribed to the inaccuracy of the measurements.

Fig. 5 gives the two-dimensional velocity field in every fourth grid point one hour before the time of low water in Harlingen, near the landward end of the Marsdiep and Vlie basins. The 0.50 ms^{-1} velocity isoline indicates the location of the main basin channels. The dotted points are the grid points taken out of the computations as tidal flats are emerging at that moment. Such maps were compared with measurements of the

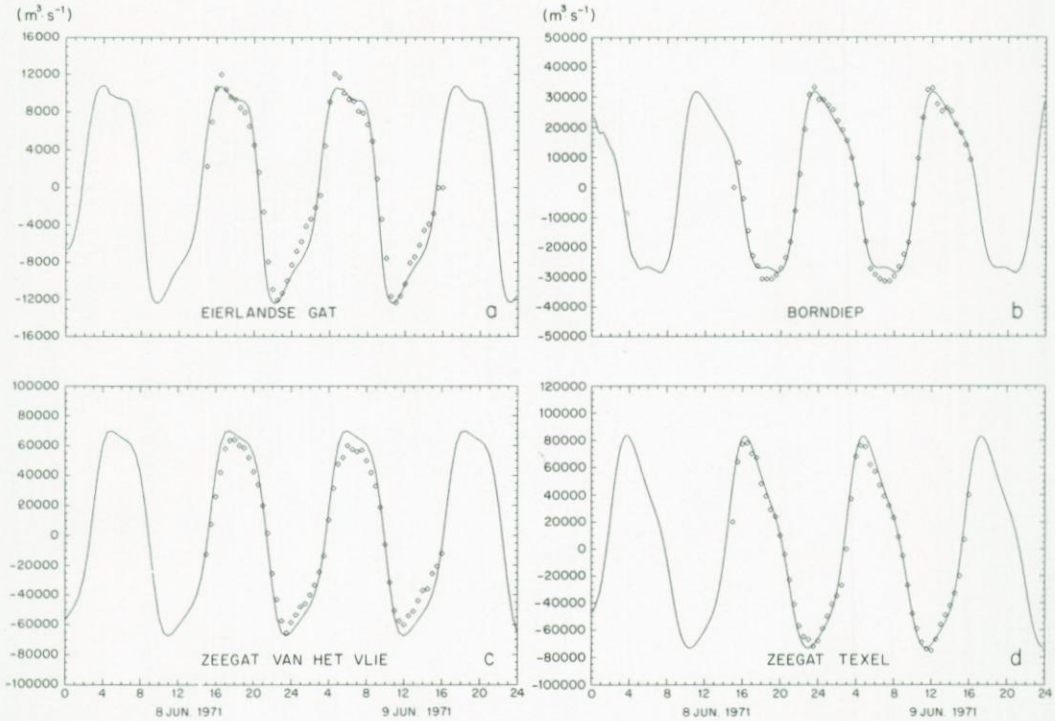

Fig. 4. Comparison of computed (——) and observed (□ □) transport rates through the inlets. a) Eierlandse Gat (between Texel and Vlieland); b) Borndiep (between Ameland and Terschelling); c) Zeegat van Vlie (between Vlieland and Terschelling); d) Zeegat van Texel (between Texel and the mainland).

global current velocity field and the location of emersed tidal flats (DE BOER *et al.*, 1984) to verify the large-scale results of the computations. A reasonable simulation of the emersion of the tidal flats was only to be achieved by excluding from the computations the grid points for which the water depth was less than 0.15 m. By this, an extreme growth of bottom friction term was prevented.

A plot showing the velocity vectors in every grid point at slack water before flood in a part of the model area near the Zeegat van Texel is given in Fig. 6. This map, in which the 5-m isobath is also indicated, demonstrates that a phenomenon like the time lag between the reversal of the tide in shallow and deeper parts of the basin is well simulated by the model.

2.4. INFLUENCE OF DIFFERENT TERMS IN THE TIDAL MOMENTUM EQUATIONS

The results of the numerical computations with the WAQUA programme, matrices of water-levels (ζ) and velocities (u, v) in staggered grid points, could only be stored at intervals of 30 min. due to limited storage facilities. These matrices have been used to compute the magnitude of the different terms in momentum equation. Although the same spatial differences were applied, the computed magnitude of these terms slightly differs from the magnitude in the numerical simulation. In the numerical simulation a time step is split up into two stages in which variables from different time levels are used by employing alternate implicit and explicit schemes (ADI method, STELLING, 1984), while in this section, as well as in section 3.4, all spatial differences are computed with variables (ζ, u, v) from the same time level. The difference hereby introduced is small and can be neglected. Furthermore, the consequence of a staggered grid is that water-levels, velocities and computed terms in the momentum equation are defined at different locations in one grid unit. Defining m as the position of the grid

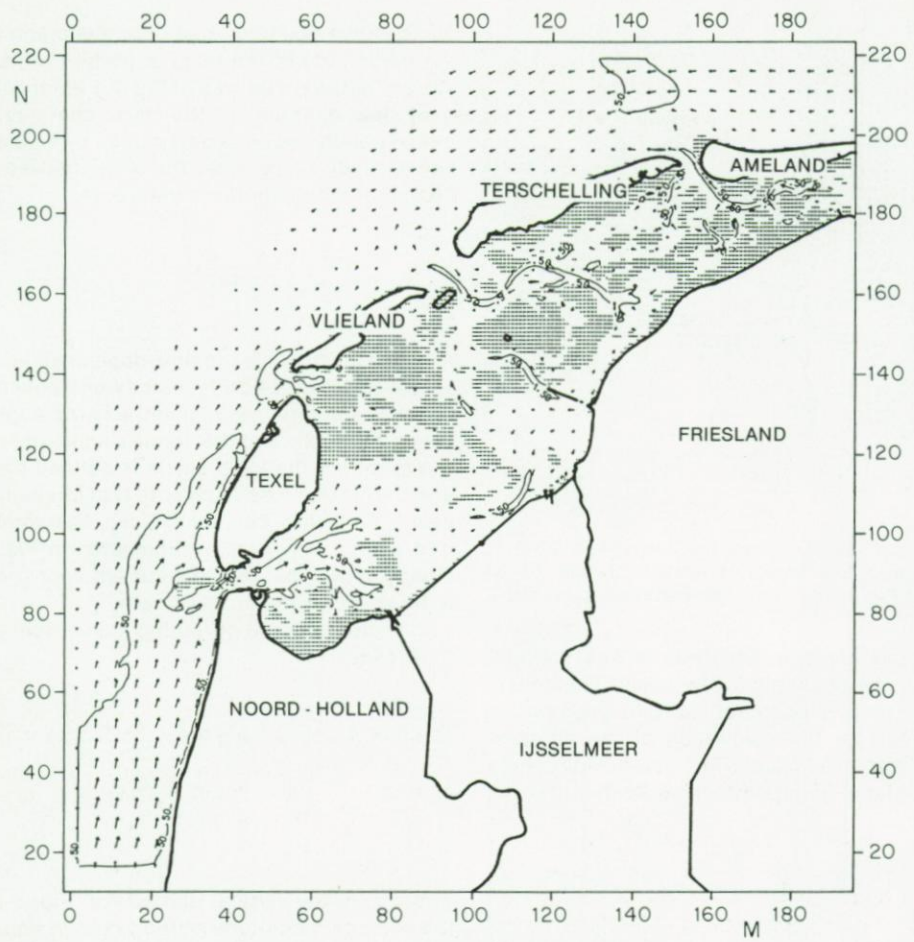

Fig. 5. Map of the two-dimensional velocity field in every fourth grid point one hour before the time of low water at Harlingen. The 0.50 ms^{-1} velocity isoline has been indicated, dotted points represent areas falling dry according the numerical model.

unit along the X-axis and n along the Y-axis, the water-levels are located at the integer values m, n, while the velocity variables and the terms in the momentum equation are located between the water-level points, in x-direction at $m + ½,n$ and in y-direction at $m,n + ½$. The magnitude and direction of a term in the momentum equation is therefore not known at one single position, which in principle prohibits a decomposition of these terms in an arbitrary direction. To enlighten the discussion in this section all terms and velocities are linearly interpolated towards the central water-level grid point (m,n) to be able to decompose these terms parallel and perpendicular to the local streamline:

$$X_{m,n} = ½(X_{m+½,n} + X_{m-½,n}) \quad (4)$$

$$Y_{m,n} = ½(Y_{m,n+½} + Y_{m,n-½}) \quad (5)$$

in which X and Y are velocities or terms in the x- and y-direction in the governing equations.

Fig. 7 shows isobaths in a part of the model near the Zeegat van het Vlie. This part encloses three different areas that are typical of the complete model and can be distinguished by their

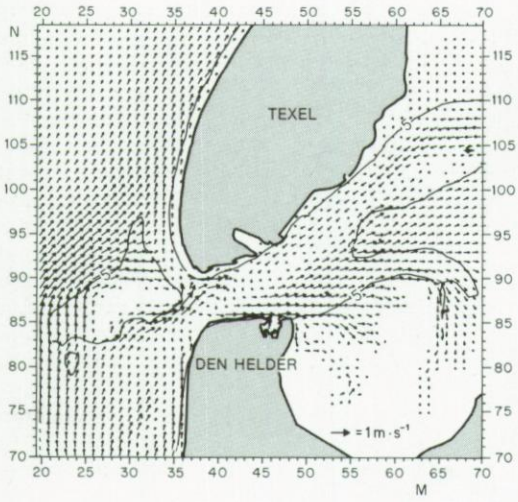

Fig. 6. Tidal velocities near the Zeegat van Texel at slack water, before flood, 1.5 hours after the time of low water at Den Helder, together with the 5 m isobath.

morphological properties: the open sea, the tidal inlet and the channels in the basin. The consequences of the topographical and geometrical differences for the magnitude of the different terms are discussed in detail for three characteristic grid points indicated in Fig. 7,

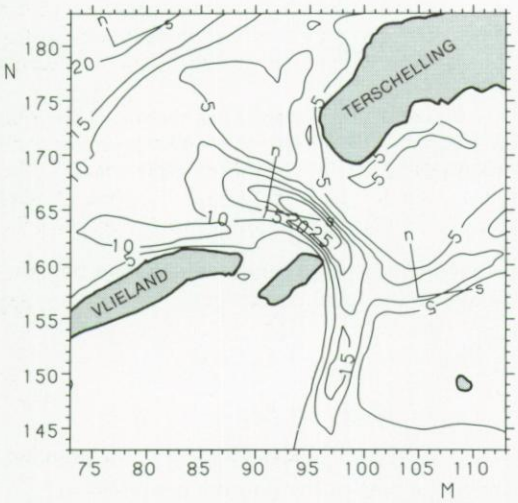

Fig. 7. Isobaths in a part of the model near the Zeegat van het Vlie (interval 5 m). The location of the characteristic grid points is given together with the local axes parallel (s) and perpendicular (n) to the dominant streamline.

while at two points of time during ebb and flood the magnitude of the most important terms are shown for the whole area of Fig. 7. First the dominant flow direction in the three characteristic model points has been determined by employing equation (6), which gives the angle between the dominant streamline and the x-axis:

$$\tan \varphi = \sum_{t=1}^{25} \left(\frac{v\,(t)}{u\,(t)} \right) \tag{6}$$

in which $(u\,(t), v(t))$ is the time-dependent velocity vector (the sign of both velocity components is reversed for negative $u\,(t)$) and φ is the angle between the x-axis and the dominant streamline. In the following the local s-axis is defined parallel and the n-axis perpendicular to that streamline in each grid point. For the chosen characteristic grid points both axes are indicated in Fig. 7. It clearly shows that the tidal current approximately flows along the local isobath.

In vector form the governing momentum equation reads:

$$\underbrace{\frac{\partial \vec{u}}{\partial t}}_{(a)} + \underbrace{\vec{u} \cdot \nabla \vec{u}}_{(b)} + \underbrace{f(\vec{j} \times \vec{u})}_{(c)} + \underbrace{g \nabla \zeta}_{(d)} + \underbrace{\frac{g \vec{u} |\vec{u}|}{C^2 (H + \zeta)}}_{(e)} - \underbrace{\nu \nabla^2 \vec{u}}_{(f)} = \underbrace{0}_{(g)} \tag{7}$$

where $\vec{j}$ is the vertical unit vector. Fig. 8 gives the average magnitude of the terms in equation (7) in the chosen grid points during the flood (solid lines) and ebb period (dashed lines). The sign of the velocity component in the local s-direction was used to separate the tidal cycle in a flood and ebb period. The average error caused by the approximations discussed above is indicated by a summation of all terms in equation (7). The magnitude of this error is also given in Fig. 8 ("term (g)") and appears to be negligible for the discussion in this section.

In general, Fig. 8 shows that the magnitude of all terms in grid point (79,180), in the open sea, is less than in both other grid points (note the different scales). Furthermore, advective terms (b) have a minor influence in this grid point. In both directions and in all grid points the relative influence of the viscosity term (f) is negligible.

The non-linear advective term (b) plays an important role in the grid points (91,165) and (105,157), especially in the direction perpen-

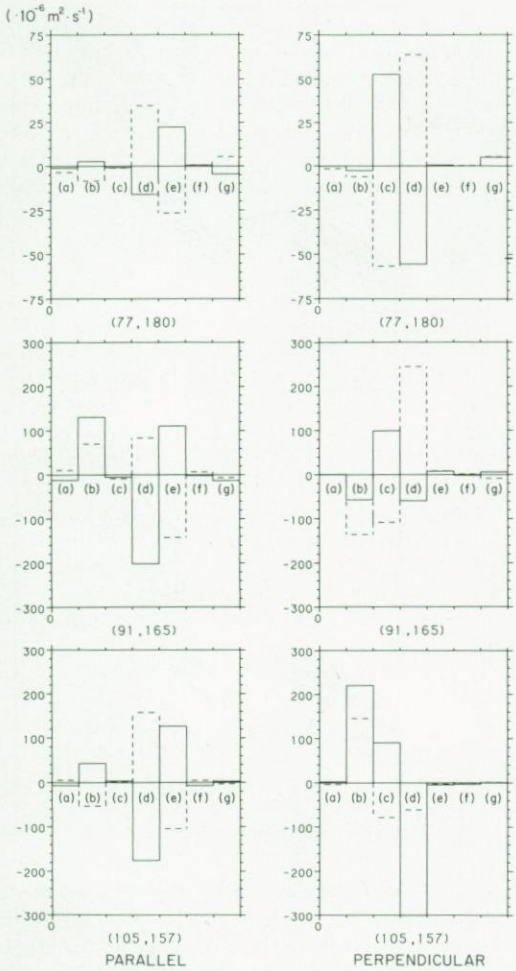

Fig. 8. Averaged magnitude of the terms (10^{-6}ms^{-2}) in equation (7) parallel (left-hand side) and perpendicular (right-hand side) to the dominant streamline in the characteristic grid points during the flood (solid) and ebb period (dashed).

dicular to the dominant streamline. LORENTZ (1926) showed that this term can be decomposed in a "Bernoulli acceleration" parallel and a "centrifugal acceleration" perpendicular to the local streamline:

$$(\vec{u} \cdot \nabla \vec{u})_s = \tfrac{1}{2} \frac{\partial}{\partial s} (u^2_s) \qquad \text{(s-direction)}$$

$$(\vec{u} \cdot \nabla \vec{u})_n = u_s \frac{\partial}{\partial s} (u_n) = \frac{u^2_s}{r} \qquad \text{(n-direction)} \qquad (8)$$

in which u_s and u_n are the velocity components in the local s-and n-direction and r is the radius of the local streamline. Such a decomposition shows that curves in the geometry of the coast and basin channels strongly influence the magnitude and direction of the centrifugal acceleration. This strong dependence on the local curvature of a streamline results in a large spatial variability in the magnitude as well as the direction in which this term acts. In the grid points in the tidal inlet and the channel the magnitude of the centrifugal acceleration about equals the coriolis acceleration while its sign does not differ between the ebb and flood periods. The consequence is that due to the rotation of the earth the magnitude of the counterbalancing water-level gradient perpendicular to the local streamline differs substantially between the ebb and flood periods.

The left-hand side of Fig. 8 shows that parallel to a streamline the bottom friction term (e) primarily balances the forcing water level gradient term (d). The advective term (b), interpreted as a Bernoulli acceleration in this direction and, together with term (d), forming the dynamic pressure gradient, plays a minor role compared to the role of the centrifugal acceleration in the n-direction. Spatial accelerations along a streamline, mainly caused by an increase/decrease in the channel cross section, determine the magnitude and relative influence of the Bernoulli term. This term has most influence at the tidal inlet grid point where the gradient in the magnitude of the flow cross section is relative large.

Term (a) in eq. 5 can be neglected at the ebb and flood phases when the tidal current reaches its maximum value. In a first approximation the governing momentum equation parallel and perpendicular to the local streamline then yields:

$$u_s \frac{\partial u_s}{\partial s} + g \frac{\partial \zeta}{\partial s} + \frac{g\, u_s |\vec{u}|}{C^2 (H + \zeta)} = 0 \qquad \text{(s-direction)}$$

(b) (d) (e) (9)

$$\frac{u^2_s}{r} + f\, u_s + g \frac{\partial \zeta}{\partial n} = 0 \qquad \text{(n-direction)}$$

(b) (c) (d) (10)

At both tidal phases the spatial distribution of these terms in the area shown in Fig. 7 is given

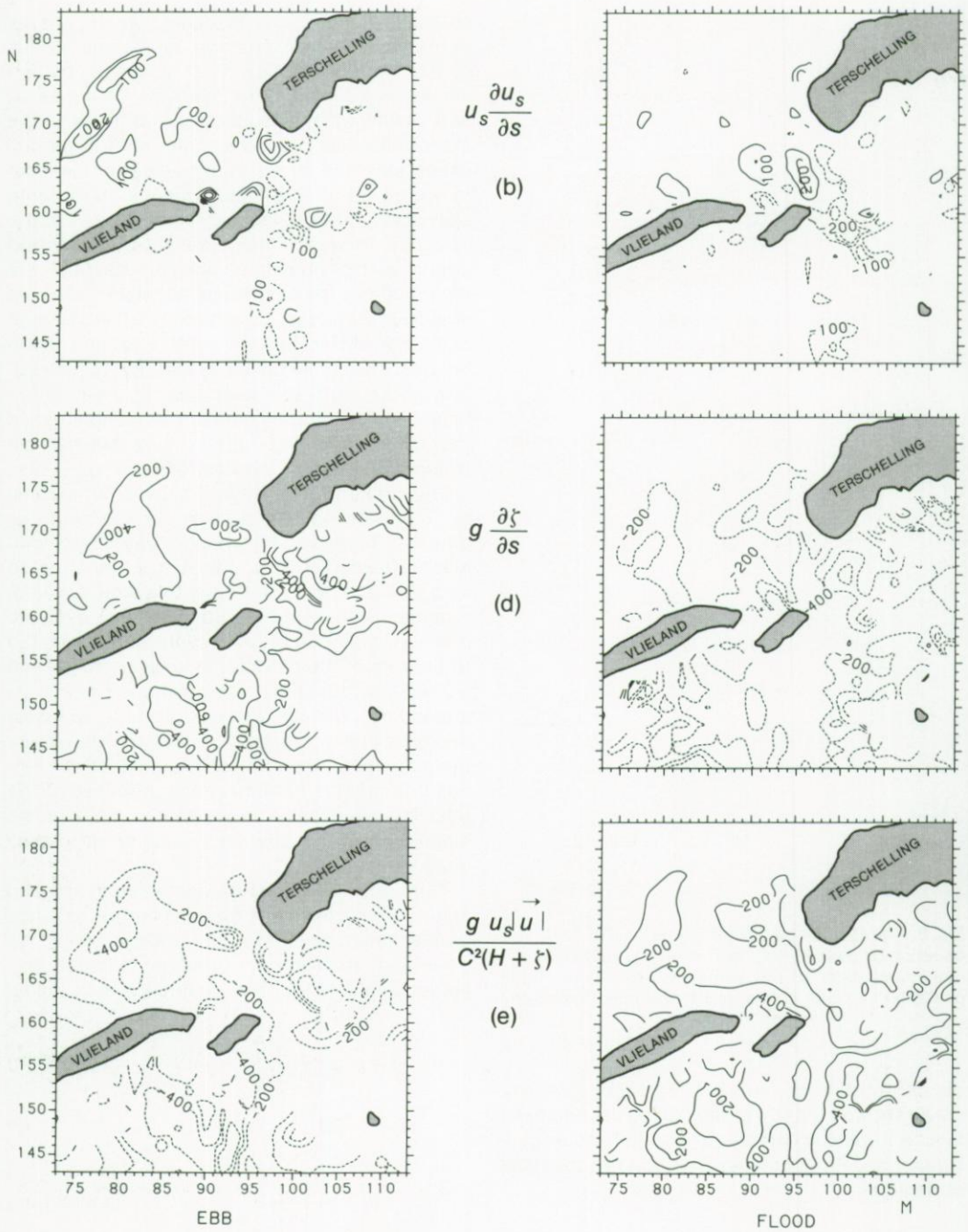

Fig. 9. (a) Isolines of the magnitude of terms b, d and e (10^{-6}ms^{-2}) in equation (9), parallel to the local momentary streamline. On the left-hand side at the time of maximum ebb, in which the positive s-axis has the same orientation as during the flood, and on the right-hand side at the time of maximum flood. Solid lines represent isolines with positive values; dashed lines represent the same range of negative values (see text).

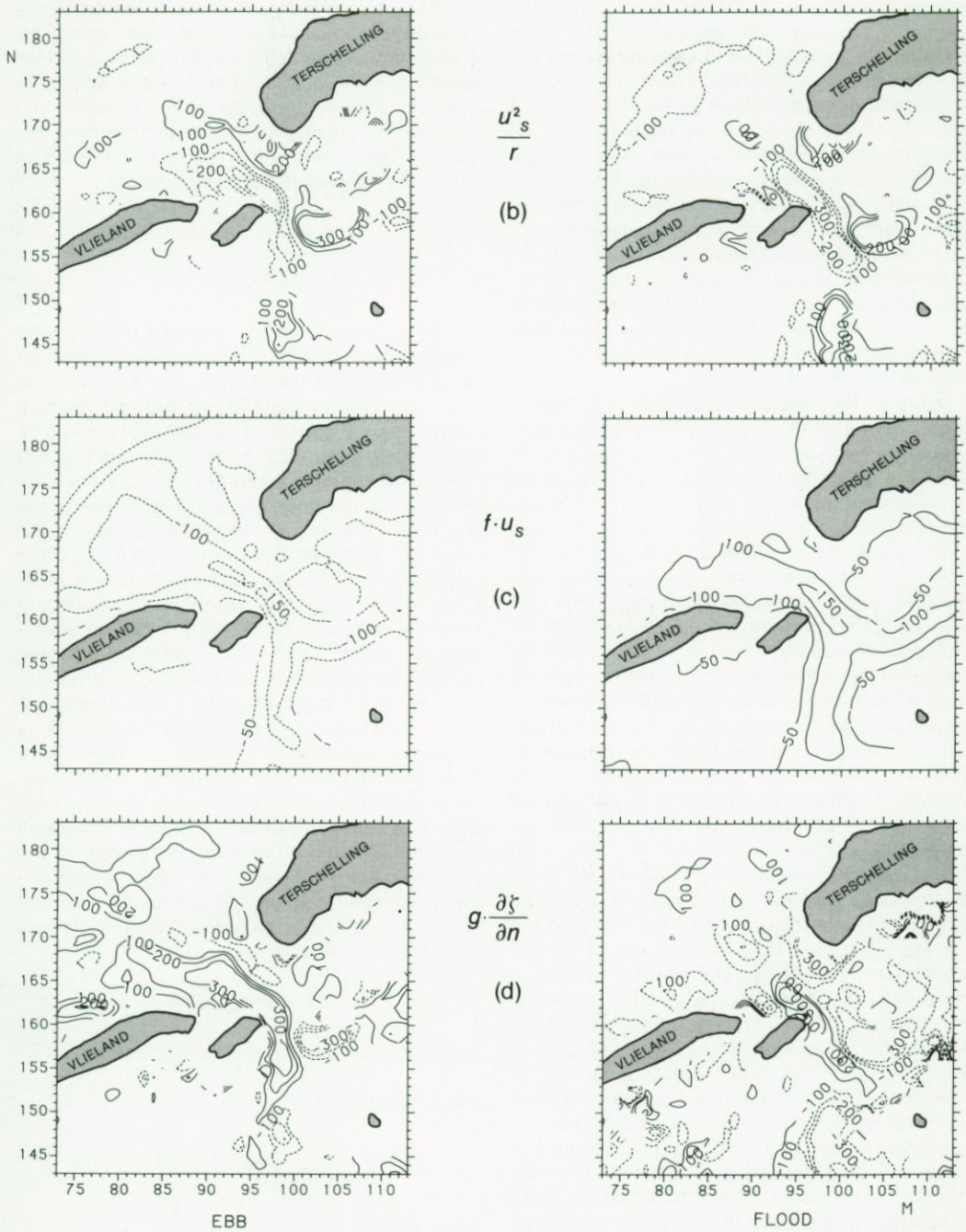

(b) Isolines of the magnitude of terms b, c and d ($10^{-6}ms^{-2}$) in equation (10), perpendicular to the local instantaneous streamline. On the left-hand side at the time of maximum ebb, in which the positive n-axis has the same orientation as during flood, and on the right-hand side at the time of maximum flood. Solid lines represent isolines with positive values; dashed lines represent the same range of negative values (see text).

in Figs 9a and b. Fig. 9a shows the isolines of the terms in equation (9) parallel to the local streamline, while Fig. 9b shows the isolines of the terms in equation (10) perpendicular to the local streamline. In both Figs the ebb phase is shown on the left-hand side. At the ebb phase the instantaneous positive s- and n-axes were chosen opposite to their computed direction to circumvent the problem of comparing terms that have been decomposed along oppositely orientated streamlines. Consequently, the difference between the local positive s- and n-axes at the ebb and flood phase is negligible. For each term solid lines represent the isolines with positive values; dashed lines represent the same range of isolines with negative values.

In Fig. 9a the intervals between the isolines for terms (d) and (e) ($2{\cdot}10^{-4}$ ms^{-2}) are greater than those for the isolines for term (b) (10^{-4}ms^{-2}). This Fig. shows that the terms (d) and (e) are the most important ones. The magnitude of these terms increases in the shallower parts. The less important Bernoulli acceleration (b) has most influence in the deeper channels, especially near the tidal inlet. Except for local deviations, the sign of the Bernoulli acceleration does not change between the ebb and flood periods. Therefore the influence of this term is relatively large in the tidally-averaged equations. The interval between the isolines of the most important terms in the n-direction, the advective term (b) and the water-level gradient term (d), is 10^{-4}ms^{-2} while the isolines for the coriolis term (c) have an interval of $0.5{\cdot}10^{-4}$ ms^{-2} between successive values (Fig. 9b). This Fig. shows that the geometry of the islands and channels causes the centrifugal acceleration (b) to be of great importance near the tidal inlet and the channel junctions. The changing curvature in a streamline is reflected in the large spatial variability in the direction in which this term acts. Furthermore, the orientation of the centrifugal acceleration does not differ between the ebb and flood periods. The water-level gradient in n-direction, term (d), balances the summation of terms (b) and (c), the centrifugal and coriolis acceleration. Depending on the local curvature of a streamline and the phase of the tide, the centrifugal and coriolis acceleration act in the same or opposite direction. In the tidal inlet the consequence is that during the ebb (flood) tide the cross inlet water-level gradient is composed of a relatively steep (small) gradient at the southern side and a relatively small (steep) gradient at the northern side. Also near channel junctions the centrifugal acceleration exceeds the coriolis acceleration so that the direction of the water-level gradient is the same during the ebb and flood periods. Only in the parts of the channel that have more or less straight streamlines does the coriolis term cause an alternating direction of the cross channel water-level gradient.

3. THE TIDAL MEAN FIELD

3.1. INTRODUCTION

In shallow seas and tidal lagoons (such as the Wadden Sea) the tidal flow generates a Eulerian residual flow pattern which can generally be regarded as a combination of isolated residual eddies and a constant flow through the sea or basin (ROBINSON, 1983). In many studies the only way to model the constant flow through the area is to impose residual boundary conditions at the open boundaries of the region under study, because a tidally-driven through-flow often depends on conditions outside the region of interest, which thus determine the open boundary conditions (PRANDLE, 1978). An important advantage of the Wadden Sea model in studying residual flows is that the open boundaries are located in the open sea, where the influence of the in and outflow through the tidal inlets is negligible. Because no residual elevations have been imposed on these open boundaries, constant flows through the inlets and between tidal basins are internally driven by the tide. Therefore special attention will be paid to this part of the residual flow field (and the residual surface elevation), even though the associated residual velocities are often one order of magnitude less than the residual eddy velocities.

3.2. DEFINITIONS

Tidal mean quantities are defined as follows:

mean water level

$$\langle \zeta \rangle = \frac{1}{T} \int_{-\frac{1}{2}T}^{\frac{1}{2}T} \zeta(t)\, dt \qquad (11)$$

mean velocity

$$\langle \vec{u} \rangle = \frac{1}{T} \int_{-\frac{1}{2}T}^{\frac{1}{2}T} \vec{u}(t)\, dt \qquad (12)$$

mean transport

$$<\vec{U}> = \frac{1}{T} \int_{-\frac{1}{2}T}^{\frac{1}{2}T} \vec{u}(t)\cdot(H + \zeta(t))\, dt \quad (13)$$

mean transport velocity

$$<\vec{u}_T> = \frac{<\vec{U}>}{\frac{1}{T} \int_{-\frac{1}{2}T}^{\frac{1}{2}T} (H + \zeta(t))\, dt} \quad (14)$$

mean stream function $\Psi(m, n)$
in which:

$$<U(m, n)> = \frac{\partial \Psi}{\partial y} \text{ and } <V(m, n)> = -\frac{\partial \Psi}{\partial x} \quad (15)$$

Averaging has been performed over a period of 12.5 h (T), the basic period in the boundary conditions. It should be stated here that all these residual quantities have been calculated in a Eulerian way, so that they cannot be used directly for Lagrangean interpretations such as residual transport of dissolved material. For instance, the mean transport velocity (14) is often interpreted as the Lagrangean residual velocity, while this is only the case for slowly varying one-dimensional velocity fields (ZIMMERMAN, 1979; VAN DE KREEKE & CHIU, 1981). In areas like the Wadden Sea, with a large spatial variability in the Eulerian velocity field, Lagrangean residual properties can only be determined by using the time-dependent velocity field to follow displacements of watermasses. This will be the subject of a subsequent paper.

3.3. RESULTS

3.3.1. MEAN WATER ELEVATION

Model results concerning mean water-levels on tidal flats are not physically meaningful because of the special treatment of these points during the simulation of their drying. The consequence is that residual water elevations are only presented for the channels in the model area.

In Figs 10a to c residual levels along the axis of the main channel of each tidal basin are drawn as a function of the distance along the channel axis. In Fig. 10c it was possible to combine in one picture the residual levels in the main chan-

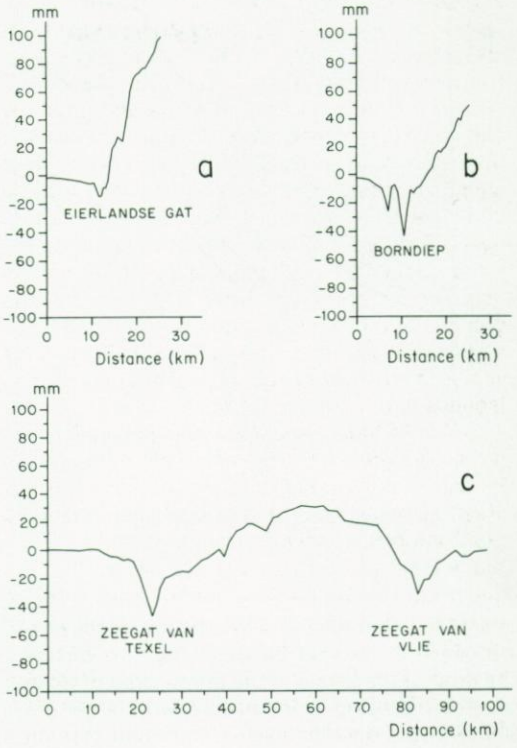

Fig. 10. Residual water elevations along the axes of the main basin channels in the tidal basins (mm) as a function of the distance from the seaward end of the inflow region. The locations of these axes are indicated in (d). (a) Eierlandse Gat; (b) Borndiep; (c) Marsdiep and Vlie basins.

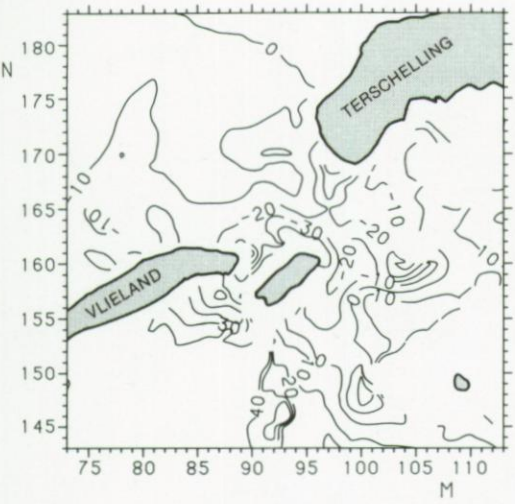

Fig. 11. Isolines of residual elevations in the area near the Zeegat van Vlie (intervals 10 mm).

nels of the Marsdiep and Vlie basin, because of the open connection between the two basins. The drop of the levels in the inflow area of all inlets and the rising in the basins, with larger gradients in the smaller basins, are characteristic features. Fig. 11 shows this phenomenon in more detail in a map of isolines of the residual level in the area near the Zeegat van Vlie (intervals of 10 mm). Two-dimensional characteristics of the distribution of mean water-levels are discussed in more detail in section 3.4.

The computed residuals at Den Helder (– 3.9 cm) and Harlingen (+ 1.8 cm) agree with observations. In the "Getijatlas voor Nederland, 1986" residual levels of – 3.9 cm and + 1.8 cm, respectively, are mentioned for these stations. These levels have been determined by analysing 12 years' records of water-levels.

3.3.2. MEAN VELOCITIES

For spatial clarity only a ninth (every 3rd grid point in both directions) of the computed mean transport velocities, $<\vec{u}_T>$ (eq. 14), in the model area is mapped in Fig. 12. The mean transport velocities near the open boundaries are not physically meaningful because they are induced by the special treatment of the advective terms at the open boundaries (STELLING, 1984). Compared to results of modelling studies in other estuaries (OEY *et al.*, 1985; TEE, 1976), Fig. 12 gives qualitatively the same picture. Residual eddies dominate the residual current field in the channels and near the tidal inlets. The existence of many of these tide-induced residual eddies in this area is supported by field observations in the western Wadden Sea (ZIMMERMAN, 1976b; DE BOER *et al.*, 1986). A qualitative comparison of observations and computations shows that the orientation of all observed eddies agrees with the orientation of the computed eddies. These eddies are induced by pronounced variations in channel geometry and bottom topography, which, in the governing equations, increase the importance of the advective terms. OEY *et al.* (1985) have shown the strong effect on the residual flow pattern of omitting the advective terms.

Tidal mean velocities, $<\vec{u}>$ (eq. 12), in every grid point in the area near the Zeegat van het Vlie are shown in Fig. 13a. On average the magnitude of the residual velocity in these eddies varies from about 0.10 ms^{-1} in the tidal basin to 0.15 ms^{-1} in the tidal inlet. Fig. 13b gives the mean transport velocities, $<\vec{u}_T>$ (eq. 14), in the same region as in Fig. 13a. Solid lines indicate the isolines of the ratio between the absolute magnitude of the mean transport velocity (eq. 14) and the absolute magnitude of the mean velocity (eq. 12). At first sight, Figs 13a and b look the same due to the domination of the residual eddies in the mean field, which do not give much difference in the orientation and only slightly in the magnitude of the two velocities. The isolines of the ratio of the magnitude of the two velocities in Fig. 13b indicate, however, that especially outside these eddies, where the mean velocities are small, the difference between the two velocities can be considerable. For one-dimensional motion this difference is in a first approximation equal to the tidal mean of $u\zeta/H$ and is often referred to as the Stokes velocity (ZIMMERMAN, 1979; VAN DE KREEKE & CHIU, 1981). The magnitude of this Stokes velocity depends strongly on local water-depth and the phase difference between tidal water-levels and velocities.

3.3.3. MEAN TRANSPORTS

Isolines for the residual stream function in the interior of the Wadden Sea between the mainland and the islands, calculated from the mean transports (eq. 15), are shown in Fig. 14 with an interval between the isolines of 200 m^3s^{-1}. This map clearly shows that the residual transport

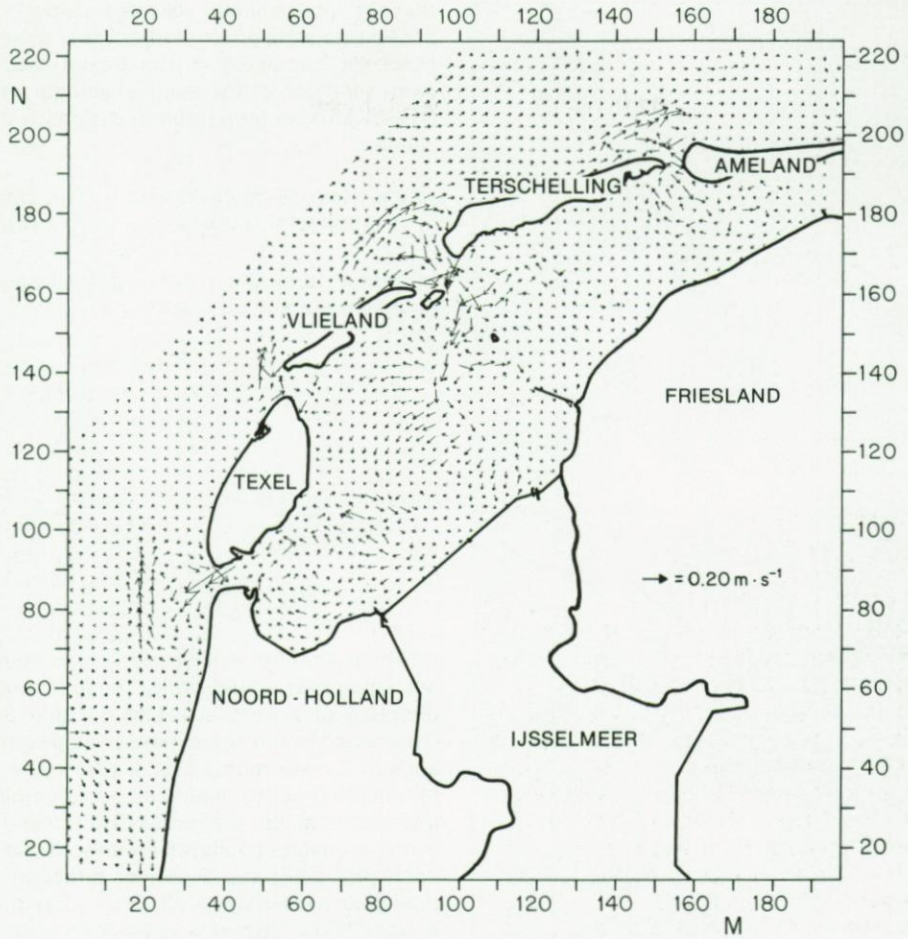

Fig. 12. Mean transport velocities, $<\vec{u}_T>$, in every 3rd grid points.

field in the Wadden Sea can be subdivided into isolated residual eddies and a constant flow through the basins. Fig. 15, which gives a picture of the area near the Zeegat van het Vlie with isoline intervals of 250 $m^3 s^{-1}$, demonstrates this in more detail. The mean transports associated with the eddies are much larger (one order of magnitude) than the constant flow. The differences between the Ψ-values of the mainland and the islands, see Fig. 14, indicate the tidally-driven ebb and/or flood surplusses through the inlets. It shows that the largest through-going volume transport takes place between the two interconnected main basins, and is directed southwards from the Vlie basin towards the Marsdiep basin. The associated transport velocities are very small ($0(10^{-2}$ $ms^{-1})$) in comparison with the tidal velocity amplitude ($0(1$ $ms^{-1})$) as well as with the transport velocities associated with the residual eddies ($0(10^{-1} ms^{-1})$). Therefore it is difficult to support the computed ebb and flood surplusses with measurements. Furthermore, in reality a mean sea-level gradient in the North Sea, along the open boundaries of the model, may possibly influence the magnitude of the residual volume transport. This possible external forcing, combined with the dependence of the residual volume transport on the wind conditions, complicates the determination of the tidally-driven part of the residual volume transport. Analyses of a series of current measurements in the

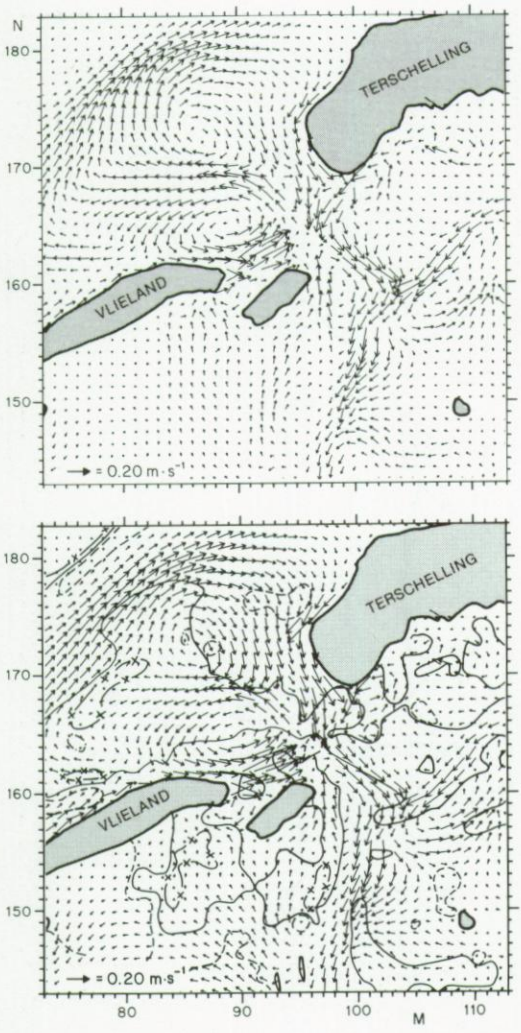

Fig. 13. (a) Mean velocities, $<\vec{u}>$, in the area near the Zeegat van Vlie.

(b) Mean transport velocities near the Zeegat van Vlie together with some isolines (0.5, 1. and 2.) of the ratio between the absolute values of the mean transport velocity and the mean velocity

$$\frac{|<\vec{u}_T>|}{|<\vec{u}>|}$$

The values of the isolines are 0.5 (---), 1.0 (———) and 2.0 (– x – x).

Zeegat van het Vlie (DE BOER *et al.*, 1986) indicate a strong variability in magnitude and direction of this part of the residual flow field and suggest that the total residual volume transport is composed of a wind-driven and a tidally-driven part. However, compared to the model results the same direction of the residual volume transport (southwards) is found during periods with weak winds.

3.3.4. INFLUENCE OF TERMS IN THE TIDALLY-AVERAGED MOMENTUM EQUATIONS

In vector form the governing tidally-averaged momentum equation reads:

$$<\vec{u}\cdot\nabla\vec{u}> + <f(\vec{j}\times\vec{u})> + <g\nabla\zeta> +$$

(b) (c) (d)

$$+ <\frac{g\vec{u}|\vec{u}|}{C^2(H+\zeta)}> - <\nu\nabla^2\vec{u}> = 0 \qquad (16)$$

(e) (f) (g)

in which as, in eqs. 11 to 15 < > stands for averaging over a tidal cycle. The magnitude and direction of a term in a specific grid point is determined in the same manner as described in section 2.4. Averaging over a tidal cycle is performed after decomposing all terms parallel and perpendicular to the dominant streamline at every available timelevel (interval 30 min.). In each grid point the dominant direction of the tidal flow is given by eq. (6); Fig. 7 gives the local s- and n-axes parallel and perpendicular to the dominant streamline in characteristic grid points in the neighbourhood of the Zeegat van het Vlie. In this section the same grid points are used to discuss the relative influence of all terms in the governing equation (16) while, as in section 2.4, the spatial distribution of the most important terms is shown for this area.

The error in the momentum balance, caused by the small differences between the computed magnitude of the terms and the magnitude in the numerical simulation (discussed in section 2.4), follows again from a summation of the terms in eq. (16). This error ("term (g)") is neglected in the discussion because it is only of importance in grid points where the magnitude of the dominating terms is relatively small.

The magnitude of all terms in equation (16) in the characteristic grid points is given in Fig. 16. A global comparison of Fig. 16 and Fig. 8, which

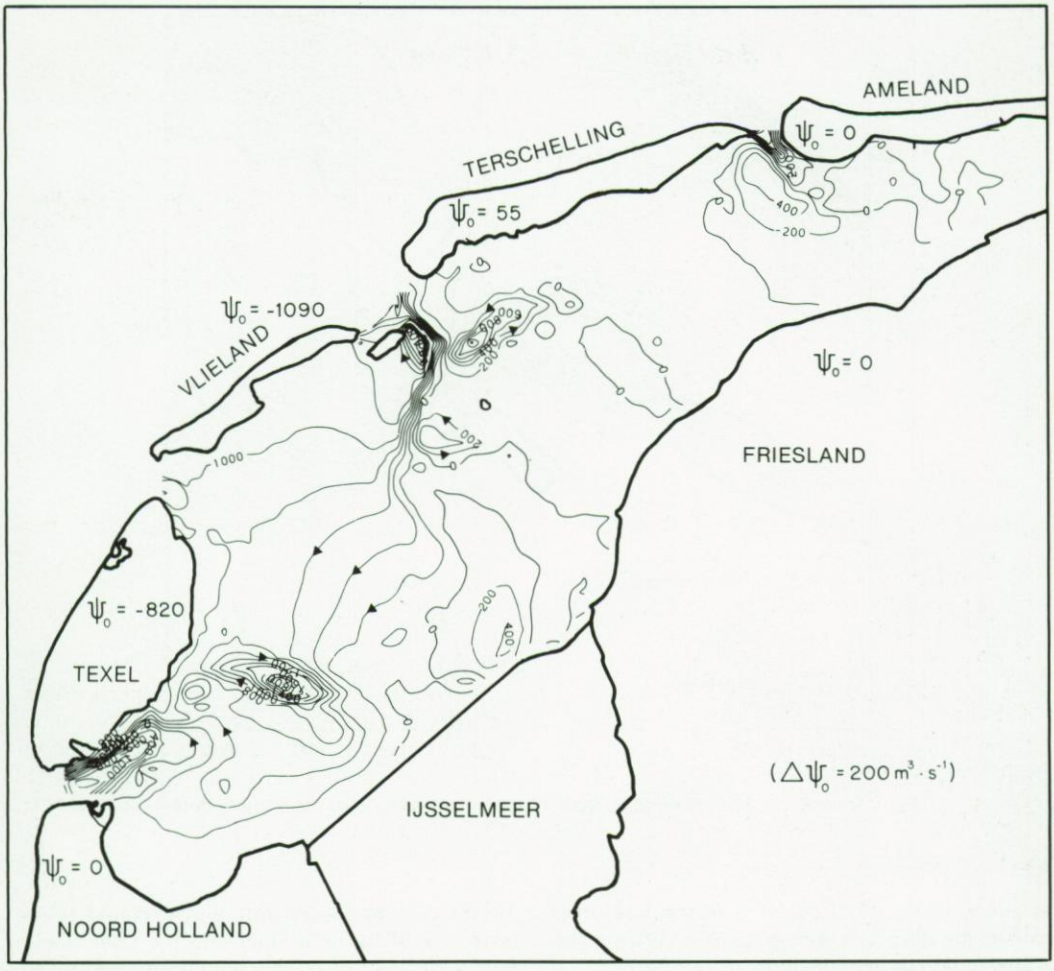

Fig. 14. Isolines of the residual stream function in the interior of the western Wadden Sea (interval 200 m^3s^{-1})

gives the average magnitude of the same terms during the ebb and flood periods, shows that there is a larger spatial variability in the magnitude of the dominant terms in the tidally-averaged equations.

Comparing the relative influence of the terms in one grid point in the tidal and tidally-averaged equations shows that parallel to the dominant streamline (s-axis) an important shift takes place: the role of the bottom friction term (e) decreases, while the role of the Bernoulli term (b) increases. Perpendicular to the streamline the relative influence of the coriolis term is diminished. Thus, in a first approximation, the non-linear term (b) is the forcing term in the mean state. This term is counterbalanced by the combination of a residual water-level gradient and a residual bottom-friction term. In the grid points shown term (d), due to a residual water-level gradient, is much larger than term (e), due to residual bottom friction.

Isolines for the magnitude of these terms are given in Fig. 17. In the left-side term, (b), (d) and (e), parallel to the dominant flow direction, are shown, in which solid lines represent the isolines ($0.5 \cdot 10^{-4} ms^{-2}$, $1 \cdot 10^{-4} ms^{-2}$ and $1.5 \cdot 10^{-4} ms^{-2}$) of terms that are positive in the local s-direction, determined according equation (6); and dashed lines represent the same range of isolines acting in the opposite direction. In general, the con-

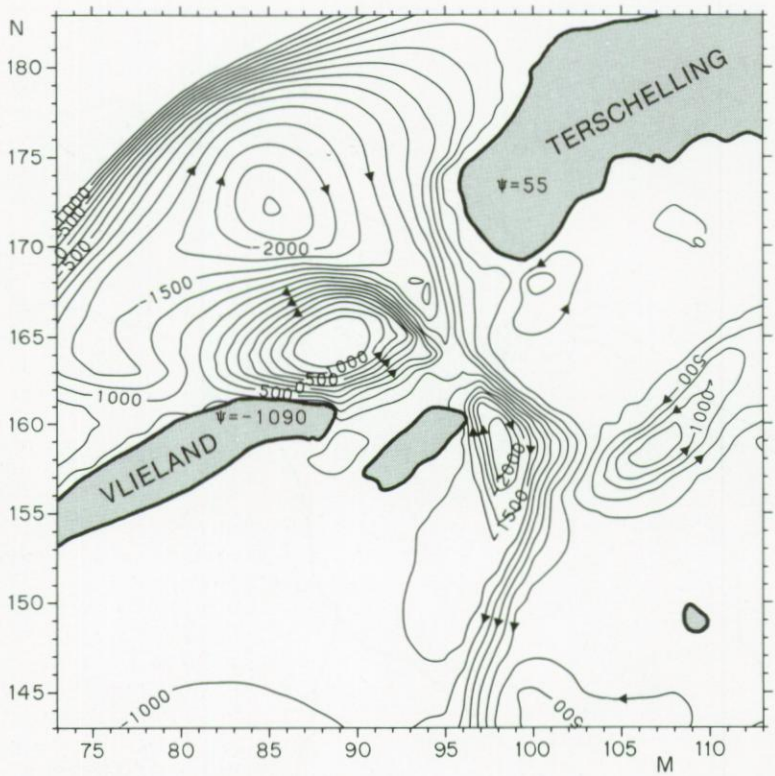

Fig. 15. Isolines of the residual stream function near the Zeegat van Vlie (interval 250 m^3s^{-1})

vergence of the tidal currents in the tidal inlet causes the Bernoulli term (b) to be positive in the inflow region of the tidal inlet and negative in the channels of the basin. The consequence is that the counterbalancing residual water-level gradient induces a drop in the residual water-level in the tidal inlet (see Fig. 10). The spatial distribution of the magnitude of the residual bottom-friction term combined with the spatial distribution of term (d) shows that in the shallower part of the area the main balance is formed by term (d) and (e), while in the deeper channels terms (b) and (d) dominate.

On the right-hand side of Fig. 17 the same terms perpendicular to the dominant streamline (in the local n-direction) are given. The range of the isolines for term (b) and (d) is greater; isolines are given for $1{\cdot}10^{-4}ms^{-2}$, $2{\cdot}10^{-4}ms^{-2}$ and $3{\cdot}10^{-4}ms^{-2}$, while term (e) has the same range of isolines as the range in the s-direction. It shows that in the n-direction the centrifugal term (b) has a large spatial variability, related to the geometry of the tidal inlet and the channels in the basin (see Fig. 7). This term is counterbalanced by a residual water-level gradient, resulting in a rising/lowering of the residual water-level in the outer/inner bend of a channel. The combined effect of the Bernoulli term and the centrifugal term on the residual levels in the tidal inlet is clearly reflected in Fig. 11. The Bernoulli term lowers the residual level in a relatively large region on both sides of the inlet and induces a drop in the centre of the inlet. A cross inlet gradient results from the more locally acting centrifugal term, which causes a further lowering of the residual levels near the islands.

Summarizing, it can be stated that in the mean state, compared to the time varying state, local geometry and bottom topography have more influence on the magnitude and spatial variability of the most important terms in the momentum equations. This is reflected in the increased in-

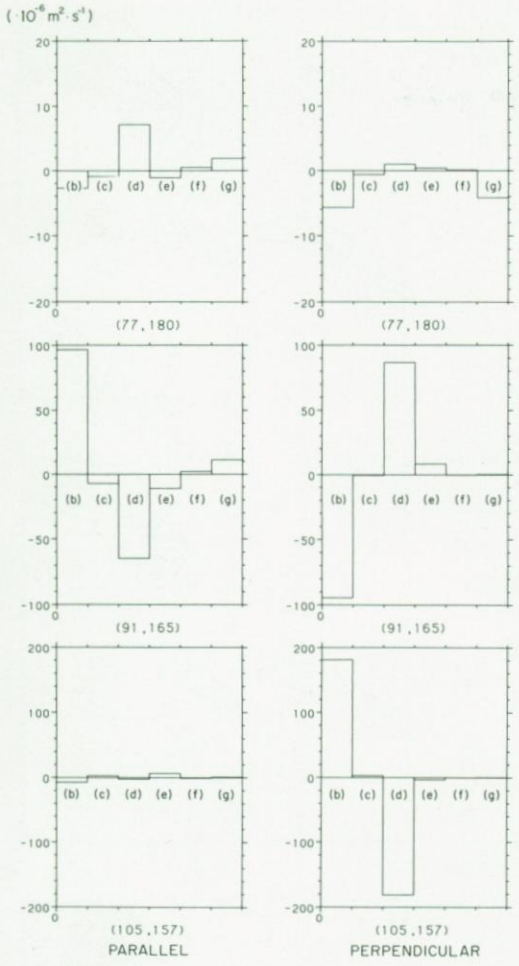

Fig. 16. Tidally averaged magnitude of the terms (in $10^{-6} ms^{-2}$) in equation (16) parallel (left-hand side) and perpendicular (right-hand side) to the dominant streamline in the characteristic grid points.

fluence of the advective terms that drive the tidally averaged field.

4. CONCLUSIONS

Simulations with a two-dimensional numerical model of the western Dutch Wadden Sea, covering four tidal basins and a part of the adjacent North Sea, show a good agreement between observed and computed water elevations, transport rates through the tidal inlets, and, on a larger scale, between measured and computed global two-dimensional current fields and between the observed and simulated area of emersed tidal flats. Averaging the computed water-levels and current velocities over a tidal cycle shows that the tidally-driven residual current velocity field is composed of isolated residual eddies and a through-flow between different basins. In the tidal inlets the residual velocities associated with the eddies, of which the orientation is supported by measurements, are one order of magnitude larger than the residual velocities associated with the through-flow. A drop in the residual elevations in the inflow areas of tidal inlets and a rise in the interior of tidal basins are general features in all tidal basins.

Rewriting the governing momentum equations in directions parallel and perpendicular to the local dominant streamline and determining the magnitude of each term in some characteristic grid points show that morphological differences strongly influence the magnitude and relative importance of most of these terms. The advective term, decomposed in a Bernoulli acceleration parallel and a centrifugal acceleration perpendicular to the local streamline, is strongly increased by pronounced variations in channel and bottom geometry, which subsequently influence the magnitude of the other terms.

Averaging these terms over a tidal period shows that in the mean state the main balance is formed by the advective and water-level gradient term. Perpendicular to the dominant flow direction, the magnitude and spatial variability of both residual terms are larger than parallel to the dominant flow direction. This difference is caused by the high number of curves in the channels that cause a high spatial variability of the centrifugal term, while variations in the magnitude of the cross section of the tidal flow, responsible for a Bernoulli acceleration, are more gentle.

5. REFERENCES

BOER, M. DE, M.F. LIESHOUT, G. KOOL & R. PEEREBOOM, 1984. Waterbeweging westelijke Waddenzee: verloop natte en droge oppervlakten en kombergingen. Nota WWKZ-84.H009, Rijkswaterstaat, The Netherlands: 1-12.

BOER, M. DE, N. DE GRAAFF & C. VISSER, 1986. Het vermogen van het Zeegat van het Vlie. Nota ANW-86.H205, Rijkswaterstaat, The Netherlands: 1-20.

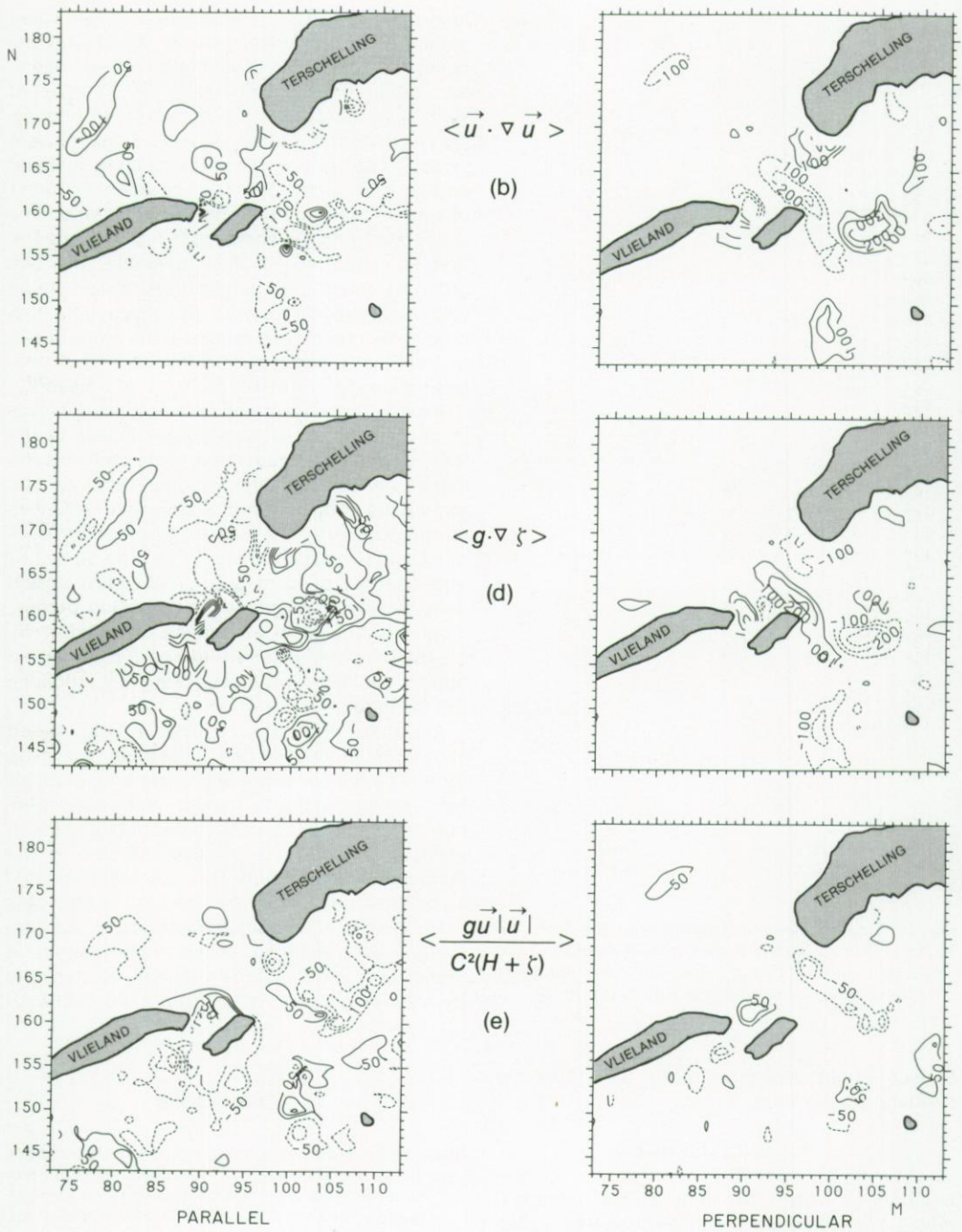

Fig. 17. Isolines of the tidally averaged magnitude of terms b, d and e (in $10^{-6} ms^{-2}$) in equation (16), parallel (left-hand side) and perpendicular (right-hand side) to the local dominant streamline. Solid lines represent isolines with positive values; dashed lines represent the same range of negative values (see text).

HEAPS, N.S., 1978. Linearized vertically integrated equations for residual circulation in coastal seas.—Dt. hydrogr. Z. **31:** 147-169.

KLATTER, H.E., J.M.C. DIJKZEUL, G. HARTSUIKER & L. BIJLSMA, 1986. Flow computations nearby a Storm Surge Barrier under Construction with Two-Dimensional Numerical Models.—Proc. Twentieth Coast. Eng. Conf., Taiwan.

KREEKE, J. VAN DE & S.S. CHIU, 1981. Tide-induced residual flow in shallow bays.—J. Hydraulic Res. **19:** 231-249.

LEENDERTSE, J.J., 1967. Aspects of a computational model for long period water wave propagation. Memorandum RM-5294-PR, Rand Corporation, Santa Monica, 1967: 1-116.

——, 1984. Verification of a Model of the Eastern Scheldt. Memorandum R-3108-NETH, Rand Corporation, Santa Monica, 1984: 1-31.

LEENDERTSE, J.J., A. LANGERAK & M.A.M. DE RAS, 1981. Two dimensional models for the Delta Works. In: H.B. FISCHER. Transport models for inland and coastal waters. Acad. Press, New York: 408-450.

LORENTZ, H.A., 1926. Verslag Staatscommissie Zuiderzee 1918-1926. Den Haag, 1926.

MADDOCK, L. & R.D. PINGREE, 1978. Numerical simulation of the Portland Tidal Eddies.—Est. Coast. Mar. Sci. **6:** 353-363.

OEY, L.Y., G.L. MELLOR & R.I. HIRES, 1985. Tidal modelling of the Hudson Raritan Estuary.—Estuar. coast. Shelf Sci. **20:** 511-527.

POSTMA, H., 1954. Hydrography of the Dutch Wadden Sea.—Archs néerl. Zool. **10:** 405-511.

PINGREE, R.D. & L. MADDOCK, 1977. Tidal eddies and coastal discharge.—J. mar. biol. Ass. U.K. **57:** 869-875.

PRANDLE, D., 1978. Residual flows and elevations in the Southern North Sea.—Proc. R. Soc. Lond. (A) **359:** 189-228.

ROBINSON, I.S., 1983. Tidally induced residual flow. In: B. JOHNS. Physical Oceanography of Coastal and Shelf Seas: 321-357.

STUDIEDIENST HOORN & DELFZIJL, 1973. De Noordzeemeting 1971. Nota W.73.1, Rijkswaterstaat, The Netherlands: 1-7.

STELLING, G.S., 1984. On the construction of computational methods for shallow water flow problems. Comm. no. 35, Rijkswaterstaat, The Netherlands: 1-226.

TEE, K.T., 1976. Tide induced residual current, a 2-d non linear numerical tidal model.—J. Mar. Res. **34:** 603-628.

VETH, C. & J.T.F. ZIMMERMAN, 1981. Observations of quasi-two-dimensional turbulence in tidal currents.—J. Phys. Oceanography **11:** 1425-1430.

VOOGT, L., 1985. Een getijmodel van de Noordzee gebaseerd op de JONSDAP-1976 meting. Nota WWKZ-84G006, Rijkswaterstaat, The Netherlands: 1-38.

ZIMMERMAN, J.T.F., 1976a. Mixing and flushing of tidal embayments in the western Dutch Wadden Sea, I: Distribution of salinity and calculation of mixing time scales.—Neth. J. Sea Res. **10:** 149-191.

——, 1976b. Mixing and flushing of tidal embayments in the western Dutch Wadden Sea, II: Analyses of mixing processes.—Neth. J. Sea Res. **10:** 397-439.

——, 1979. On the Euler-Lagrange transformation and the Stokes drift in the presence of oscillatory and residual currents. Deep-Sea Res. **26A:** 505-520.

(received 22 December 1987; revised 9 February 1988)

CHAPTER 3

TIDAL AND RESIDUAL FLOWS IN THE WESTERN DUTCH WADDEN SEA II: AN ANALYTICAL MODEL TO STUDY THE CONSTANT FLOW BETWEEN CONNECTED TIDAL BASINS*

H. RIDDERINKHOF

Netherlands Institute for Sea Research, P.O.Box 59, 1790 AB Den Burg, Texel, The Netherlands

ABSTRACT

In a one-dimensional analytical model the origin of constant flows between connected tidal basins, as well as the origin of the associated residual levels, is examined. Linearized shallow water equations are used to describe the propagation and damping of a tidal wave in schematized (uniform width and depth) connected basins. Analytical expressions are derived for the tidal stress terms, including the contribution of the non-linear bottom-friction term, which serve as the forcing functions in the equations for the mean field. It is shown that in a first approximation the residual levels in the tidal inlets, which give boundary conditions for the tidally-averaged equations, are dependent on the tidal velocities in the inlet because of a "Bernoulli effect". The model shows that in general differences between the fluctuating water levels at the inlets influence the residual flow more than morphological differences between two connected basins. The tidally-driven mass transport in the western Dutch Wadden Sea, directed southwards from the Vlie basin towards the Marsdiep basin, can be explained from the larger water-level amplitude at the inlet of the Vlie basin.

1. INTRODUCTION

In a preceding paper on tidal and residual flows in the western Dutch Wadden Sea, in which results from a detailed two-dimensional numerical model were discussed, it has been shown that the tidally-driven mean flows in this area can be subdivided into a large-scale part, the constant flow between connected tidal basins, and a small-scale part, the isolated residual eddies (RIDDERINKHOF, 1988). The boundaries with the open sea of this numerical model are located outside the region of influence of the tidal inlets in the adjacent, relatively deep, North Sea (Fig. 1). In contrast to most modelling studies on residual flows (*e.g.* PRANDLE, 1978), in which boundary conditions often directly induce a constant flow through the region under interest, no residual levels are prescribed on the boundaries of this numerical model. So the computed large-scale residual flow between the different tidal basins is internally driven by the tide.

The magnitude of the mean transport, 900 m^3s^{-1}, between the two major Wadden Sea basins, the Vlie and Marsdiep basins, is only about one percent of the transport amplitude in the inlets. However, this tide-induced constant flow can play an important role when for instance the composition or flushing time scale of water masses in the Marsdiep basin is considered. For comparison, the average supply of fresh water from the IJsselmeer is about 450 m^3s^{-1}. To gain more insight into the origin of this large-scale residual flow as well as of the associated residual elevations, a one-dimensional analytical model has been developed. This model is used to examine how the tidal mean field is influenced by morphological asymmetries between the two basins as well as by the influence of differences between the fluctuating water levels at the two inlets. A comparable analytical study on mass transport induced by tidal asymmetries at the inlets of a tidal canal was performed by VAN DE KREEKE & DEAN (1975). Studies on the effect of inlet asymmetries on the tide induced flow are presented in VAN DE KREEKE (1976) and VAN DE KREEKE & COTTER (1974).

Acknowledgements.—I am grateful to L.R.M. Maas for his interest and discussions during the set up of the analytical model.

Publication no. 22 of the project "Ecological Research North Sea and Wadden Sea" (EON)

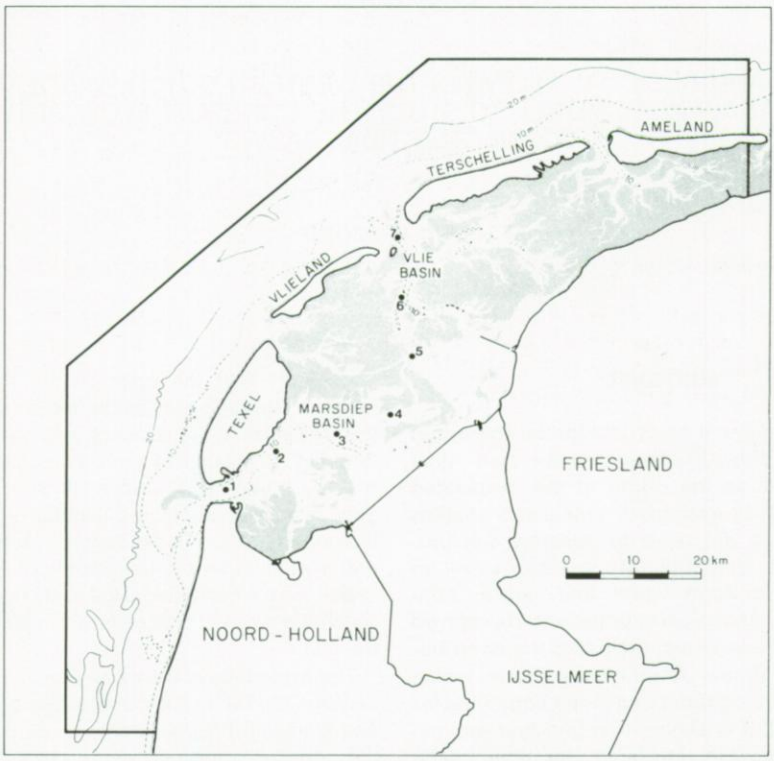

Fig. 1. Map of the western Dutch Wadden Sea showing some isobaths (10 m, 20 m), emersing tidal flats and the location of the boundaries of the numerical model (RIDDERINKHOF, 1988). Results in the gridpoints 1 to 7 are used in Fig. 4.

2. DESCRIPTION OF THE ANALYTICAL MODEL

In schematizing the western Wadden Sea only the two main basins, the Marsdiep and the Vlie basins, have been considered. Fig. 2 shows the schematization of the two-dimensional reality of these basins in a one-dimensional system. Either basin is schematized as a tidal channel with a constant width and depth. The chosen value of the morphological parameters of these channels is discussed in section 3.2. The transition between the tidal basins and the open sea, the in and outflow areas of the basins, is schematized as a funnel-shaped area with a length short compared with the basin length and the tidal wave length. From hereon the boundary between this inflow area and the tidal channels is referred to as the inlet of the channels. For this model the basic shallow water equations read:

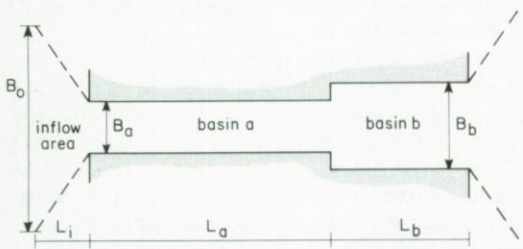

Fig. 2. Schematization of the tidal basins and adjacent inflow regions. Basin a represents the schematized Marsdiep basin and basin b represents the schematized Vlie basin.

$$\frac{\partial Q}{\partial t} + \frac{\partial}{\partial x}\left(\frac{Q^2}{BD}\right) + gBD\frac{\partial \zeta}{\partial x} + \frac{k\,Q|Q|}{BD^2} = 0 \qquad (1)$$

$$\frac{\partial Q}{\partial x} + B\frac{\partial \zeta}{\partial t} = 0 \qquad (2)$$

in which:
Q volume transport
D total water depth $H + \zeta$
H mean water depth
B width
ζ water elevation relative to the mean water depth
k bottom-friction coefficient.

Compared to the governing equations in the numerical model (RIDDERINKHOF, 1988), the Coriolis and horizontal turbulent viscosity terms are neglected. The equations are written in terms of the volume transport, Q, to have non-linear terms only in the momentum equation. These basic equations have to be linearized to find analytical expressions for the tidal water levels and volume transports. Using the method of LORENTZ (1926) to reduce the quadratic bottom-friction term, in which in a tidal period the energy dissipation of a single harmonic tidal constituent due to the linearized bottom friction term equals the energy dissipation due to the non-linear term, and assuming the amplitude of the fluctuating water levels to be much less than the mean water depth ($\zeta << H$), the following set of linear tidal equations can be deduced:

$$\frac{\partial Q}{\partial t} + gBH\frac{\partial \zeta}{\partial x} + \frac{\lambda_1 Q}{H} = 0 \tag{3}$$

$$\frac{\partial Q}{\partial x} + B\frac{\partial \zeta}{\partial t} = 0 \tag{4}$$

in which:

$$\lambda_1 = \frac{8k}{3\pi}\frac{|Q_m|}{BH} \tag{5}$$

where $(|Q_m|/BH)$ represents a characteristic value of the tidal velocity amplitude in the area.

To find the equations which describe the tidal mean flow and elevations the basic equations (1) and (2) have to be averaged over a tidal cycle. In this averaging procedure it is assumed that:

$$Q = Q_0 + Q_1; \quad \overline{Q_1} = 0; \quad Q_0 << Q_1 \tag{6}$$

$$\zeta = \zeta_0 + \zeta_1; \quad \overline{\zeta_1} = 0; \quad \zeta_0 << \zeta_1 << H \tag{7}$$

in which:

Q_0, ζ_0 = residual components
Q_1, ζ_1 = tidal components

$$\overline{a} = \frac{1}{T}\int_{-T/2}^{T/2} a\,dt, \qquad T = \text{tidal period}$$

In this averaging procedure especially the linearization of the bottom-friction term needs care. Therefore the reduction of this term is discussed in detail. HEAPS (1978), using the method of HUNTER (1975) with complex variables, showed that use of (6) in the numerator of the quadratic friction term and averaging over a tidal period yields (see appendix A):

$$\frac{\overline{kQ|Q|}}{B(H+\zeta)^2} = \frac{\overline{2k|Q_1|Q_0}}{B(H+\zeta)^2} + \frac{\overline{kQ_1|Q_1|}}{B(H+\zeta)^2} \tag{8}$$

The assumption of a tidal motion associated with a single harmonic constituent together with condition (7) gives a further simplification of the first term in the right-hand side of eq. (8):

$$\frac{\overline{2k|Q_1|Q_0}}{B(H+\zeta)^2} = \frac{\lambda_0 Q_0}{H} \tag{9}$$

in which, analogous to eq. (6), the residual friction coefficient is dependent on the average tidal velocity amplitude:

$$\lambda_0 = \frac{4k}{\pi}\frac{|Q_m|}{BH} = 1.5\lambda_1 \tag{10}$$

Equation (10) shows that the term that is linearly dependent on the mean transport requires an increased friction coefficient. The numerator in the second term at the right-hand side of eq. (8) can be linearized by expanding $Q_1|Q_1|$ in a Fourier series. Retaining only the first term of this series gives:

$$\frac{\overline{kQ_1|Q_1|}}{B(H+\zeta)^2} = \frac{8}{3\pi}\frac{\overline{kQ_1}}{B(H+\zeta)^2} = \frac{\overline{\lambda_1 Q_1}}{(H+\zeta)} \tag{11}$$

in which the same expression as in eq. (5) is used for the friction coefficient. Expanding the denominator in the last term of eq. (11) and substituting condition (7) subsequently gives:

$$\frac{\overline{\lambda_1 Q_1}}{(H+\zeta)} = \frac{\overline{\lambda_1 Q_1}}{H} - \frac{\overline{\lambda_1 Q_1 \zeta_1}}{H^2} \tag{12}$$

Combining eqs. (8), (9), (11) and (12) together with conditions (6) and (7) finally gives the tidally-averaged linearized bottom-friction term:

$$\frac{\overline{kQ|Q|}}{B(H+\zeta)^2} = \frac{\lambda_0 Q_0}{H} - \frac{\overline{\lambda_1 Q_1 \zeta_1}}{H^2} \tag{13}$$

Equation (13) gives the required form of a term linear in the mean transport and a term quadratic in tidal quantities. It is of interest to note that an analysis exactly parallelling the above may be carried out working in terms of depth mean currents (u_1 and u_0) rather than volume transports. As a result it can be shown that in eq. (13) Q_1 is replaced by u_1 and Q_0 by u_0. In both cases the second term on the right-hand side of eq. (13) can be interpreted as a frictional effect acting on the Stokes drift, here expressed as a Stokes transport ($\overline{Q\zeta/H}$) and as a Stokes velocity ($\overline{u\zeta/H}$) when depth mean currents are used. Another method to linearize the bottom friction term is followed by VAN DE KREEKE & DEAN (1975). Their result is equal to eq. (13) if λ_1 in the first term on the right hand side of (13) is replaced by λ_0. This stems from a different treatment of the factor $kQ|Q|$ in the basic expression. The coefficient λ_1 is found when the procedure is started with the linearization of $kQ|Q|$ to $\lambda_1 Q$ before substituting (6). An increased coefficient, λ_0, is found when the procedure is started with substituting (6), as is shown above. Here the latter procedure is followed because it is analogous to the treatment of the other terms in eqs. (1) and (2).

Returning to the basic equations (1) and (2), making use of the inequalities in (6) and (7), substituting eq. (13) and assuming small non-linear advection we finally find the following set of equations for the mean field:

$$\overline{\frac{\partial}{\partial x}\left(\frac{Q_1^2}{BH}\right)} + \overline{gB\frac{\partial}{\partial x}\left(\frac{\zeta_1^2}{2}\right)} + gBH\frac{\partial \zeta_0}{\partial x} + \frac{\lambda_0 Q_0}{H} - \frac{\overline{\lambda_1 Q_1 \zeta_1}}{H^2} = 0 \qquad (14)$$

$$\frac{\partial Q_0}{\partial x} = 0 \qquad (15)$$

The first two terms of the momentum equation (eq. 14) are the well-known tidal stress terms (NIHOUL & RONDAY, 1976), which, together with the last term that originates from the non-linear bottom friction, are the forcing terms for the mean state. This total tidal stress must be balanced by a residual water-level gradient and/or a bottom-friction term caused by a residual transport (in the case of open basins). To derive expressions for the mean field, the linearized tidal equations (3 and 4) are used to determine the tidal water levels and volume transports which subsequently give analytical expressions for the forcing terms in eq. (14). After integrating eq. (14) the residual water levels in the interior of both basins can be expressed as a function of the tidal stresses, the residual flow (Q_0) and two integration constants. These integration constants can only be determined when the residual level is known at two positions, presumably the boundaries with the open sea. As these boundary conditions are not known *a priori*, but are in fact part of the problem of finding the tidal mean state, the schematized model area was extended over a relatively short distance to the open sea. To circumvent the "open boundary" problem for the tidal mean state it is now assumed that at the seaward boundaries of the inflow area the residual levels are not influenced by the tidal flows in the basins. A difference between the residual levels at both seaward boundaries can therefore only be caused by the tidal flows in the open sea and has to be interpreted as an external forcing. As such an externally forced pressure gradient is absent in the numerical model simulations (RIDDERINKHOF, 1988), it is also neglected here. So, when the tidal stresses in the inflow area are known, the residual level at both inlets can be computed and subsequently used to determine the internally-driven mean field in both basins.

3. RESULTS FOR THE TIDAL AND TIDAL MEAN FIELD

3.1. INFLOW AREA

The length of the funnel-shaped inflow area can be assumed to be much smaller than the tidal basin length. Having now two horizontal length scales over which variables may vary, it seems appropriate to

TABLE 1

Scales and non-dimensional parameters in the analytical model.

$B = B_A b'$	B_A = width basin a
$H = H_A h'$	H_A = depth basin a
$x = L_i x_i' + L_A x'$	L_A = length basin a, L_i = length inflow area
$\zeta = Z_A \zeta'$	Z_A = tidal amplitude at $x = -L$ ($x' = -1$)
$t = t'/\sigma$	σ = frequency tidal wave
$q = <Q> q'$	$<Q> = B_A L_A Z_A \sigma$
$\lambda_1 = \sigma H_A \lambda'_1$	λ_1 = linearized bottom friction coefficient
$k = k' / L_A$	$k = \frac{\sigma}{\sqrt{gH_\alpha}}$ = wave number
$\zeta_0 = <\zeta_0> \zeta_0'$	$<\zeta_0> = Z_A^2 H_A^{-1}$
$q_0 = <q> q_0'$	$<q_0> = <Q>\ Z_A\ H_A^{-1}$
$\lambda_0 = \sigma H_A \lambda_0'$	$\lambda_0' = 1.5 \lambda_1'$

apply a multiple scale expansion (MAAS *et al.*, 1987) which in a first approximation simplifies the governing equations for the inflow area. Table 1 lists the introduced scaling and non-dimensional parameters. A consequence of using two horizontal coordinates is that the $\partial/\partial x$ operator reads:

$$\frac{\partial}{\partial x} = L_A^{-1} \left(\frac{\partial}{\partial x'} + \epsilon^{-1} \frac{\partial}{\partial x_i'} \right), \quad \epsilon = \frac{L_i}{L_A} << 1 \qquad (16)$$

Using (16) and scaling (3) and (4) according to Table 1, the dimensionless form of the linear tidal equations (3 and 4) (dropping primes), is

$$\epsilon \frac{\partial q}{\partial t} + \epsilon \frac{bh}{k^2} \frac{\partial \zeta}{\partial x} + \frac{bh}{k^2} \frac{\partial \zeta}{\partial x_i} + \epsilon \frac{\lambda_1 q}{h} = 0 \qquad (17)$$

$$\epsilon \frac{\partial q}{\partial x} + \frac{\partial q}{\partial x_i} + \epsilon b \frac{\partial \zeta}{\partial t} = 0 \qquad (18)$$

Expanding the dependent variables in (17) and (18) in a perturbation series (using ϵ as a small parameter) yields at zeroth order for the tidal field in the inflow area

$$\frac{\partial \zeta}{\partial x_i} = 0, \quad \frac{\partial q}{\partial x_i} = 0 \qquad (19)$$

Thus on the relatively small length scale of the inflow area the tidal wave propagates in a first approximation as if it has a rigid upper surface. The same procedure is followed to determine the governing equations for the mean field in the inflow area. Using the governing equations for the mean field (14) and (15), extending the set of non-dimensional parameters with non-dimensional variables for the tidal mean variables, ζ_0' and q_0' (Table 1), expanding these variables in a perturbation series, and substituting (16) yield at zeroth order for the mean field in the inflow area (dropping primes)

$$\overline{\frac{\partial}{\partial x_i} \frac{q_1^2}{bh}} + \overline{\frac{b}{k^2} \frac{\partial \zeta_1^2}{\partial x_i}} + \frac{bh}{k^2} \frac{\partial \zeta_0}{\partial x_i} = 0 \qquad (20)$$

$$\frac{\partial q_0}{\partial x_i} = 0 \qquad (21)$$

Using (19), eq. (20) can be further simplified

$$\overline{\frac{q_1^2}{h} \frac{\partial}{\partial x_i} b^{-1}} + \frac{bh}{k^2} \frac{\partial \zeta_0}{\partial x_i} = 0 \qquad (22)$$

To find the required expression for the residual levels at the transition between the tidal channel and the inflow area eq. (22) has to be integrated. Taking the residual level at the seaward end of the inflow area as a boundary condition ($\zeta_0 = 0$) and assuming a fast decrease of the inflow width in this region ($B_A << B_0$, Fig. 2) yields the following expression for the residual level at the open boundary of the tidal channel

$$\zeta_0 = \overline{-q_1^2} \frac{k^2}{2bh} \quad \left(= -\frac{\overline{Q_1^2}}{2gB^2D^2} = -\frac{\overline{u_1^2}}{2g} \right) \qquad (23)$$

Substitution of the relevant scales gives the term in brackets in (23). The resulting drop in the residual water level in a tidal inlet, about 2.5 cm for $u = 1$ ms^{-1}, can be interpreted as a Bernoulli effect caused by a fast reduction of the inflow section over a relatively short distance. This phenomenon can be recognized in the numerical model (RIDDERINKHOF, 1988) as well as in the analysis of observations (RIJKSWATERSTAAT, 1987).

3.2. SCHEMATIZED BASINS

3.2.1. TIDAL FLOWS AND WATER LEVELS

Of course the "rigid lid" approximation of the tidal flow in the inflow area cannot be used to describe the

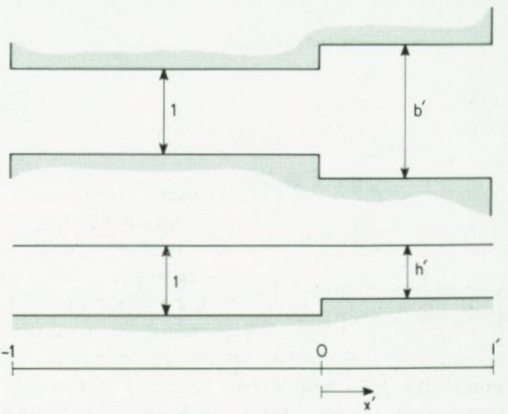

Fig. 3. Schematization of the tidal basins in non-dimensional parameters. The upper part shows a plan view of both basins and the lower part shows the longitudinal cross-section.

tidal field in the interior of the two basins. To determine the tidal stresses an analytical model has been developed. This model has to represent the tidal transports and water elevations as reasonably as can be done by approximating the two-dimensional reality of our numerical model to a one-dimensional system. Choosing the boundary between the two channels as the origin for the non-dimensional x-coordinate (Fig. 3) and omitting hereafter the accents for the non-dimensional variables results in the following sets of tidal equations:

$-1<x<0$ basin a $b=h=1$

$$\frac{\partial q}{\partial t}+\frac{1}{k^2}\frac{\partial \zeta}{\partial x}+\lambda_1 q=0 \qquad (24)$$

$$\frac{\partial q}{\partial x}+\frac{\partial \zeta}{\partial t}=0 \qquad (25)$$

$0<x<l$ basin b

$$\frac{\partial q}{\partial t}+\frac{bh}{k^2}\frac{\partial \zeta}{\partial x}+\frac{\lambda_1 q}{h}=0 \qquad (26)$$

$$\frac{\partial q}{\partial x}+b\frac{\partial \zeta}{\partial t}=0 \qquad (27)$$

Combining the momentum and continuity equation and substituting (*c.c* means the complex conjugate function):

$-1<x<0$

$$\zeta_A(x,t)=\zeta_A(x)\,e^{it}+c.c$$

$$\zeta_A(x)=A\,e^{i\tau_A x}+B\,e^{-i\tau_A x}$$

$$q_A(x,t)=q_A(x)\,e^{it}+c.c \qquad (28)$$

$0<x<l$

$$\zeta_B(x,t)=\zeta_B(x)\,e^{it}+c.c$$

$$\zeta_B(x)=C\,e^{i\tau_B x}+D\,e^{-i\tau_B x}$$

$$q_B(x,t)=q_B(x)\,e^{it}+c.c \qquad (29)$$

in which A, B, C and D are complex integration constants, we find for τ and q:

$-1<x<0$

$$\tau_A^2=k^2(1-\lambda i) \qquad (30)$$

$$q_A(x)=\frac{i}{\tau_A^2}\frac{\partial \zeta_A}{\partial x} \qquad (31)$$

$0<x<l$

$$\tau_B^2=\frac{k^2}{h}\left(1-\frac{\lambda}{h}i\right) \qquad (32)$$

$$q_B(x)=\frac{bi}{\tau_B^2}\frac{\partial \zeta_B}{\partial x} \qquad (33)$$

To find the complete solution of the propagation and damping of the tidal wave in both basins we need to impose 4 boundary conditions:

1) $x=-1$ $\quad \zeta_A(-1,t)=e^{it}+c.c$

2) $x=l$ $\quad \zeta_B(l,t)=Z\,e^{i(t+\varphi)}+c.c$

3) $x=0$ $\quad \zeta_A(0,t)=\zeta_B(0,t)$

4) $x=0$ $\quad q_A(0,t)=q_B(0,t)$ $\qquad (34)$

The first two boundary conditions represent the fluctuating water levels at both inlets, which can differ both in amplitude and phase. Boundary conditions 3) and 4) at $x=0$ guarantee the continuity of sea level and volume transport at the boundary between the two basins. Condition 4) implies that partial reflection of the tidal wave at the transition between the two basins is neglected. Substituting these boundary conditions yields:

$$C=\frac{(\cos\tau_A+i\gamma\sin\tau_A)Ze^{i\varphi}-e^{-i\tau_B l}}{2i(\cos\tau_A\sin(\tau_B l)+\gamma\sin\tau_A\cos(\tau_B l))}$$

$$D=\frac{(-\cos\tau_A+i\gamma\sin\tau_A)ze^{i\varphi}+e^{i\tau_B l}}{2i(\cos\tau_A\sin(\tau_B l)+\gamma\sin\tau_A\cos(\tau_B l))}$$

$$A=\frac{1}{2}((C+D)+\gamma(C-D))$$

$$B=\frac{1}{2}((C+D)+\gamma(C-D))$$

$$\gamma=b\tau_A/\tau_B \qquad (35)$$

In both basins $Q(x,t)$ and $\zeta(x,t)$ can now be computed depending on the choice of tidal and morphological parameters. The combination of parameters which appears to give reasonable results with regard to the observed amplitudes and phases

TABLE 2

Parameters and coefficients as used in the schematization of the Wadden Sea basins. H_A, B_A and λ_1 were tuned according to the conditions given in the text.

$L_A = 40 \cdot 10^3$m	$L_B = 20 \cdot 10^3$m	($l' = 0.5$)
$H_A = 4.5$ m	$H_B = 3.00$ m	($h' = 0.66$)
$B_A = 15 \cdot 10^3$m	$B_B = 24 \cdot 10^3$m	($b' = 1.6$)
$Z_A = 0.70$ m	$Z_B = 0.86$ m	($z' = 1.23$)
$\sigma = 1.4 \cdot 10^{-4}$s^{-1}	$\varphi = -0.63$	
$g = 9.81$ ms^{-2}	$\lambda_1 = 2.0 \cdot 10^{-3} \cdot$ms^{-1}	

of transport in both basins is listed in Table 2. Global characteristics of the topography in the Marsdiep and Vlie basins show a significant depth (h=0.66) and length difference (l=0.5) between the two. The width ratio chosen (b=1.6), in combination with the length ratio, is in agreement with the known small difference between the total surface area of the Vlie and Marsdiep basins (ZIMMERMAN, 1976).

In tuning the analytical model, the morphological ratios (h, b, l) and the length of basin a, (L_A), as well as the tidal boundary conditions (Z, φ), well known from observed data, were kept constant. The friction coefficient, λ_1, and depth scale of basin a, H_A, which determine the damping and the phase speed of the tidal wave, have to meet the following requirements: 1) the boundary at $x = 0$ should coincide with a transport amplitude minimum 2) the amplitude of the tidal velocities in both inlets should be approximately equal. The first requirement ensures that the incoming tidal waves meet at the transition between the two basins, in the prototype resulting in the formation of tidal watersheds. The second requirement concerning the velocity ratios in the inlets, which equal the

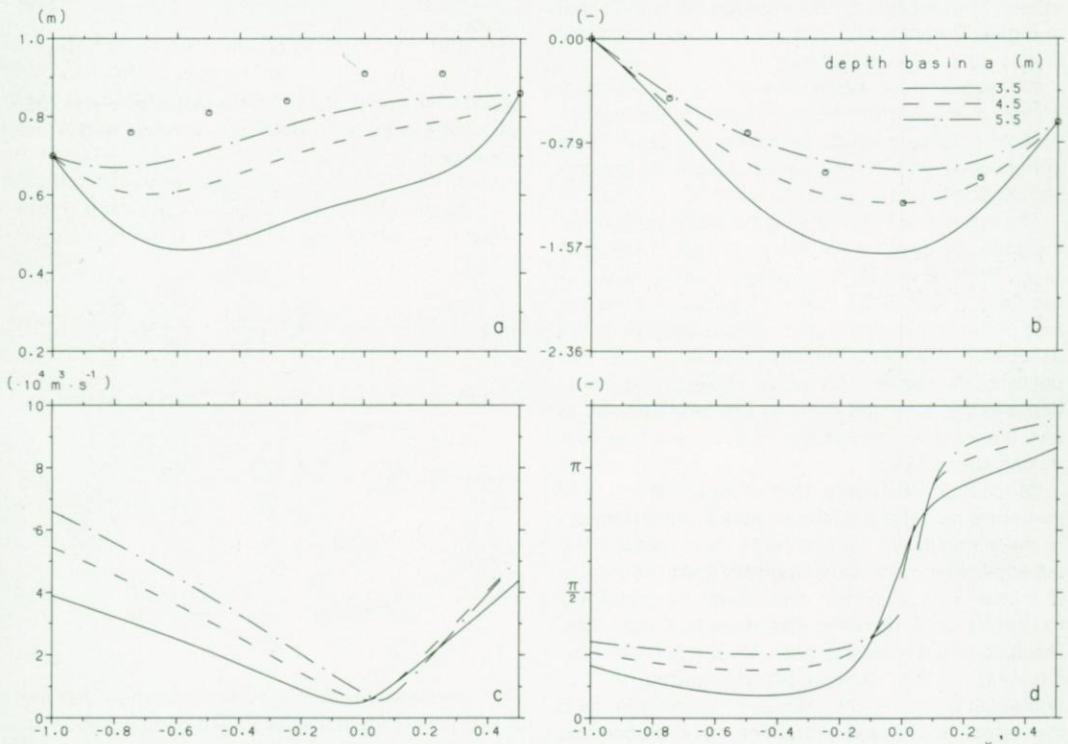

Fig. 4. Water level and transport amplitudes and phases dependent on the depth of basin a, as a function of the non-dimensional x'- coordinate. For comparison results in corresponding grid points in the numerical model are shown (O O O). The grid points 1 to 7 in the numerical model correspond with resp. $x' = -1.0$, -0.75, -0.50, -0.25, 0., 0.25, 0.50 in the analytical model.

(a) Phase of tidal sea level relative to the tidal sea level at $x' = -1$ (-)

(b) Amplitude of tidal sea level (m)

(c) Phase of volume transport relative to the tidal sea level at $x' = -1$ (-)

(d) Amplitude of volume transports (10^4m$^3 \cdot$s^{-1})

transport ratios because of the width and depth ratio chosen, follows from observations and numerical model results (RIDDERINKHOF, 1988). This is an important requirement as it influences the tidal stress ratio at both open boundaries as well as the residual level boundary conditions for the mean state. Furthermore, this condition justifies the assumption that the bottom friction coefficient, being dependent on a representative value of the tidal velocity amplitude according to eq. (5), does not differ in the two basins. Finally, the width of basin a was varied to tune the transport amplitudes in the two inlets. The final outcome of this tuning was a value of $2 \cdot 10^{-3}$ ms^{-1} for the friction coefficient, λ_1, 4.5 m for the depth scale, H_A, and $15 \cdot 10^3$m for the width scale, B_A. Fig. 4a to d gives the resulting amplitudes and phases of the fluctuating water levels and volume transports in both channels. For some positions Fig. 4a and b shows results in corresponding gridpoints of the numerical model. The position of these gridpoints is indicated in Fig. 1. The influence of changing the depth scale is also given in these figures.

Although it is not shown here, changing the bottom friction coefficient or length of basin a yields comparable results, in which an increasing depth scale corresponds with a decreasing length or bottom-friction coefficient.

The major effect of changing the depth scale is the increase/decrease in the phase speed of the tidal wave. With respect to the transport amplitudes this results in a shift of the transport minimum while the ratio of the amplitudes in both inlets is adapted to the associated changing "effective" basin length. The depth scale chosen, 4.5 m, is close to the mean depth in the Marsdiep basin, 4.3 m, and appears to give the most reasonable results in terms of the conditions stated before.

Of course, compared to the observations and numerical model results the analytical model can only meet qualitative requirements. For instance the schematization of a morphologically irregular area into a basin with a uniform depth leads to a relatively too strong damping of the tidal wave near the inlets, resulting in a decreasing water-level amplitude (see Fig. 4a), which cannot be recognized in the numerical model results. However, keeping in mind the rather crude schematization, this model can serve as a basis for a qualitative study of the mean field.

3.2.2. THE TIDAL MEAN FIELD

The set of non-dimensional equations for the mean field, based on eqs. (14 and 15), reads:

$-1 < x < 0 \qquad b = h = 1$

$$\overline{2q_1 \frac{\partial q_1}{\partial x}} + \frac{1}{k^2} \overline{\zeta_1 \frac{\partial \zeta_1}{\partial x}} + \frac{1}{k^2} \overline{\frac{\partial \zeta_0}{\partial x}} + \lambda_0 q_0 - \lambda_1 \overline{q_1 \zeta_1} = 0 \tag{36}$$

$$\frac{\partial q_0}{\partial x} = 0 \tag{37}$$

$0 < x < l$

$$\frac{2}{bh} \overline{q_1 \frac{\partial q_1}{\partial x}} + \frac{b}{k^2} \overline{\zeta_1 \frac{\partial \zeta_1}{\partial x}} + \frac{bh}{k^2} \overline{\frac{\partial \zeta_0}{\partial x}} + \frac{\lambda_0 q_0}{h} - \frac{\lambda_1 \overline{q_1 \zeta_1}}{h^2} = 0 \tag{38}$$

$$\frac{\partial q_0}{\partial x} = 0 \tag{39}$$

Making use of eqs. (24 to 27) the last term in eqs. (36) and (38) can be expressed as a function of the first two terms:

$$-1 < x < 0 \qquad \lambda_1 \overline{q_1 \zeta_1} = -\frac{1}{k^2} \overline{\zeta_1 \frac{\partial \zeta_1}{\partial x}} + \overline{q_1 \frac{\partial q_1}{\partial x}} \tag{40}$$

$$0 < x < l \qquad \frac{\lambda_1 \overline{q_1 \zeta_1}}{h^2} = -\frac{b}{k^2} \overline{\zeta_1 \frac{\partial \zeta_1}{\partial x}} + \frac{1}{bh} \overline{q_1 \frac{\partial q_1}{\partial x}} \tag{41}$$

so that the tidal stress term, T_{xx}, can be written as:

$$-1 < x < 0 \qquad T_{xx_A} = \frac{2}{k^2} \overline{\zeta_1 \frac{\partial \zeta_1}{\partial x}} + \overline{q_1 \frac{\partial q_1}{\partial x}} \tag{42}$$

$$0 < x < l \qquad T_{xx_B} = \frac{2b}{k^2} \overline{\zeta_1 \frac{\partial \zeta_1}{\partial x}} + \frac{1}{bh} \overline{q_1 \frac{\partial q_1}{\partial x}} \tag{43}$$

These expressions for the tidal stress show that the Stokes part of the tidally-averaged bottom friction increases the contribution of the water-level component to the total tidal stress while the contribution of the transport component decreases.

Substituting (42) and (43) in (36) and (38) and integrating yields:

$$-1 < x < 0 \qquad \int T_{xx_A} dx + \frac{1}{k^2} \zeta_0 + \lambda_0 q_0 x = A \tag{44}$$

$$q_0 = \text{constant}$$

$$0<x<l \quad \int T_{xx_B} dx + \frac{bh}{k^2}\zeta_0 + \frac{\lambda_0 q_0}{h}x = B \qquad (45)$$

$$q_0 = \text{constant}$$

in which A and B are integration constants. In these equations (44 and 45) the tidal stress terms can be computed by substitution of eqs. (28) and (29). For instance averaging and integrating of the water-level components gives a simple expression:

$$\overline{\zeta_1 \frac{\partial \zeta_1}{\partial x}} = \zeta_1^* \frac{\partial \zeta_1}{\partial x} + \zeta_1 \frac{\partial \zeta_1^*}{\partial x} \qquad (46)$$

$$\int \overline{\zeta_1 \frac{\partial \zeta_1}{\partial x}} dx = \zeta_1 \zeta_1^* = |\zeta_1|^2 \qquad (47)$$

where an asterisk indicates the complex conjugate and (| |) the tidal amplitude. The transport component of the tidal stress can be simplified in an analogous way.

Again we need 4 boundary conditions to be able to find the solution of this set of equations:

1) $x=-1 \quad \zeta_0 = Z_{0_{-1}}$

2) $x=l \quad \zeta_0 = Z_{0_l}$

3) $x=0 \quad \zeta_{0_A} = \zeta_{0_B}$

4) $x=0 \quad q_{0_A} = q_{0_B}$ (48)

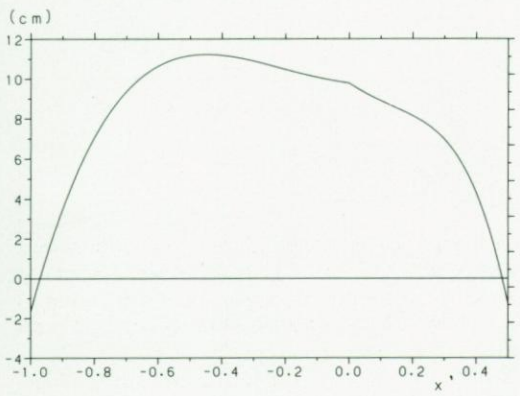

Fig. 5. Residual water elevation in the schematized tidal channels (cm) as a function of the non-dimensional x-coordinate.

Conditions 1) and 2) impose a residual level at both inlets. These are a function of the tidal transports and can be computed by employing eqs. (31) and (33). The conditions 3) and 4) guarantee the continuity of residual level and residual flow at the connection of the two basins.

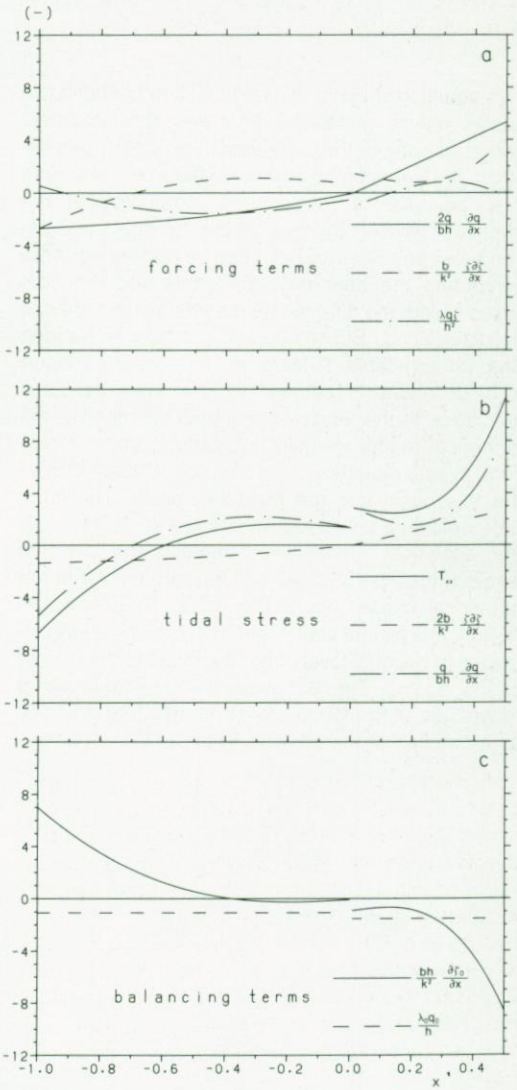

Fig. 6. Non-dimensional magnitude of the terms in eqs. (36), (38), (42) and (43) as a function of the non-dimensional x-coordinate. (a) Forcing terms in eqs. (36) and (38). (b) Composing terms of tidal stress and total tidal stress, eqs. (42) and (43). (c) Terms associated with tidal mean variables in eqs. (36) and (38).

Substitution of these conditions yields:

$$q_0 = \frac{1}{\lambda_0 + \frac{\lambda_0^{\prime}}{bh^2}} \left\{ \frac{Z_{0_{-1}} - Z_{0_l}}{k^2} + \int_0^{-1} T_{xx_A}\, dx + \frac{1}{bh\,l} \int^0 T_{xx_B} dx \right\} \quad (49)$$

This equation shows that a residual flow between two basins will be generated whenever the integrated tidal stress and/or the difference in residual levels between the two open boundaries differ from zero. Note that, because of the chosen morphological differences between the two basins, no direct integration between $x=-1$ and $x=l$ can be performed. After computing the boundary conditions and the tidal stresses with the tidal model the tidal mean field can be determined. Substitution of the typical Wadden Sea values (Table 1) leads to a residual transport (Q_0) of about 3 percent of the tidal transport amplitude in the inlets while computations with the numerical model resulted in a ratio of about 1 percent. In both models the residual flow is directed from the Vlie basin into the Marsdiep basin. The computed residual levels are shown in Fig. 5. Although the analytical model overestimates the residual levels in the interior of the basins compared with the numerical model results (fig. 9c in RIDDERINKHOF (1988)), this picture clearly shows the same strong increase in residual levels from the inlets to the middle of the basins. Fig. 6a gives the non-dimensional magnitude of the forcing terms in eqs. (36) and (38) as a function of the position in the basins. It shows that the relative importance of these three terms is approximately equal. Fig. 6b gives the magnitude of the total tidal stress as well as the magnitude of both components, defined according to eqs. (42) and (43). This figure clearly shows that the water-level component is more important than the transport component. The magnitude of the counterbalancing terms, associated with tidal mean variables, is shown in Fig. 6c.

4. DISCUSSION

Before examining the influence of morphological asymmetries and asymmetrical boundary conditions on the residual flow, attention is paid to the sensitivity of the analytical model to the schematization of the morphology of the Wadden Sea and to the bottom friction parameter. As in the tidal model, the boundary conditions for the tidal fluctuations, $z=1.23$ and $\varphi=-0.63$, and the depth and width ratio between the two basins, $h=0.66$ and $b=1.6$, were kept constant, as these are well known from the observed data. The influence of changing the depth scale or bottom coefficient on the residual flow as a function of the length ratio between the two basins is shown in Fig. 7a and b, where the percentage of the residual transport compared with the tidal transport amplitude at the inlet of basin a is given on the vertical axis. Both figures show that the magnitude of the residual flow is only slightly sensitive to a variation in these parameters, while the direction of this flow does not change. As in the tidal model, a comparison of Fig. 7a with 7b shows that varying the depth scale of basin a or the bottom-friction coefficient gives qualitatively the same results: a greater depth corresponding with a smaller friction coefficient.

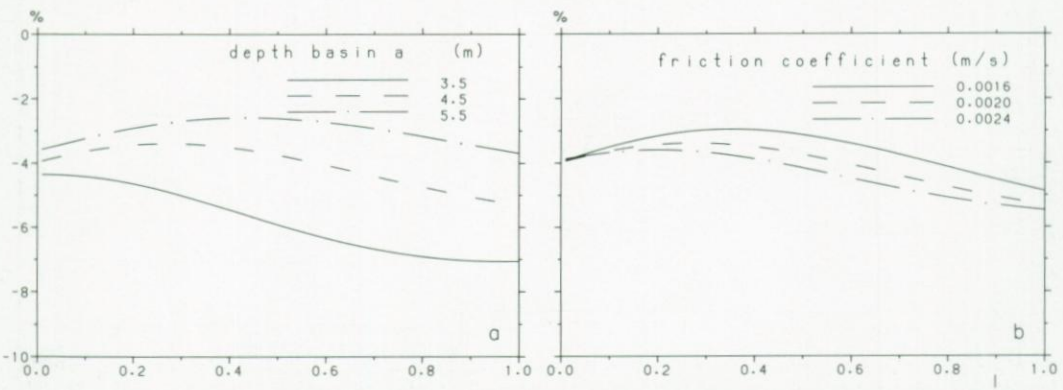

Fig. 7. Ratio between residual transport and tidal transport amplitude at the inlet of basin a (%) as a function of the length ratio between the two basins. (a) Influence chosen depth scale of basin a. (b) Influence bottom-friction coefficient.

Internal tidally-driven residual volume transports between connected basins can only exist when there are asymmetries between the two basins. These asymmetries are either of a morphological nature, *i.e.* length, width or depth differences, or of a tidal nature, *i.e.* amplitude or phase differences between the fluctuating water levels at the two inlets. The analytical model for constant morphological scales (Table 1) is used to examine the relative contribution of both asymmetries to the residual flow.

4.1. TIDAL ASYMMETRIES

To illustrate the consequences of different water-level boundary conditions at both inlets it is assumed that there are no morphological differences between the two basins ($h = b = 1$). This schematization is equal to a model of a single channel with different water-level boundary conditions at both ends. Making use of eq. (47) eq. (49) can now be simplified as:

$$q_0 = \frac{1}{\lambda_0(1+l)}$$

$$\left\{ \frac{Z_{0_{-1}} - Z_{0_l} + 2|\zeta|^2_{-1} - 2|\zeta|^2_l}{k^2} + |q|^2_{-1} - |q|^2_l \right\} \quad (50)$$

which shows that a difference in tidal amplitude of the transport and/or water levels between the two inlets induces a residual flow towards the lowest amplitude. The difference in residual level, connected with a transport amplitude difference by the Bernouilli effect (eq. (22)), acts in the opposite direction. Using eq. (23) the residual pressure gradient term can be written as:

$$\frac{Z_{0_{-1}} - Z_{0_l}}{k^2} = -\frac{1}{2}\left(\overline{q^2_{-1}} - \overline{q^2_l}\right) = \frac{1}{4}\left(|q|^2_{-1} - |q|^2_l\right) \quad (51)$$

which shows that the magnitude of the residual flow is only reduced by the counterbalancing residual level gradient, but its sign is not reversed. Using eq. (31) the transport component of the tidal stress in eq. (50) can be written as a function of the differences in amplitude (Z) and phase (φ) of the water-level boundary conditions

$$|q|^2_{-1} - |q|^2_1 = F\,(Z^2 - 1) + G\,Z\sin\varphi \quad (52)$$

where the real parameters F and G can be expressed as (* means complex conjugate):

$$F = (PP^* - QQ^*), \quad G = \frac{(PQ^* - QP^*)}{2i} \quad (53)$$

with:

$$P = \frac{2}{\tau e^{-i\tau(1+l)} - \tau e^{i\tau(1+l)}},$$

$$Q = \frac{e^{i\tau(1+l)} + e^{-i\tau(1+l)}}{\tau e^{-i\tau(1+l)} - \tau e^{i\tau(1+l)}} \quad (54)$$

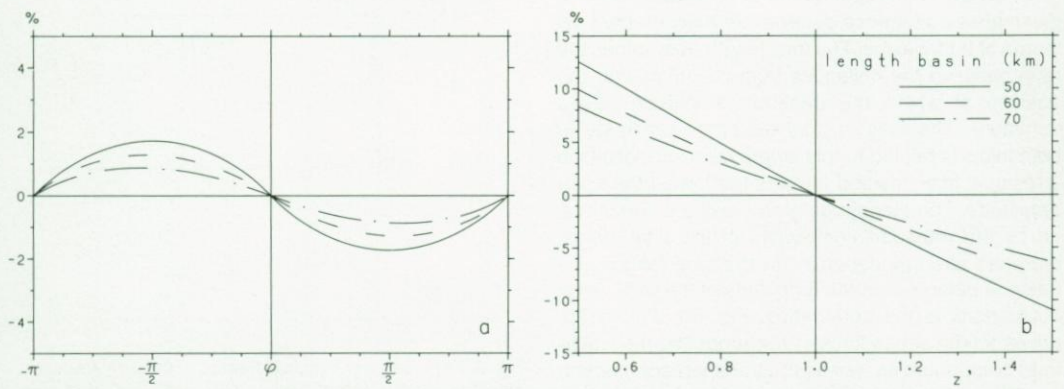

Fig. 8. Effects of differences in the fluctuating water levels at the open boundaries of a single channel. 8a. Ratio between residual transport and tidal transport amplitude at the inlet where the tidal wave enters first as a function of phase differences (%). 8b. Ratio between residual transport and tidal transport amplitude at the inlet of basin a as a function of amplitude differences (%).

Finally substituting eqs. (51) and (53) in eq. (50) yields

$$q_0 = \frac{1}{\lambda_0(1+l)} \left[\left(\frac{3}{4}F - \frac{2}{k^2} \right) (Z^2 - 1) + \frac{3}{4} G Z \sin\varphi \right] \qquad (55)$$

which demonstrates the independent effects of differences in amplitude and in phases of the water-level boundary conditions. A comparable study on mass transport induced by different water-level boundary conditions at both ends of a single canal has been performed by VAN DE KREEKE & DEAN (1975). Their final equation for the residual flow is equal to eq. (55) with respect to the effects of phase and amplitude differences on the direction of the residual flow. Minor differences stem from the contribution of the internally-driven residual pressure gradient and the increased friction coefficient for the residual flow in the final equation here presented (55). Both adjustments reduce the magnitude of the residual volume transport compared with the results of VAN DE KREEKE & DEAN.

In Fig. 8a and b the ratio between residual transport and the tidal transport amplitude at the inlet of the basin where the tidal wave enters first, basin a for positive phases and basin b for negative phases, is shown as a function of a phase difference ($z=1$, Fig. 8a), or an amplitude difference at the inlets ($\varphi=0$, Fig. 8b) and the total length of both basins (mind the different scales of the vertical axes in Fig. 8a and b). Fig. 8a shows that a phase difference results in a residual flow that is directed from the basin where the tidal wave first enters towards the other basin. The magnitude of the residual flow at a given phase difference depends strongly on the total length of both basins. The total length determines the ratio between the distances from the inlets and the position at which the transport amplitude has a minimum. The ratio in tidal transport amplitude in both inlets is related to this length ratio and results in a residual flow directed towards the lowest transport amplitude. The magnitude of the residual flow, caused by the transport component of the tidal stress, therefore strongly depends on the total length of a basin. A difference in the amplitude of the water-level fluctuations at the boundaries, Fig. 8b, directly imposes a tidal stress force in the model by the water-level component as well as the transport component, resulting in a residual flow towards the lowest water-level amplitude. The dependence of the magnitude of the tidal stress gradient on the length of both basins is reflected in the magnitude of this residual flow. A comparison of Fig. 8a with Fig. 8b shows that the residual flow is larger in the case of amplitude differences than in the case of phase differences. This is caused by the relatively small influence of the transport component in the total tidal stress.

4.2. MORPHOLOGICAL ASYMMETRIES

Assuming the water-level boundary conditions at both inlets to be equal ($z=1$, $\varphi=0$), the influence of morphological differences on the residual flow can be examined. In Fig. 9a the influence of a depth difference is illustrated. In the prototype the boundary between the two basins is located at the position where the transport amplitude has its minimum. Thus the length ratio is a function of the phase speed ratio of the tidal waves in both basins. This ratio is proportional to the square of the depth ratio ($l=\sqrt{h}$) in the case of zero bottom friction, and in a first approximation proportional to the depth ratio ($l=h$) in the case of strong, depth-dependent bottom friction

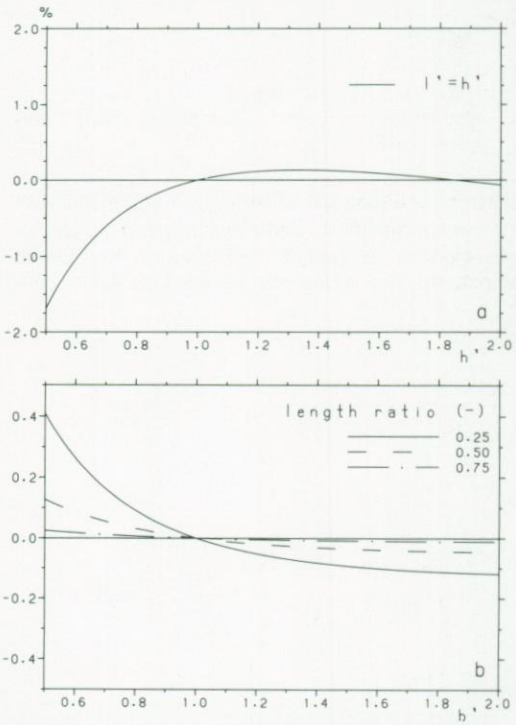

Fig. 9. Ratio between residual transport and tidal transport amplitude at the inlet of basin a (%) as a function of morphological asymmetries between connected tidal basins. 9a. Influence depth and associated length ratio (l'=h') between the two basins. 9b. Influence width ratio for different length ratios.

($\lambda >> \sigma$, eqs. 30 and 32). Hence by using the transport amplitude minimum as a criterion the length ratio is linearly dependent on the depth ratio. The latter ratio is used in Fig. 9a. It shows that a depth difference in general induces a residual flow towards the deeper basin. However, the magnitude of this residual flow is small (mind the difference between Figs 8 and 9 in the scale of the vertical axes) compared with the residual flow caused by tidal asymmetries.

The influence of a width ratio at different length ratios is illustrated in Fig. 9b. Because of the boundary condition at the connection between the two basins (continuity of transports), a width ratio primarily influences the magnitude of the tidal velocities at both sides of this connection. The increased velocity in the narrower basin reduces the tidal stress force on this side of the connection, resulting in a residual flow towards the narrow basin. Fig. 9b shows that the magnitude of this residual flow is very small when the transition between the two basins is located near a transport minimum of the tidal flow (l'=0.75).

5. CONCLUSIONS

The analyses with the analytical model show that in general asymmetries in morphology and boundary tides between basins induce a residual flow between the two. In a single channel this residual flow is directed towards the inlet where, in the case of phase differences, the tidal wave enters last, or, in the case of amplitude differences, towards the inlet with the lowest water-level amplitude. When morphological differences are considered, a residual flow is induced towards the deeper and/or narrower part.

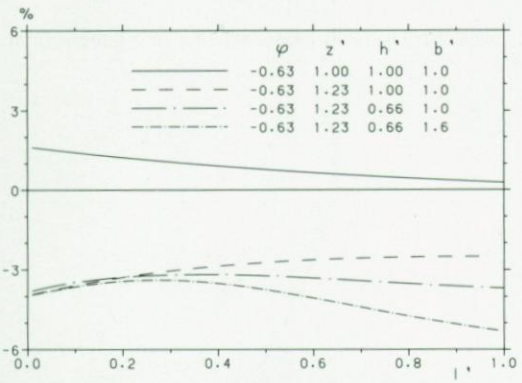

Fig. 10. Influence of different combinations of tidal and morphological asymmetries on the ratio between residual transport and tidal transport amplitude at the inlet of basin a (Marsdiep basin), as a function of the length ratio between the Vlie and Marsdiep basins. In reality the length ratio is approximately 0.5.

In Fig. 10 the consequences of a combination of these asymmetries are summarized for a schematization of the connected Marsdiep and Vlie basins. For different combinations of asymmetries the ratio between the residual transport and the tidal transport amplitude at the inlet of the Marsdiep basin is given as a function of the length ratio. In reality the length ratio is approximately 0.5. For this length ratio Fig. 10 shows that the amplitude difference of the water-level boundary conditions is the most important factor that causes the residual flow to be directed from the Vlie basin towards the Marsdiep basin.

Summarizing it can be concluded that the difference in water-level amplitude at the inlets as well as the depth and width ratio between the two basins directs the residual flow from the Vlie basin towards the Marsdiep basin, whereas phase differences direct the flow in the opposite direction. The combined effect of morphological differences and differences in water-level amplitude at the inlets appears to be larger than the effect of phase differences.

6. REFERENCES

DRONKERS, J.J., 1964. Tidal computations in rivers and coastal waters. Wiley, New York.

HEAPS, N.S., 1978. Linearized vertically integrated equations for residual circulation in coastal seas.—Dt. hydrogr. Z. **31:** 147-169.

HUNTER, J.R., 1975. A note on quadratic friction in the presence of tides.—Estuar. coast. mar. Sci. **3:** 473-475.

KREEKE, J. VAN DE, 1976. Increasing the mean current in coastal channels.—J. Waterw. Harb. Coast. Eng. Div. ASCE **102:** WW2: 223-234.

KREEKE, J. VAN DE & D.C. COTTER, 1974. Tide-induced mass transport in lagoon-inlet systems.—Proc. XIV Conf. Coast Eng. Copenhagen, Denmark: 2290-2301.

KREEKE, J. VAN DE & R.G. DEAN, 1975. Tide induced mass transport in lagoons.—J. Waterw. Harb. Coast. Eng. Div. ASCE **101:** WW4: 393-403.

LORENTZ, H.A., 1926. Verslag Staatscommissie Zuiderzee 1918-1926. Den Haag.

MAAS, L.R.M., J.T.F. ZIMMERMAN & N.M. TEMME, 1986. On the exact shape of the horizontal profile of a topographically rectified tidal flow.—Geophys. Astrophys. Fluid Dyn. **38:** 105-129.

NIHOUL, J.C.J. & F.C. RONDAY, 1975. The influence of the "tidal stress" on the residual circulation.—Tellus **27:** 484-489.

PRANDLE, D., 1978. Residual flows and elevations in the Southern North Sea.—Proc. R. Soc. Lond. (A) **359:** 189-228.

RIDDERINKHOF, H., 1988. Tidal and residual flows in the western Dutch Wadden Sea. I: Numerical model results.—Neth. J. Sea Res. **22:** 1-21.

RIJKSWATERSTAAT, 1986. Getijatlas van Nederland 1986.
ZIMMERMAN, J.T.F., 1976. Mixing and flushing of tidal embayments in the western Dutch Wadden Sea, I: Distribution of salinity and calculation of mixing time scales.—Neth. J. Sea Res. **10:** 149-191.

(received 23-12-1988; revised 2-5-1988)

APPENDIX Linearization of $Q|Q|$

The method of HUNTER (1975) and HEAPS (1978) is followed to average the numerator of the quadratic friction term. Substituting

$$Q = Q_0 + Q_1 \; ; \quad Q_0 << Q_1 \tag{A1}$$

gives:

$$\overline{Q|Q|} = \overline{(Q_0 + Q_1)|Q_0 + Q_1|}$$

$$= \overline{(Q_0 + Q_1)\sqrt{[(Q_0 + Q_1)(Q_0^* + Q_1^*)]}} \tag{A2}$$

where the asterisk denotes a complex conjugate. Neglecting terms of order Q_0^2 under the square root sign and expanding this equals:

$$\overline{(Q_0 + Q_1)|Q_1| \left\{1 + \frac{Q_0 Q_1^* + Q_0^* Q_1}{2|Q_1|^2}\right\}}$$

$$= \frac{3}{2}\overline{|Q_1|Q_0} + \overline{\frac{Q_1^2 Q_0^*}{2|Q_1|}} + \overline{Q_1|Q_1|} \tag{A3}$$

Finally substituting:

$$Q_1 = A_1 + iA_2 \; ; \quad Q_0 = B_1 + iB_2 \tag{A4}$$

in (A3) and choosing axes such that $A_2 = 0$ and $B_2 = 0$ gives the following expression for one-dimensional motion:

$$\overline{Q|Q|} = \overline{2|Q_1|Q_0} + \overline{Q_1|Q_1|}$$

CHAPTER 4

TIDAL AND RESIDUAL FLOWS IN THE WESTERN DUTCH WADDEN SEA III: VORTICITY BALANCES*

H. RIDDERINKHOF

Netherlands Institute for Oceanic Sciences, P.O. Box 59, 1790 AB Den Burg, Texel, The Netherlands

ABSTRACT

A vorticity-dynamics approach is used to examine the origin of the small-scale residual current field in the western Dutch Wadden Sea. For a representative part of the Wadden Sea, the magnitude of vorticity and of terms in the balance equation for vorticity is determined on the basis of results from a two-dimensional numerical model. The torque from bottom friction along the side walls of the tidal channels appears to be the dominating mechanism in generating tidal relative vorticity, the magnitude of which is much larger than planetary vorticity. Especially near a tidal inlet, stretching and squeezing of fluid columns is of importance in increasing/decreasing relative vorticity. Averaging over a tidal period shows, compared to the tidal equations, an increased influence of the non-linear advective and streching/squeezing terms in the tidally-averaged balance. However, although the relative influence of these strong non-linear terms increases, the influence of the weak non-linear terms originating in bottom friction cannot be ignored. The mechanism responsible for the headland eddies near a tidal inlet and the topographical eddies in the channels of the Wadden Sea is essentially the same, *viz.* the transfer of vorticity from a source region where this vorticity is produced by differential bottom friction, to adjacent regions. This transfer of tidal vorticity, or advection, is most effective near a transition from straight to curved isobaths where a gradient in the production of tidal vorticity occurs. This is illustrated by showing the vorticity possessed by a particular fluid column during a tidal excursion. The dominant influence of the bathymetry on the small scale residual current pattern is used for a qualitative discussion of the residual flow field in other parts of our numerical model.

1. INTRODUCTION

In a preceeding paper results from a two-dimensional numerical model have been used to describe tidal and tidally-driven residual flows in the western Dutch Wadden Sea (RIDDERINKHOF, 1988a). The computed Eulerian residual flow field has been interpreted as a combination of a large scale internally driven volume transport between connected tidal basins and small scale isolated residual eddies. In an analytical study it has been shown that the origin of the throughgoing volume transport can largely be explained from asymmetrical water-level fluctuations at the inlets of connected tidal basins (RIDDERINKHOF, 1988b). In the present paper the conservation equation for vorticity is used to explain the origin of the small-scale residual current field. The use of a vorticity-dynamics approach to discuss the origin of the residual flow pattern stems from the dominating presence of closed residual streamlines in the outcome of the numerical model (RIDDERINKHOF, 1988a). This implies the presence of non-vanishing residual vorticity, which must be accounted for (ZIMMERMAN, 1980b). Another reason to focus on vorticity is that this approach implicitly quantifies and explains the shear in the velocity field. This velocity shear is of great importance for the dispersion of material, which will be the subject of a following article (Ridderinkhof, in ms). Furthermore, numerical analysis of the different terms in the governing vorticity equation enables us to make a comparison with results of other studies in the same field. These studies differ from each other in that each treats a particular type of residual eddy, whereas residual eddies due to a variety of causes are to be expected in a shallow estuary such as the Wadden Sea. The origin of topographical eddies in the open sea has been the subject of analytical studies by HUTHNANCE (1973) and ZIMMERMAN (1978, 1980a). Results of theoretical studies on topographical eddies have been compared with measurements of tidal vorticity in the Southern Bight of the North Sea by RIEPMA (1987). The effect of the grid size in a numerical model with respect to the computed tidal and residual vorticity in the open sea has been studied by ABRAHAM *et al.* (1987). TEE (1976, 1977) and PINGREE & MADDOCK (1979) used a numerical model to study the residual current pattern near a promontory in the coastline of a relatively deep tidal area, while YANAGI

**Publication no 32 of the project 'Ecological Research North Sea and Wadden Sea'*

(1976, 1978) and OONISHI (1977) studied the effects of lateral friction in a schematized rectangular basin. IMASATO (1983, 1987) discussed the physical meaning of tide-induced residual eddies. A general conclusion from these studies is that residual vorticity is generated by the advection of tidal vorticity by the oscillating flow (ROBINSON, 1983). Thus the inclusion of advective terms as well as terms representing the mechanisms that produce tidal vorticity in the governing equations is essential to be able to reproduce a realistic residual current field. These terms are incorporated in our numerical model, which solves the non-linear shallow water equations. A vorticity-dynamics approach to the model results enables us to identify the dominating mechanisms that account for the presence of residual eddies in the complex geometrical and topographical reality of a shallow estuary.

Acknowledgements.—The author is much indebted to Rijkswaterstaat, Dienst Informatieverwerking, for the use of their computer and the support in employing the extended system of computer programs for simulating two-dimensional tidal flows (WAQUA system).

2. MODEL AND METHOD TO PROCESS THE RESULTS

2.1. MODEL DESCRIPTION

This paragraph summarizes characteristics of the numerical model, results of which are used to determine the magnitude and origin of tidal and residual vorticity. A more extensive discussion can be found in RIDDERINKHOF (1988a).

Fig. 1 gives the boundaries and some isobaths of our western Wadden Sea model. It covers four tidal

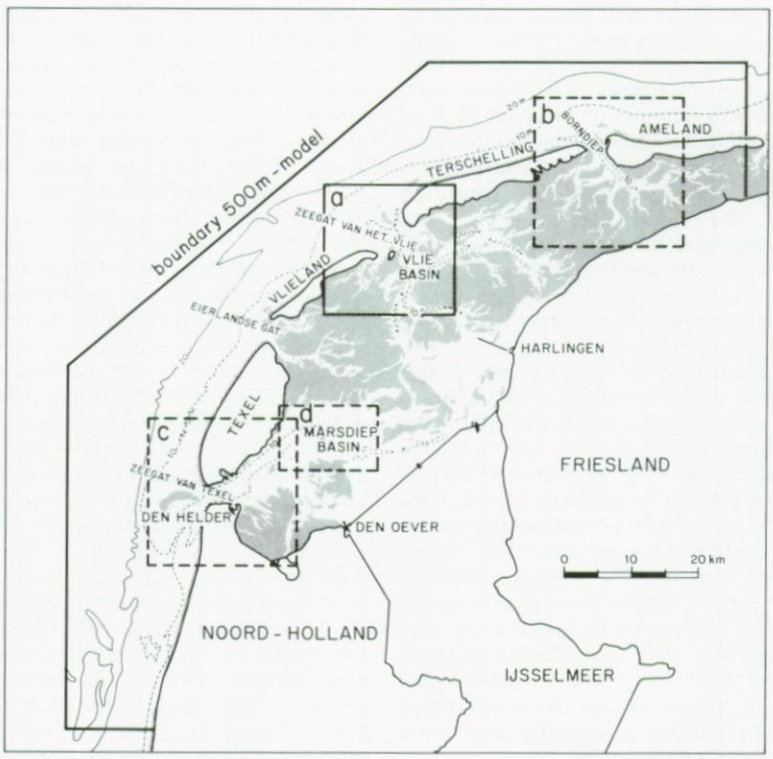

Fig. 1. Area covered by the two-dimensional numerical model for the western Dutch Wadden Sea. Open boundaries are located in the adjacent North Sea. Isobaths indicate that the model covers 4 tidal basins. Results for a representative part of the model, indicated by a solid square (region a), are used for an extensive discussion. Dashed lines represent areas that are used for a qualitative discussion of the residual velocity field. (Fig. 13 gives results for region b, Fig. 14 for region c and Fig. 15 for region d).

basins as well as an adjacent part of the North Sea. The hydrodynamic equations used in the model are given by the following set:

$$\frac{\partial u}{\partial t}+u\frac{\partial u}{\partial x}+v\frac{\partial u}{\partial y}-fv=-g\frac{\partial \zeta}{\partial x}-g\frac{u\sqrt{(u^2+v^2)}}{C^2(H+\zeta)}+\nu\left(\frac{\partial^2 u}{\partial x^2}+\frac{\partial^2 u}{\partial y^2}\right) \tag{1}$$

$$\frac{\partial v}{\partial t}+u\frac{\partial v}{\partial x}+v\frac{\partial v}{\partial y}+fu=-g\frac{\partial \zeta}{\partial y}-g\frac{v\sqrt{(u^2+v^2)}}{C^2(H+\zeta)}+\nu\left(\frac{\partial^2 v}{\partial x^2}+\frac{\partial^2 v}{\partial y^2}\right) \tag{2}$$

$$\frac{\partial \zeta}{\partial t}+\frac{\partial (H+\zeta)\,u}{\partial x}+\frac{\partial (H+\zeta)\,v}{\partial y}=0 \tag{3}$$

in which:

u, v = vertically averaged velocity components
ζ = water elevation relative to a reference plane
H = depth relative to a reference plane
f = coriolis parameter
g = acceleration of gravity
ν = horizontal eddy viscosity coefficient
C = bottom friction coefficient (Chezy coefficient)

These well-known shallow-water equations are solved numerically by employing the ADI (Alternating Direction Implicit) method on a staggered grid (LEENDERTSE, 1967; STELLING, 1984). The grid size is 500 m, resulting in a matrix of 196 x 222 elements, and the standard timestep is 150 s. Water levels, having a mean amplitude of about 0.80 m, are prescribed at the open boundaries in the North Sea. For the present paper it is of interest that a perfect slip condition is imposed along the closed boundaries of the coastline. Thus a lateral frictional, coastal boundary layer cannot be simulated in our model. A depth-dependent formulation (Manning's formulation) has been applied for the bottom-friction coefficent:

$$C=\frac{(H+\zeta)^{1/6}}{n},\quad n=0.023 \tag{4}$$

The coefficient for horizontal eddy viscosity was chosen to be 7 m^2s^{-1} in the standard simulation.

Tidal results insensitive to small scale variations in bottom topography such as water elevations in the deeper tidal channels, volume transports through the tidal inlets and global current velocity fields have been compared with observations. It has been concluded that the model simulates these aspects fairly well. A result of special interest for the present study is that in those areas for which field measurements are available, the location and orientation of computed residual eddies agree with current measurements.

2.2. METHOD TO DETERMINE TERMS IN THE VORTICITY EQUATION

In the present article we discuss the mechanisms that govern the production, advection and damping of vorticity in the western Wadden Sea. The vertical component of relative vorticity, ω, is defined as:

$$\omega=\frac{\partial v}{\partial x}-\frac{\partial u}{\partial y} \tag{5}$$

which implies that the local rate of change of vorticity during a tidal cycle is given by:

$$\frac{\partial \omega}{\partial t}=\frac{\partial}{\partial x}\frac{\partial v}{\partial t}-\frac{\partial}{\partial y}\frac{\partial u}{\partial t} \tag{6}$$

Equation (6) suggests that the contribution of the different terms to the local rate of change of relative vorticity can be computed whenever the magnitude of the terms in eqs (1) and (2) is known in every discrete grid point. However the numerical method used to solve eqs (1), (2) and (3) in principle prohibits such a treatment of eq. (6).

Defining m as the position of the grid unit along the X-axis and n along the Y-axis, the use of a staggered grid implies that the water levels are defined at the integer values m,n while the velocity variables and the terms in the momentum equation are located between the water level points, in x-direction at $m+\frac{1}{2},n$ and in y-direction at $m,n+\frac{1}{2}$. Defining ω at $m+\frac{1}{2},n+\frac{1}{2}$, eq. (5) can be discretised by applying:

$$\left.\frac{\partial \omega}{\partial t}\right|_{m+\frac{1}{2},n+\frac{1}{2}}=\frac{\left(\left.\frac{\partial v}{\partial t}\right|_{m+1,n+\frac{1}{2}}-\left.\frac{\partial v}{\partial t}\right|_{m,n+\frac{1}{2}}\right)}{\Delta x}-\frac{\left(\left.\frac{\partial u}{\partial t}\right|_{m+\frac{1}{2},n+1}-\left.\frac{\partial u}{\partial t}\right|_{m+\frac{1}{2},n}\right)}{\Delta y} \tag{7}$$

which suggests that the contribution of the different terms at a specific time level can directly be computed from their value in the numerical simulation. However, the ADI-method also implies that a time step is split up into two stages in which variables from different time levels are used by employing alternately explicit and implicit schemes, terms in the momentum equation in the x-direction being centred in time

around the level $j\Delta t$ and terms in the y-direction around the level $(j+\frac{1}{2})\Delta t$. Thus eq. (7) cannot be defined at a specific time level. This in priciple prohibits a discussion of the relative influence of the composing terms in the balance equation for vorticity, eq. (6), on the basis of the value of terms during the numerical simulation. This problem now was circumvented by determining numerical values for terms in eq. (7) (and in eqs (1) and (2)) with variables from exactly the same time level ($j\Delta t$). Using the same spatial differences as in the ADI-method, the difference between the magnitude of a term in the numerical simulation and the magnitude of a term computed with variables from the same time level was reduced by decreasing the applied time step from 150 sec. (standard) to 37.5 sec.

However, a consequence of this method remains that the balance in eq. (7) does not exactly add up to zero. The deviation is small, however, as will be shown in the following sections.

The time interval used for the computation of vorticity related quantities is 30 min, which is equal to the interval used for storage of the matrices for u,v and ζ.

3. TIDAL VORTICITY AND BALANCES

Substituting (1) and (2) in the rigth-hand side of (6), rearranging and making use of (4), gives the conservation equation for vorticity:

$$\underset{a}{\frac{\partial\omega}{\partial t}} + \underbrace{u\frac{\partial\omega}{\partial x}+v\frac{\partial\omega}{\partial y}}_{b} = \underbrace{-\omega\left(\frac{\partial u}{\partial x}+\frac{\partial v}{\partial y}\right)}_{c} \underbrace{-f\left(\frac{\partial u}{\partial x}+\frac{\partial v}{\partial y}\right)}_{d} + \underbrace{\frac{gn^2}{(H+\zeta)^{4/3}}\left(u\frac{\partial\sqrt{(u^2+v^2)}}{\partial y}-v\frac{\partial\sqrt{(u^2+v^2)}}{\partial x}\right)}_{e} +$$

$$\underbrace{+gn^2\sqrt{(u+v^2)}\left(u\frac{\partial(H+\zeta)^{-4/3}}{\partial y}-v\frac{\partial(H+\zeta)^{-4/3}}{\partial x}\right)}_{f} \underbrace{-\frac{gn^2\sqrt{(u^2+v^2)}}{(H+\zeta)^{4/3}}\omega}_{g} \underbrace{+\nu\left(\frac{\partial^2\omega}{\partial x^2}+\frac{\partial^2\omega}{\partial y^2}\right)}_{h} \qquad (8)$$

The sum of terms on the right-hand side of eq. (8) gives the total change of vorticity with time as seen when moving at velocity (u,v) and represents the mechanisms that produce and damp vorticity. Terms (c) and (d) represent the conservation of potential vorticity when fluid columns spin up or down by column stretching or squeezing. Term (e) derives from bottom friction and represents the production of vorticity due to velocity shear (for quadratic friction law). Term (f) also originates in bottom friction and represents the production of vorticity due to depth gradients transverse to the direction of the tidal flow. This term combines the effects of a depth-distributed frictionforce and a depth-dependent friction coefficient. Term (g) is the damping part of bottom friction. Term (h) represents the damping of vorticity by lateral shear. A schematic representation and detailed discussion of the generating and damping mechanisms are given by ROBINSON (1983). Eq. (8) can also be written as:

$$\underset{(A)}{\frac{\partial\omega}{\partial t}} + \text{advection} = \underset{(P)}{\text{production}} + \underset{(D)}{\text{damping}} \qquad (9)$$

in which term (A) is equal to term (b) in (8), term (P) represents the production terms, (c)+(d)+(e)+(f) in (8), and term (D) represents the damping terms, (g)+(h) in (8). In the following, the magnitude of relative vorticity, ω, as well as of the terms in eq. (8) during a tidal cycle is shown in some characteristic grid points, while at two points of time, during ebb and flood, vorticity and the magnitude of the terms in eq. (9) are shown for a representative part of the numerical model. The position of the characteristic grid points is indicated in Fig. 2 which also gives isobaths in a representative part of the numerical model near the tidal inlet between Vlieland and Terschelling, draining the Vlie basin. This part of the model is used to discuss the magnitude of the composite terms in eq. (9). Grid point 1 is representative of the the seaside of a tidal inlet, grid point 2 is located near the centre of the inlet, grid point 3 at the basin side of the inlet where the isobaths are relatively straight, and grid point 4 is located near a channel junction in the tidal basin where isobaths are strongly curved and the mean water depth is relatively small.

Fig. 3 gives the relative vorticity in these grid points during a tidal cycle. This figure shows that relative vorticity in these points is about an order of magnitude larger than planetary vorticity ($f = 1.15\cdot10^{-4}\ s^{-1}$). In contrast to the other gridpoints the absolute magnitude of vorticity in grid point 1, at the seaside of the tidal inlet, is much larger during the ebb period than during the flood period. The left

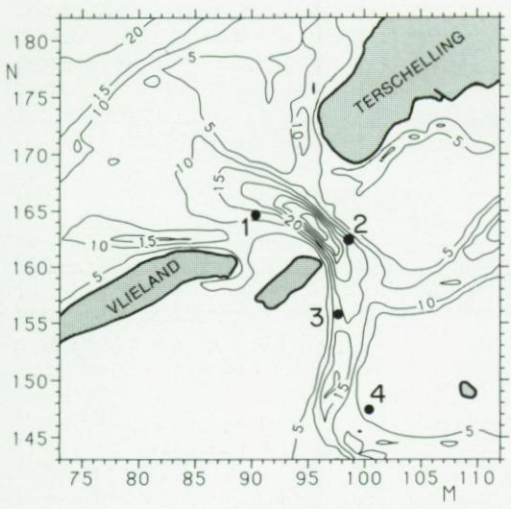

Fig. 2. Isobaths in a representative part of the numerical model. Numerical values of the terms in the vorticity equation are discussed in detail for grid points 1 to 4.

column of Fig. 4 gives the magnitude of the terms at the left-hand side of eq. (8) in these grid points. The magnitude of term (a), given by a solid line, has been determined by applying:

$$\frac{\partial \omega}{\partial t} = \frac{(\omega \mid_{t+\Delta t} - \omega \mid_{t-\Delta t})}{2\Delta t}, \quad \Delta t = 30 \text{ min.} \qquad (10)$$

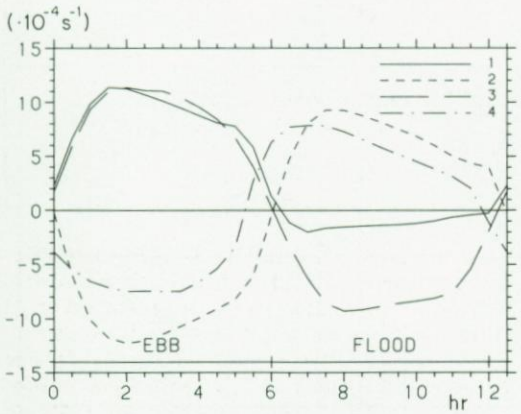

Fig. 3. Relative vorticity, ω ($\cdot 10^{-4} s^{-1}$), during a tidal cycle in grid points 1 to 4. (See Fig. 2 for the position of these grid points).

while the dotted points (a') give the magnitude of term (a) when it is computed on the basis of the balance in eq. (8). The difference between the two, compared with the magnitude of the other terms, gives an idea of the accuracy of the method that has been used to determine the value of the terms in eq. (8). This difference can be neglected for the discussion in this paragraph. The left column shows that in the grid points 1 and 2 during almost the complete tidal cycle, the advective term (b) is negative. In grid points 3 and 4 this term is only of relative importance during the flood period.

The middle column of Fig. 4. gives the magnitude of the terms that produce vorticity, (c), (d), (e) and (f) in eq. (7). Term (f) is the most important term in the grid points considered. Depth gradients perpendicular to the tidal flow appear to be a very important source of tidal vorticity, especially in grid point 4 where the water depth is relatively small (Note the difference in vertical scale between grid points 1,2 and 3 and grid point 4). Terms (c) and (d) represent the effect of stretching and squeezing of fluid columns. Due to the large relative vorticity ($\omega >> f$) the contribution of the planetary vorticity to this mechanism, term (d), is negligible. Generation of vorticity by velocity shear, term (e), is less important than the generation by transverse depth gradients (f). Because term (e) always acts in an opposite direction to term (f), the resulting production of vorticity by bottom friction decreases when a quadratic friction law is used. In grid points (2) and (3) at the basin side of the tidal inlet, the contribution of term (c), due to stretching/squeezing, is about equal to the total contribution of bottom friction. An important difference between the two mechanisms is that the sign of term (c) does not change during a tidal cycle. The general conclusion from the magnitude of terms producing tidal vorticity is that in a first approximation in a tidal basin and near a tidal inlet only the Coriolis effect, term (d), can be ignored.

The right column of Fig. 4 gives the magnitude of the mechanisms that damp vorticity. In the grid points concerned, damping by bottom friction, term (g), is the most important term. In grid point 4 the damping by lateral shear, term (h), can even be neglected. However, the influence of term (h) is strongly dependent on the chosen value of the horizontal eddy diffusion coefficient and on the imposed perfect slip condition at closed boundaries. The consequences of varying this parameter on the residual eddies is shown in section 5. Combining the value of damping by bottom friction, term (g), with the value of relative vorticity, ω (Fig. 3), gives an order of magnitude of the damping time scale, T_d:

$$T_d = \frac{\text{term(f)}}{\omega} = \frac{gn^2\sqrt{(u^2+v^2)}}{(H+\zeta)^{3/4}} \qquad (11)$$

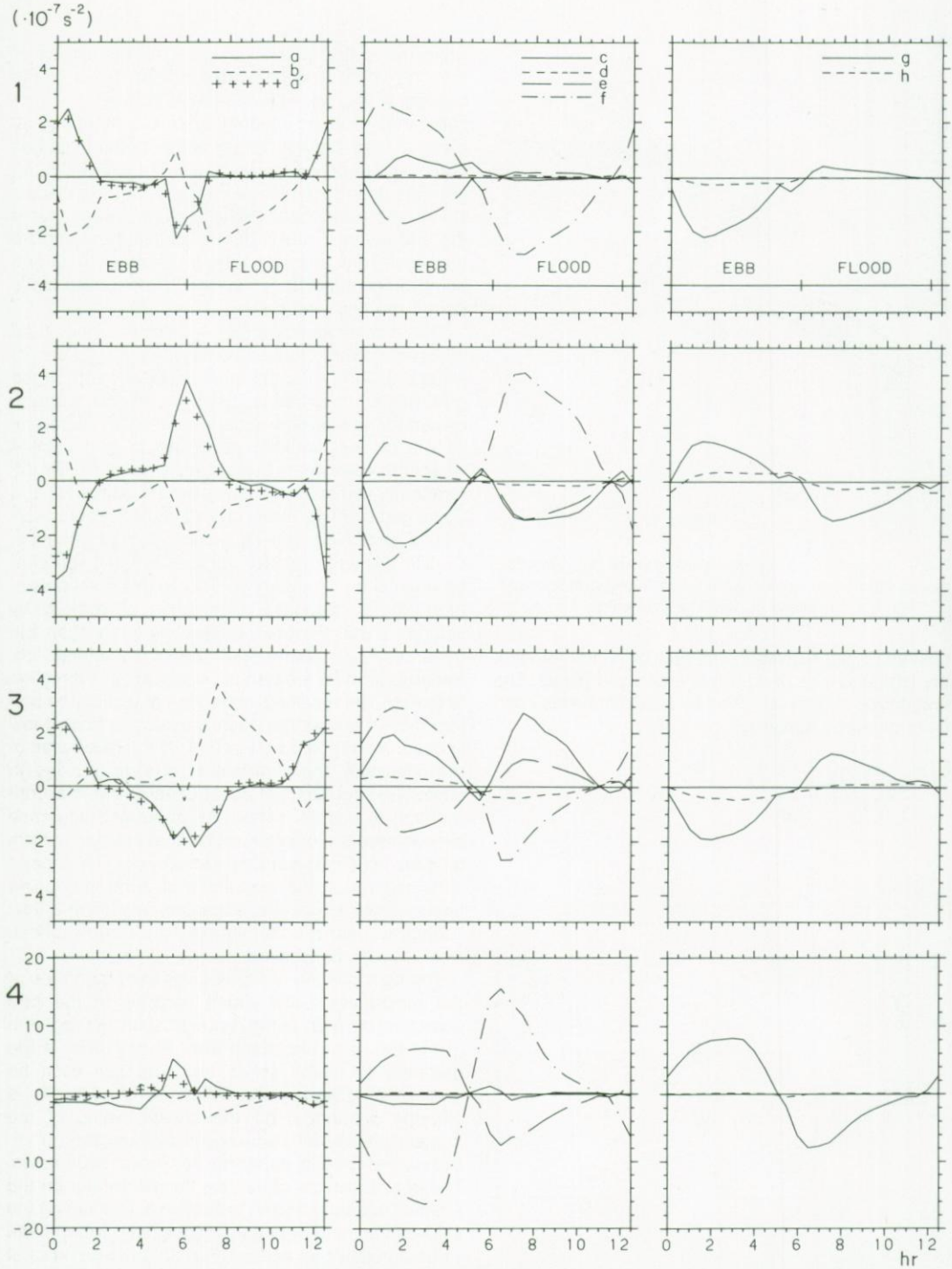

Fig. 4. Magnitude of terms in eq. (8) ($\cdot 10^{-7} s^{-2}$) during a tidal cycle in grid points 1 to 4. The left column gives the terms at the left-hand side of eq. (8) (see text), the middle column gives the terms producing vorticity and the rigth column gives the terms damping vorticity. Terms belonging to a specific grid point are given in a row. Note that the range of the vertical scale for grid point 4 differs from the other grid points.

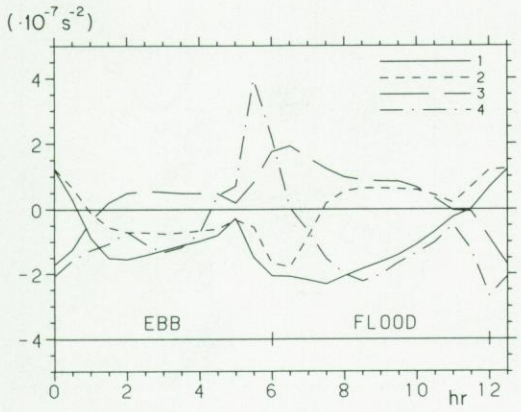

Fig. 5. Total rate of change of vorticity by bottom friction in the characteristic grid points ($\cdot 10^{-7} s^{-2}$).

This time scale varies from about 0.5 hours in grid point 4 to 2 hours in grid point 2. Thus tidal vorticity is destroyed within a tidal period.

Comparing the terms originating in bottom friction shows that the order of magnitude of damping, term (g), about equals the total production, (e)+(f). This suggests that the effective influence of bottom friction is only small. However, Fig. 5, giving the total effect of bottom friction, (e)+(f)+(g) in eq. (8), shows that the bottom friction term still has considerable influence on the rate of change of vorticity if these terms are added. The dominating character of this term depends on the specific situation, *e.g.* in grid point 1 the local damping of vorticity by this term is larger than the local production during the ebb period, while production is larger than damping during the flood period.

Fig. 6 gives the current velocity field and the spatial distribution of relative vorticity at two characteristic time levels during the ebb tide and the flood tide. The left side of Fig. 6 corresponds with $t=2$ in Fig. 4 and the right side with $t=8$. This figure shows that, except for a change of sign, there is not

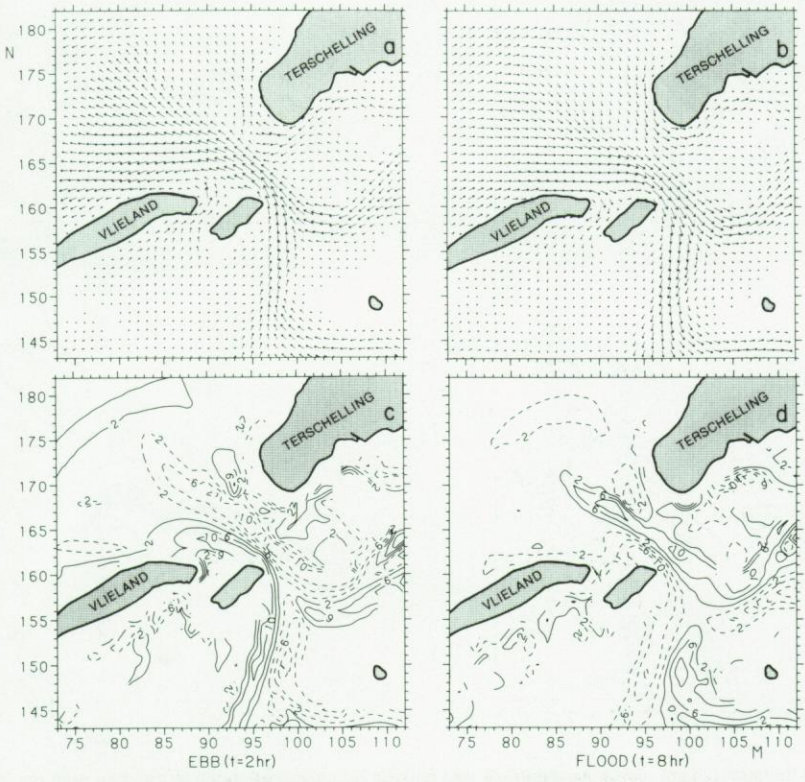

Fig. 6. Current velocities and isolines of relative vorticity ($\cdot 10^{-4} s^{-1}$) in a representative part of the model near the Zeegat van het Vlie. Left, for a characteristic time level during ebb ($t=2$ in Fig. 4); rigth, for a characteristic time level during flood ($t=8$ in Fig. 4). Solid lines indicate vorticity with positive sign, dashed lines vorticity with negative sign.

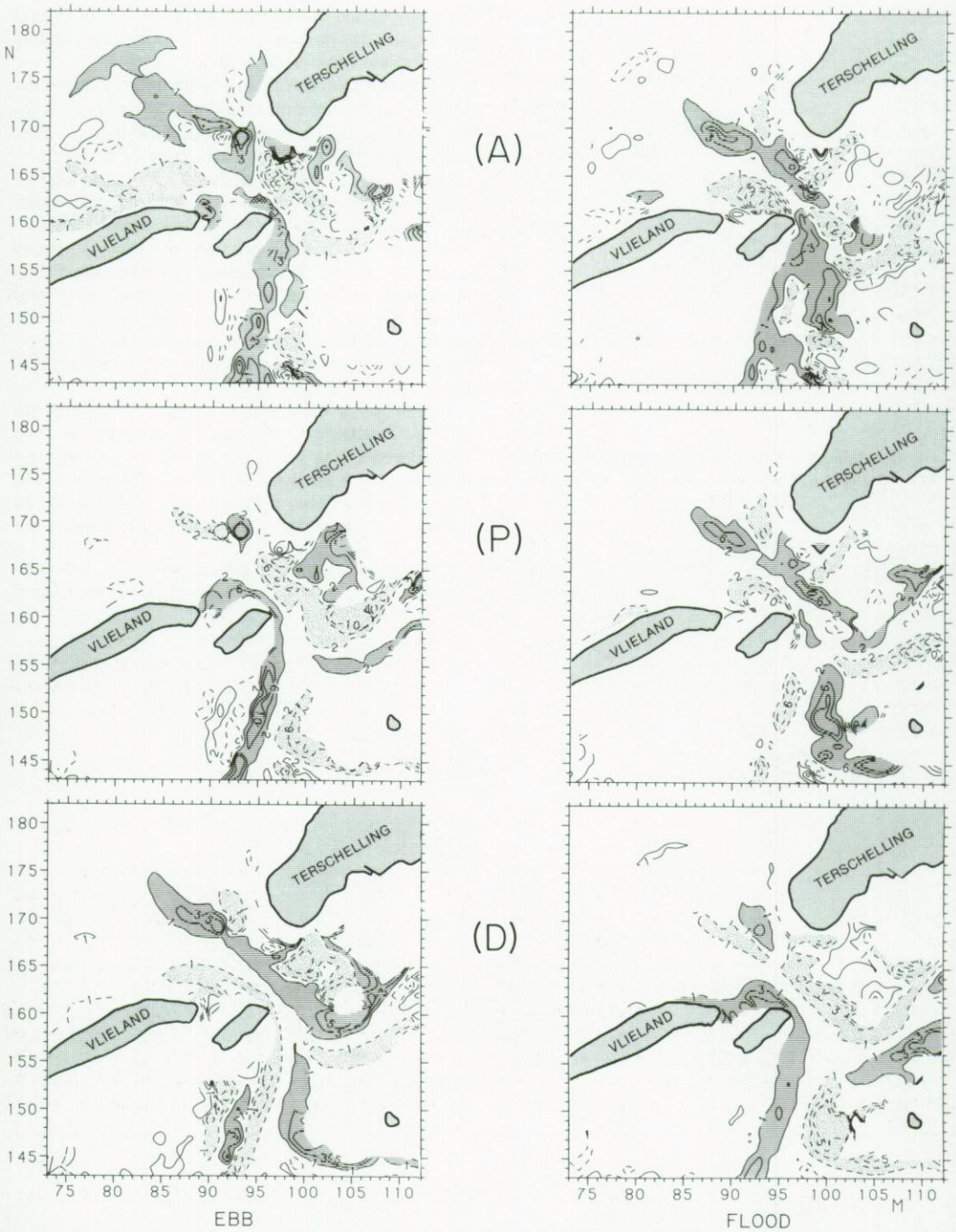

Fig. 7. Isolines for the terms in eq. (9) during ebb ($t=2$, left) and during flood ($t=8$, right) in the area near the Zeegat van het Vlie. The interval between successive isolines is $4 \cdot 10^{-7} s^{-2}$ for production and $2 \cdot 10^{-7} s^{-2}$ for advection and damping. The absolute value of the lower limit of the range of isolines is $2 \cdot 10^{-7} s^{-2}$ for production and $1 \cdot 10^{-7} s^{-2}$ for advection and damping. Solid lines indicate positive values, dashed lines the same range of negative values.

much difference between the two velocity fields and the magnitude of relative vorticity during the ebb tide and the flood tide. In most grid points of the tidal channels relative vorticity is larger than planetary vorticity. A comparison with Fig. 2 shows that the largest relative vorticity is found along the side walls of the tidal channels where production of relative vorticity by differential bottom friction (term (f) in eq. 8) is relatively high. A detailed comparison of both synoptic vorticity distributions shows that in some regions vorticity is larger during ebb than during flood, for instance at the seaside of the inlet. Such regions where the magnitude of relative vorticity substantially differs between the ebb and flood periods can also be found near channel junctions in the tidal basin.

Fig. 7 gives isolines for the magnitude of the terms in eq. (9), total production (P), advection (A) and damping (D) at specific time levels during the ebb period ($t=2$, left side) and flood period ($t=8$, right side), when the local rate of change of vorticity can be ignored. For production the interval between successive isolines is $2 \cdot 10^{-7} s^{-2}$ and for advection as well as damping the interval is $1 \cdot 10^{-7} s^{-2}$. Solid lines indicate isolines having positive values and dashed lines indicate the same range of negative values. Production of relative vorticity is largest on the relatively steep side walls of the tidal channels. The sign of this term differs between the ebb and flood periods. However, the absolute value of production of vorticity can substantially differ between the ebb and flood periods. This is partly caused by differences in current velocities and water levels at both tidal phases, resulting in different contributions of the bottom friction term. Another contribution to this difference in production stems from the stretching/squeezing term because it has the same sign during the ebb and flood periods (see also Fig. 4). This term is of importance near the inlet where the divergence and convergence of the tidal currents as well as the tidal vorticity are relatively large. Damping is large in the same region as where vorticity and production of vorticity are large. However, in general the production of vorticity on the side walls of the channels is larger than the damping. Therefore a part of the tidal vorticity is advected to other regions. This is reflected in the isolines of the advection term. Although the advective term is still large near the

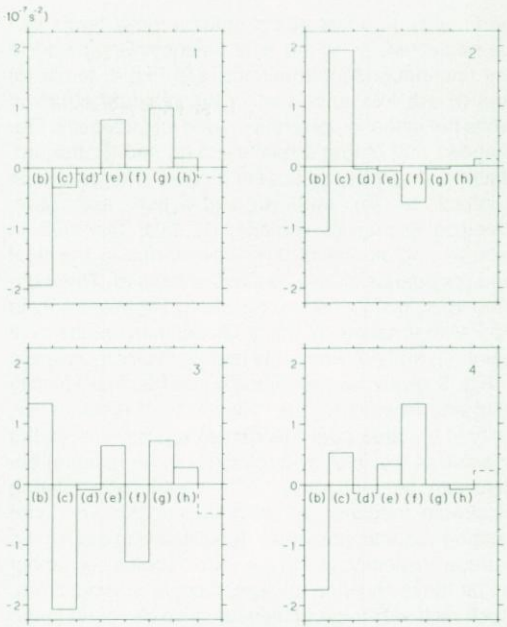

Fig. 8. Magnitude of tidally-averaged terms in eq. (12) in the characteristic grid points ($10^{-7} s^{-2}$). (Fig. 2 gives the position of these gridpoints).

'source regions', its magnitude is also of importance outside these regions, *e.g.* in the centre of the channels and, especially during ebb, at the seaside of the inlet.

4. RESIDUAL VORTICITY AND BALANCES

In vector form the tidally averaged vorticity equation reads: see eq. (12).

In eq. (12) —— means averaging over a tidal period and j is the vertical unit vector. Fig. 8 gives the magnitude of these terms in the chosen characteristic grid points. The last column in this figure gives the summation of all terms and indicates the discrepancy between the balance in eq. (12) and the balance in the shown numerical values. This discrepancy is again neglected in this paragraph. In general Fig. 8 shows that in these grid points only term (d), the Coriolis effect, and (h), damping by lateral friction, appear to be of minor importance in all

$$\underbrace{\overline{u \cdot \nabla \omega}}_{b} \; \underbrace{\overline{+\omega \nabla \cdot u}}_{c} \; \underbrace{\overline{+f \nabla \cdot u}}_{d} \; \underbrace{\overline{-\frac{gn^2 j}{(H+\zeta)^{4/3}} \cdot (ux \nabla \mid u \mid)}}_{e} \; \underbrace{\overline{-gn^2 j \cdot (u \mid u \mid x \nabla (H+\zeta)^{-4/3})}}_{f} \; \underbrace{\overline{+\frac{gn^2 \mid u \mid}{(H+\zeta)^{4/3}} \omega}}_{g} \; \underbrace{\overline{-\nu \nabla^2 \omega}}_{h} = 0 \qquad (12)$$

grid points. In a first approximation these terms can be neglected, as in the tidal balance. Compared to the time-dependent equations, see Fig. 4, terms (e) and (f) are less important in the residual equation while the influence of terms (b) and (c) increases. Fig. 4 shows that during a tidal cycle (e) and (f), the production of vorticity by bottom friction, change sign in contrast to (b) and (c), advection and stretching/squeezing of vorticity. By this, the shift in relative importance of the above terms in the tidal and residual balance equations is caused. The damping term, mainly bottom friction (g), appears only to be of importance in the total balance in the grid points (1) and (3), where the residual vorticity is large.

Fig. 9 gives the two-dimensional residual velocity field and isolines for the magnitude of residual vorticity in the area near the Zeegat van het Vlie. At the seaside of the inlet, two relatively large residual eddies can be recognized, at the east side rotating clockwise (negative vorticity) and at the west side rotating counterclockwise (positive vorticity). The residual velocity in these two eddies is about 0.10-0.15 ms^{-1}, while the length scale is about 5 km. Such relatively large eddies can also be found in the channels of the inner basin, especially near channel junctions. It is more difficult to recognize the smaller eddies, but the isolines in Fig. 9 show that in the tidal basin and close to the inlet relative large regions of residual vorticity of the same sign are often composed of a series of residual eddies with the same rotation sense. A quadrupole structure of the residual current field can be recognized from the sign of residual vorticity at both sides of the inlet. However, at the basinside of the inlet this quadrupole is rather distorted. At this side the associated residual current field is much more irregular than at the seaside. Furthermore the residual flow field is composed of a large-scale and a small-scale part, which complicates the current pattern. Near the tidal inlet the influence of the through going volume transport is only small because velocities associated with this large-scale part of the residual flow field, $O(10^{-2}ms^{-1})$, are an order of magnitude lower than velocities associated with the residual eddies, $O(10^{-1}ms^{-1})$.

Fig. 10 gives the spatial distribution of the dominating tidally-averaged terms in eq. (12) in the area near the Zeegat van het Vlie. In this area the absolute value of terms (d) and (h) is less that $0.5 \cdot 10^{-7}$ s^{-2}, the lower limit of the range of isolines for the other terms, and therefore these terms are not shown in this figure. In general this figure shows that the relative influence of the bottom friction term, (e), (f) and (g), is less than in the time-dependent situation. This is due to the weak non-linearity in terms of the residual velocity. Fig. 10 shows that despite this weakened non-linearity the contribution of these terms cannot be ignored along the side walls of the tidal channels, where the water depth is relatively small and the depth gradients are relatively large. The strong non-linearity of terms (b) and (c) is reflected in the increased influence of these terms in the tidally averaged situation. Term (c) is of importance in those regions where relative vorticity as well as the divergence/convergence of the tidal flow is relatively large. This term primarily gives the effect of variations in bottom topography causing stretching and squeezing of fluid columns. Therefore its influence is largest near contractions in the channel

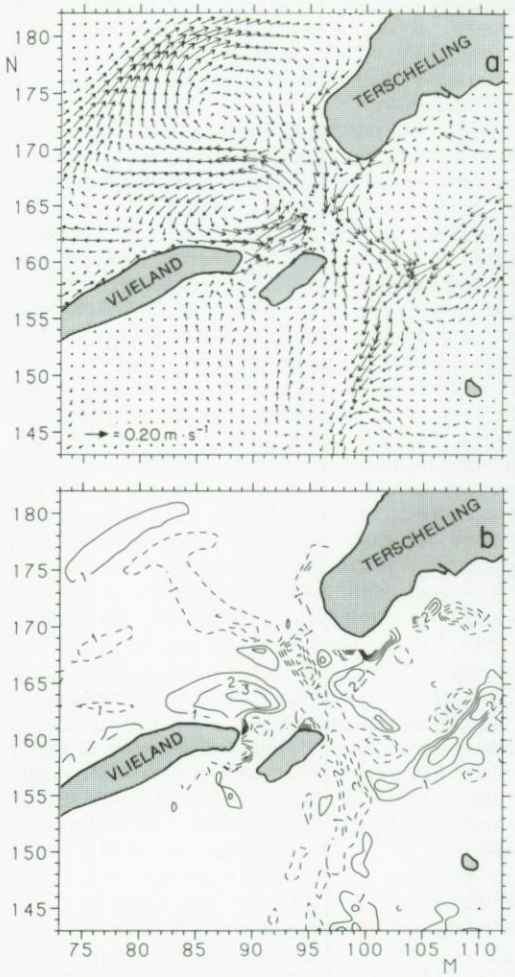

Fig. 9. Residual velocities and isolines for the magnitude of residual relative vorticity, ω_0, in the area near the Zeegat van het Vlie. The residual vorticity distribution has been derived from the residual velocities. The absolute value of the lower limit of the range of isolines is $1 \cdot 10^{-4}s^{-1}$ and the interval between successive isolines is $1 \cdot 10^{-4}s^{-1}$. Dashed lines represent residual vorticity with negative sign and solid lines residual vorticity with positive sign.

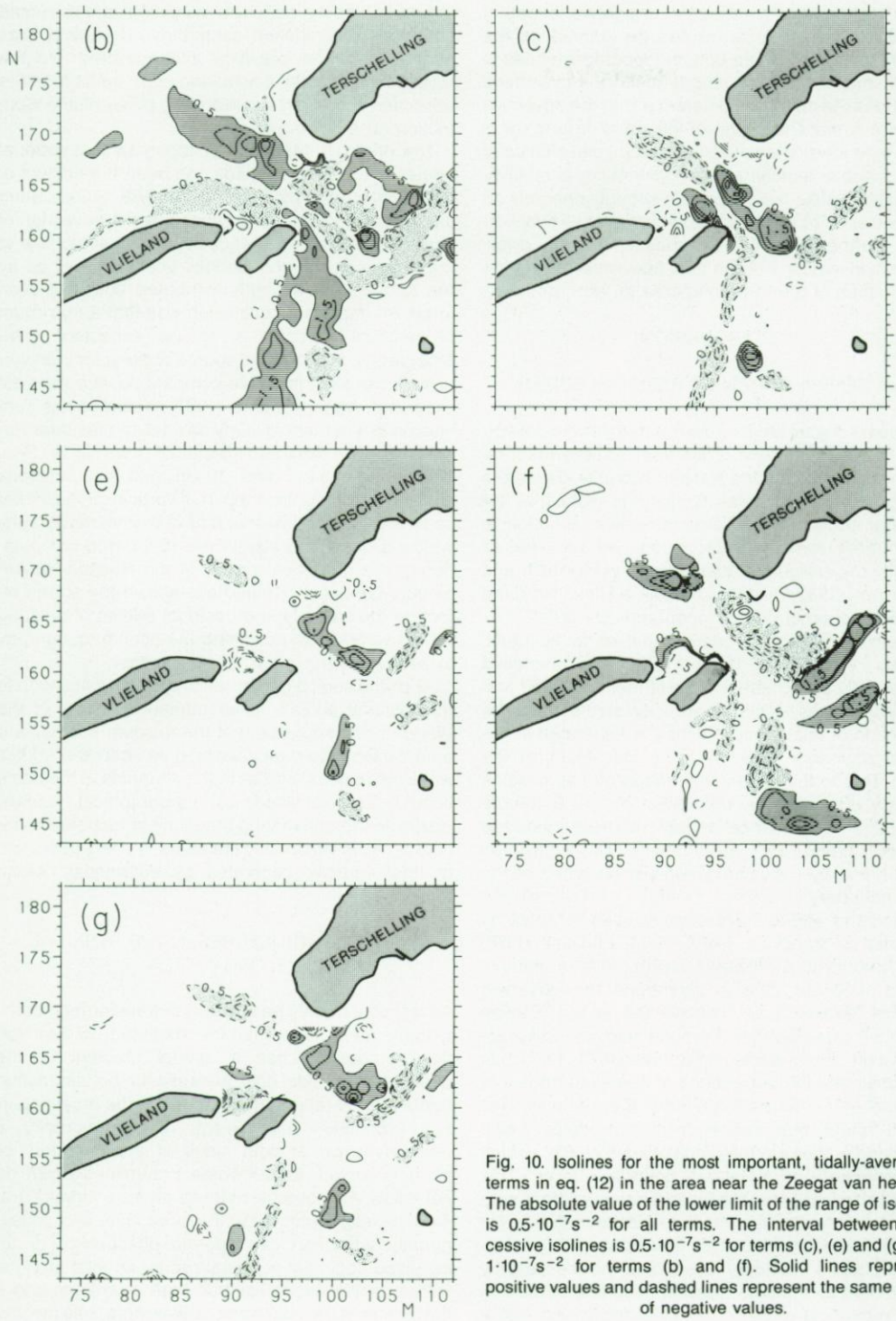

Fig. 10. Isolines for the most important, tidally-averaged, terms in eq. (12) in the area near the Zeegat van het Vlie. The absolute value of the lower limit of the range of isolines is $0.5 \cdot 10^{-7} s^{-2}$ for all terms. The interval between successive isolines is $0.5 \cdot 10^{-7} s^{-2}$ for terms (c), (e) and (g) and $1 \cdot 10^{-7} s^{-2}$ for terms (b) and (f). Solid lines represent positive values and dashed lines represent the same range of negative values.

cross-section. The contribution of tidal variations in the water level to term (c) can be ignored as the length scale over which bottom topography varies is much smaller than the length scale of sea surface variations. An important difference with the advective term (b) is that the region of influence of term (b) is more extended. The advective term (b) can also be of importance in regions where tidal vorticity is relatively small because the magnitude strongly depends on the existence of a spatial gradient of relative tidal vorticity. Furthermore, the dependence on the divergence/convergence of the tidal flow limits the region of influence of term (c) compared to term (b).

5. DISCUSSION

5.1. CLASSIFICATION OF RESIDUAL EDDIES

Residual vorticity stems from the transfer of tidal vorticity to the mean field. Thus tidal vorticity must be present to make such a transfer possible. Therefore the production of tidal vorticity is essential for residual eddies. The geomorphological situation in which tidal vorticity is produced can be used to classify the residual eddies. ZIMMERMAN (1981) and ROBINSON (1983) distinguish basin eddies, headland eddies and sandridge or topographical eddies.

Basin eddies have been identified in hydraulic models by YANAGI (1976, 1978) and modelled numerically by OONISHI (1977). In their idealised rectangular basins, residual vorticity stems from the advection of tidal vorticity which is generated in the lateral boundary layer near the side walls of the basin. Due to the rectangular shape of these basins vorticity production by differential bottom friction is absent. In a numerical model of these idealized basins, production of vorticity can only be guaranteed by imposing a non-slip condition at the rigid boundary.

Headland eddies have been studied in detail by PINGREE & MADDOCK (1977, 1979), PINGREE (1978) and MADDOCK & PINGREE (1978). In a numerical model they are able to reproduce the observed residual eddies near Portland Bill in the English Channel, provided that the non-linear advective acceleration terms are included. TEE (1976, 1977) has demonstrated the occurrence of headland eddies in a model of the Minas Basin in the Bay of Fundy. TEE (1977) found that similar to basin eddies these headland eddies are the result of advection of vorticity generated in a lateral boundary layer. This mechanism indicates the importance of using a non-slip boundary condition at the rigid boundary in his model. However, PINGREE & MADDOCK (1980) showed that lateral boundary layers need not necessarily be present to simulate residual headland eddies. In their numerical model of an idealized island with a regularly sloping beach, a condition at the closed boundary was chosen such that no vorticity was generated at the coastline and advected into the model. In this model a headland eddy stems from the advection of vorticity generated by differential bottom friction on a sloping beach.

The origin of sandridge or topographical residual eddies in an open tidal sea has been the subject of analytical studies by ZIMMERMAN (1978, 1980a). Such topographical eddies are caused by the advection of vorticity generated by squeezing and stretching of planetary vorticity, the Coriolis effect, as well as by the torque from a depth-distributed bottom friction force. An important conclusion was that a maximum of residual vorticity is to be expected when topographic features, *i.e.* source regions for tidal vorticity, have a length scale comparable with the tidal excursion. ABRAHAM *et al.* (1987) confirmed this conclusion in a numerical study on tidal and residual vorticity in the Southern Bight of the North Sea. Comparing 1.5-km and 10-km grid computations showed that a significant part of vorticity at the 10-km scale was induced by that part of bottom topography which is of subgrid size in the 10 km grid computations. In a numerical model of the Hudson-Raritan estuary OEY *et al.* (1985) have shown the strong effect on the same type of residual eddies of omitting advective terms or assuming the bottom topography to be constant in a part of their model.

Applying such a geomorphological classification to the residual eddies in our numerical model of the Wadden Sea suggests that the residual eddies near a tidal inlet should be classified as headland eddies while the residual eddies in the channels of the basin should be classified as topographical eddies. However, the dominating mechanism responsible for both types is essentially the same, namely advection of tidal vorticity generated by differential bottom friction.

5.2. BASIC STRUCTURES IN THE RESIDUAL VELOCITY FIELD

Advection can only be effective in transferring vorticity to the mean field when the magnitude of tidal vorticity production has a spatial gradient in the direction of the tidal flow. Because the bottom friction torque, terms (e) and (f) in eq. (8), is the most important production mechanism, residual vorticity is relatively large at both sides of a promontory or strongly curved isobath where streamlines locally do not follow the isobaths. In these areas a vorticity gradient develops parallel to the streamline and consequently advection can operate effectively. For an idealized tidal inlet schematized by an inlet channel with a regular slope towards both coastlines and a flat bottom in the inflow and outflow area, this mecha-

nism results in a basic quadrupole structure of the residual current field. In such a schematization of the Zeegat van het Vlie, positive (negative) vorticity is advected towards the sea from the southwestern (northeastern) slope of the inlet channel during ebb and vorticity with the opposite sign is advected towards the basin from the inlet channel during flood. Averaging this (transient) phenomenon over a tidal period gives a quadrupole of residual eddies. Both eddies at the seaside of the inlet in Fig. 9 can be interpreted as the seaside part of this basic quadrupole structure. The asymmetrical location of these eddies is due to the shoal at the northern side of the inlet which lenghtens the vorticity production region and moves the centre of the clockwise rotating residual eddy in a seaward direction. This shows that the centre of the residual eddies is close to the end of a source region for tidal vorticity. The dimension of the eddies is much smaller than the excursion length of the fluid columns, which stems from the relatively strong bottom friction dissipating tidal vorticity within a few hours.

At the basin side of the inlet the residual velocity field in Fig. 9 is rather complicated. This is caused by the irregular bathymetry (see Fig. 2) which is far from the above discussed flat bathymetry in the idealized situation. At this side the bathymetry is such that distances between successive source regions for tidal vorticity are relatively small (see also Fig. 7). However, comparing Fig. 2 with Fig. 9, shows that even in this area the basic pattern can be recognized in that residual vorticity is most pronounced near strongly curved isobaths, such as channel junctions, where during part of the tidal cycle the tidal flow advects tidal vorticity from the region where it is produced.

5.3. INFLUENCE OF LATERAL FRICTION

The small influence of the lateral friction term on the residual flow pattern is illustrated in Fig. 11, which gives the residual current field in the area near the Zeegat van het Vlie when this term is neglected (ν=0 m^2s^{-1}, Fig. 11a) and when the eddy viscosity parameter is increased by a factor of 10 compared to the original computations (ν=70 m^2s^{-1}, Fig. 11b). It shows that both computations give the same results compared to the original computations with respect to the location, orientation and global dimensions of the residual eddies. Only the magnitude of the residual velocities increases/decreases somewhat by decreasing/increasing the magnitude of lateral friction. The small influence of lateral friction is partly caused by the use of a perfect slip condition in our numerical model. In reality, a coastal boundary layer acts as a source for tidal vorticity. However, the influence of such a boundary layer on the residual velocity pattern is only restricted to a small region (DE SWART & ZIMMERMAN, 1987). Furthermore, the water depth is relatively small near the coast in this area, which makes it plausible that even near the coastline differential bottom friction is the most important mechanism for producing vorticity.

5.4. LAGRANGEAN REPRESENTATION

The transfer of vorticity from source regions can also be illustrated in a Lagrangean way (ROBINSON, 1981).

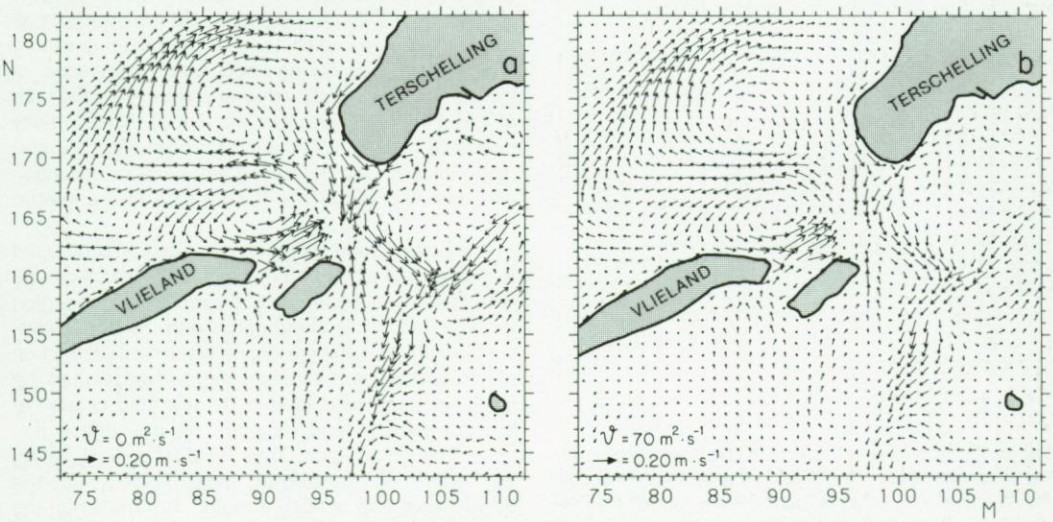

Fig. 11. Residual velocity field in the area near the Zeegat van het Vlie when lateral friction is neglected (ν=0 m^2s^{-1}, left side) and when lateral friction is increased (ν=70 m^2s^{-1}, right side) in the numerical simulation.

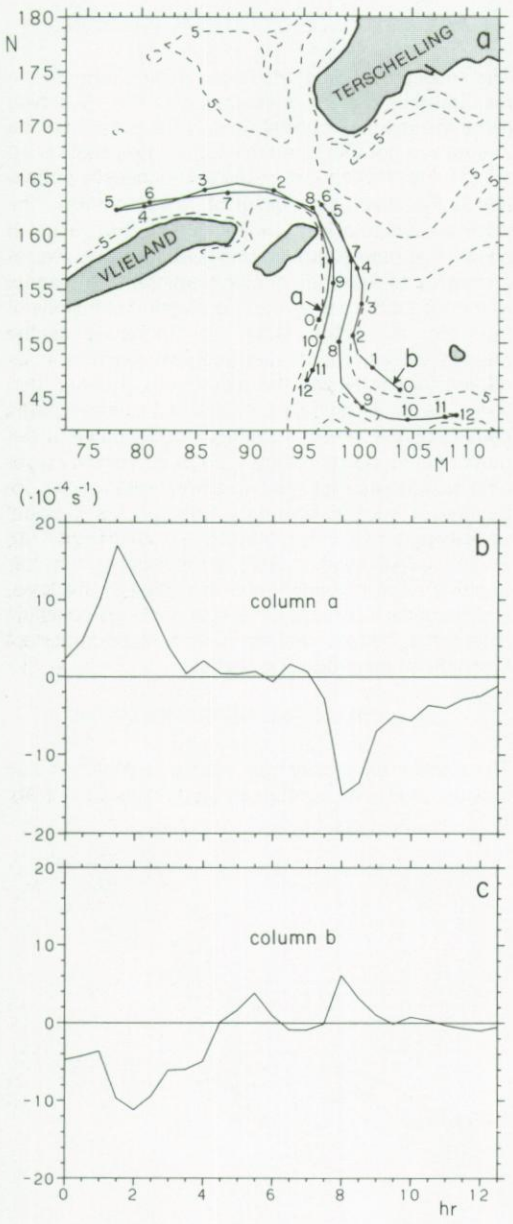

Fig. 12. Relative vorticity of two particular fluid columns during a tidal excursion. The time in this figure corresponds with the time axis in Fig. 4. (a) Trajectory of both fluid columns; (b) Relative vorticity ($\cdot 10^{-4} s^{-1}$) of column a; (c) Relative vorticity ($\cdot 10^{-4} s^{-1}$) of column b.

Fig. 12a gives computed trajectories of two particular fluid columns. The time step used for computing the Lagrangean track of these columns is 2.5 min. Figs 12b and 12c shows the relative vorticity possessed by these fluid columns (with an interval of 30 min) during their tidal excursion. The values in these figures are equal to the vorticity in the nearest grid point at the specific time level and the time axis corresponds with the time axis in Fig. 4. Fig. 12b shows that the fluid column concerned obtains positive vorticity when it moves in a seaward direction along the southwestern side of the inlet. This positive vorticity is transported towards the open sea. Before the turn of the tide, vorticity is almost completely damped away (mainly by bottom friction). During the flood period negative vorticity is obtained when the column passes the source region of the inlet. This negative vorticity is partly locally damped and partly transported to the basin side of the inlet. Fig. 12c shows that during ebb, negative vorticity produced at the eastern side wall of the main channel is transported to the basin (southeastern) side of the inlet, the same region as where during flood negative vorticity comes from the inlet promontory. This indicates that different sources can contribute vorticity to a specific region and explains the irregularity of the resulting residual vorticity pattern. The first part of the track of column b during flood is close to the centre of the main channel, which causes the vorticity possessed to be relatively small. Near a channel junction it obtains positive vorticity which is partly carried downstream.

The vorticity possessed by these fluid columns can also be discussed by comparing their trajectory with the zones for production, advection and damping during flood and ebb in Fig. 7. For instance, Fig. 7. shows that the southwestern side of the inlet acts as a strong source region for vorticity, positive during ebb and negative during flood, which is reflected in the maximum vorticity value of column a in Fig. 12b at t=1.5 hr (ebb) and t=8 hr (flood). The vorticity decrease after t=1.5 hr and t=8 hr in Fig. 12b corresponds with the increased influence of advection and damping at the sea (basin) side of the inlet in Fig. 7.

The Lagrangean representation can also be used to explain that a maximum of residual vorticity can be expected when the length of a specific source region for tidal vorticity is comparable with the tidal excursion length. Assuming a region where the production of tidal vorticity is of constant sign and larger than the local damping, relative vorticity of a fluid column at the downstream end depends on the time it has spent in such a region. Thus residual vorticity, being the result of transferring tidal vorticity at the downstream end of such a region, is large when the tidal excursion length about equals the length of the production zone. Qualitatively this agrees with results

for the open, relatively deep sea, as found analytically by ZIMMERMAN (1978, 1980a), although the conditions behind his basic, linearized, equation prevent a direct application of his analytical model to the area discussed here. The qualitative correspondence stems from the presence of the term responsible for transferring vorticity to the mean field in his and our model, *viz.* tidal advection of vorticity, while his linearized equation differs mainly from the governing equation in our numerical model in the terms producing tidal vorticity. Furthermore, the Lagrangean approach clearly illustrates that both tidal and residual vorticity cannot penetrate further than a tidal excursion length beyond the end of a production region. In the present model, this distance is even smaller due to the relatively short damping time scale. The Lagrangean approach also clarifies the restrictions to the physical meaning of Eulerian residual eddies. Fig. 12b clearly shows that the seaside of the inlet only possesses positive vorticity during ebb (t=2-3.5 for column a), while the same region does not possess voriticity during flood (t=6-7.5 for column a). Residual vorticity is the result if the vorticity present in this region is averaged over a tidal period. Thus the residual eddies are the result of averaging a transient phenomenon, only present during a relatively short period, over a complete tidal cycle, as argued by IMASATO (1983, 1987) .

5.5. THE RESIDUAL CURRENT PATTERN IN OTHER PARTS OF THE MODEL

Bottom topography and channel geometry appear to have a dominant influence on the spatial structure of the residual current velocity field near the Zeegat van het Vlie. It is now of interest to see whether the residual current field in other parts of the model can qualitatively be understood from the bathymetry.

5.5.1. ZEEGAT VAN AMELAND

Fig. 13 gives the residual current velocity field and some isobaths in the area near the Zeegat van Ameland, between Terschelling and Ameland, in the northern part of the model. At the seaside, three residual eddies can clearly be distinguished. The centre of the two clockwise eddies is located close to the downstream end of a shoal during ebb. In these regions negative vorticity produced at the sides of the shoal during ebb can be transferred to the mean field. The anticlockwise eddy close to the inlet can be classified as a headland eddy and forms the anticyclonic part of the vortex pair to be expected at this side of the inlet. The eddy at the western side dominates the flow field due to the asymmetrical geometry of the inflow area, which causes a larger spatial gradient of tidal vorticity at this side. The residual current field at the basin side of the inlet shows that the high number of promontories and channel junctions in this area causes the residual flow field to be rather irregular. However, the basic structure of a vortex pair of opposite signs at both sides of a source region for tidal vorticity can still be recognized when the velocity field is compared with the bathymetry.

5.5.2. ZEEGAT VAN TEXEL

The residual current field around the Zeegat van Texel in the southern part of the model, Fig. 14, also

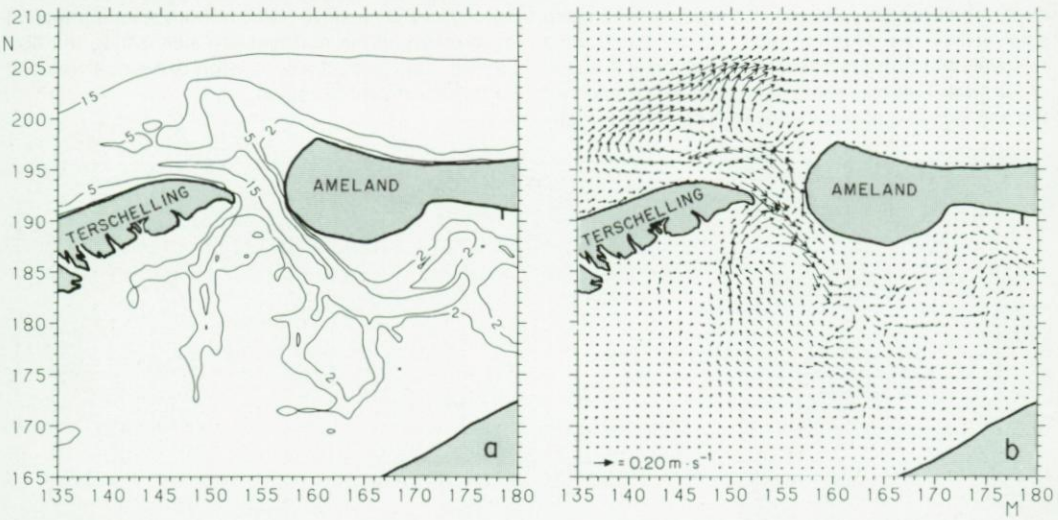

Fig. 13. Isobaths (2, 5 and 15 m) and residual velocity field in the northern part of the model, near the Zeegat van Ameland.

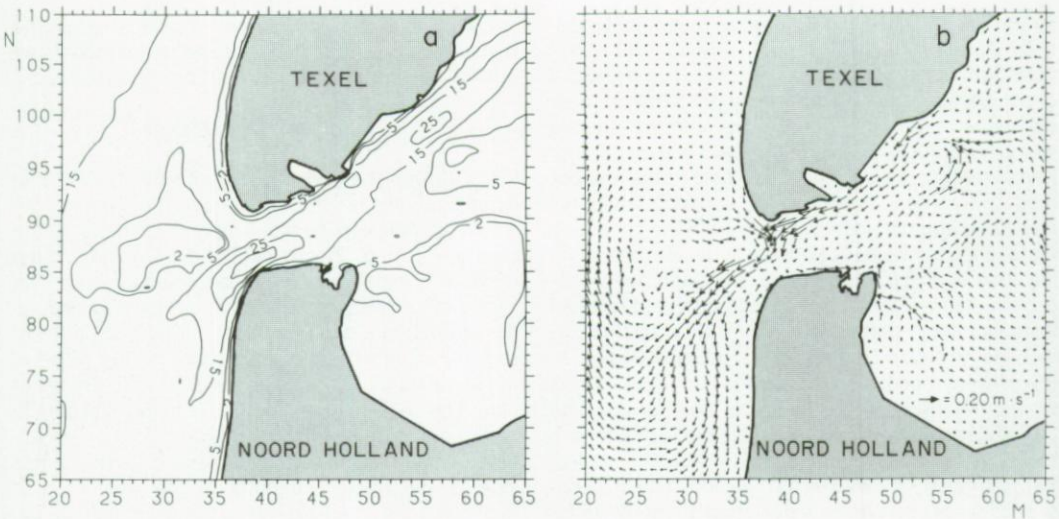

Fig. 14. Isobaths (2, 5, 15, 25 and 35 m) and residual velocity field in the southern part of the model, near the Zeegat van Texel.

deviates strongly from the quadrupole structure to be expected. The isobaths of this model part show that the depth profile around the inlet is far from regular and symmetrical. At the seaside of the inlet the residual current field is strongly influenced by a shoal which is partly emersed throughout the tidal cycle. Residual currents near this shoal are locally induced and can therefore not be associated directly with a headland eddy. The residual vorticity at the southern side of this inflow area is caused by the advection of positive vorticity generated at the southern slope of the inlet. The velocities of this headland eddy are relatively small. This is caused by the asymmetrical depth profile of the inlet with a deep hole and steep side wall at the southern side, which results in a relatively small torque from bottom friction at this side of the inlet. This also gives part of the explanation for the absence of a residual eddy with negative vorticity at the basin side of the inlet. The use of a perfect slip condition, especially at this side, can also contribute to the absence of a negatively orientated eddy in this area. However, the existence of this single, anticlockwise orientated, residual eddy is supported by field measurements (ZIMMERMAN, 1976). Thus positive vorticity generated at the northern side of the inlet during flood appears to have a dominant influence on the residual vorticity pattern. The advection of positive vorticity from the northern branch of the inflow area during flood also contributes to the sign of the resulting residual eddy. The length of this eddy is relatively large, which can be explained by the supply of positive vorticity from a topographical promontory at the northeastern side during the ebb period. This gives the same sign of residual vorticity in a relatively large region.

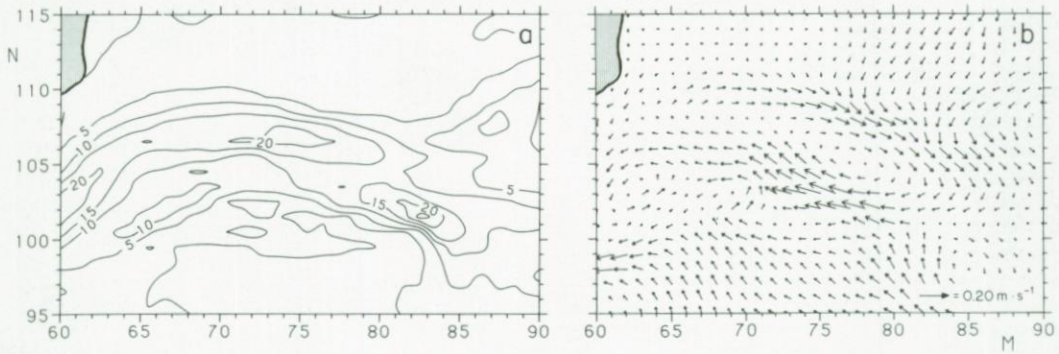

Fig. 15. Isobaths (2, 5, 15, 20 and 25 m) and residual velocity field in a channel in the inner part of the Marsdiep basin.

$$\overline{u\cdot\nabla\omega}+\overline{\omega\nabla\cdot u}-\overline{\frac{gn^2j}{(H+\zeta)^{4/3}}\cdot[ux\nabla\mid u\mid]}-\overline{gn^2j\cdot[u\mid u\mid x\nabla(H+\zeta)^{-4/3}]}+\overline{\frac{gn^2\mid u\mid}{(H+\zeta)^{4/3}}\omega}=0 \qquad (13)$$

5.5.3. INNER PART OF THE MARSDIEP BASIN

Fig. 15 shows the residual current field in the inner part of the southern basin, the Marsdiep basin, in more detail. Topographical eddies dominate the flow field in the channel. Again the bathymetry can be used to explain these eddies. The residual eddy in the centre of this figure is relatively large because this part of the channel is supplied with negative vorticity during the flood tide as well as during the ebb tide. During both tidal phases this area is just behind a source region for tidal vorticity with negative sign. Other eddies have the same type of connection with the bathymetry although their strength is less because these eddies are only present during part of the tidal cycle.

6. CONCLUSIONS

Rewriting the basic shallow water equations into a conservation equation for relative vorticity and determining the value of the different terms appear to be an appropriate way to get insight into the origin of the small-scale residual current field, the tide induced residual eddies. Numerical findings confirm that the mechanism for the generation of residual vorticity is tidal advection of a gradient of tidal vorticity, as found before in theoretical studies.

In the channels of a shallow estuary like the Wadden Sea, tidal relative vorticity is much larger than planetary vorticity. This tidal vorticity is mainly produced by differential bottom friction along the sides of the channels. Near a tidal inlet the effect of stretching/squeezing of fluid columns on the rate of change of tidal vorticity is of comparable influence as the effect of differential bottom friction. In a first approximation, the contribution of the Coriolis effect to this mechanism can be ignored, due to the large relative vorticity. Bottom friction also acts as the most important term for damping tidal vorticity and damps vorticity within one hour in the channels of the estuary and within a few hours near the tidal inlets.

Averaging the terms in the vorticity equation over a tidal period shows that the influence of the non-linear terms increases compared to the non-averaged field. However, numerical results show that for the channels of an estuary the tidally averaged vorticity equation cannot be simplified into a balance between the non-linear advection term and the damping of residual vorticity, as has been suggested for the open sea (ZIMMERMAN, 1978; ROBINSON, 1983). The non-linear stretching/squeezing term, due to the large tidal vorticity, and the non-damping part of residual bottom friction, due to the relatively large residual velocities, cannot be ignored. Thus in a first approximation the governing equation for the residual vorticity field reads: see eq. (13).

Vorticity possessed by a specific column during a tidal excursion clearly illustrates the mechanism responsible for the small scale residual current field and shows that the transfer of vorticity to the mean field is most effective at the downstream end of a source region for tidal vorticity. In our numerical model, the torque from bottom friction by depth gradients transverse to the tidal flow appears to be the dominant source of tidal vorticity. Thus residual vorticity is to be expected near a transition from straight to curved isobaths where the tidal flow locally does not follow the isobath and a gradient in production of tidal vorticity occurs. This explains the basic pattern of a quadrupole of residual eddies near a tidal inlet and a pair of residual eddies of opposite signs at both sides of a promontory in a tidal channel. However, the actual bathymetry near the tidal inlets and in the channels of the Wadden Sea is far from symmetrical and regular. This causes the actual residual eddy pattern to be rather disturbed although the basic structure can still be recognized.

According to the geomorphological background, these residual eddies can be classified as headland eddies near the tidal inlet and topographical eddies in the channels. The mechanism responsible for both types is essentially the same, *viz.* advection of tidal vorticity generated by differential bottom friction.

7. REFERENCES

ABRAHAM, G., H. GERRITSEN & G.J.H. LINDIJER, 1987. Subgrid tidally induced residual circulations.—Cont. Shelf Res. **7:** 285-305.

HUTHNANCE, J.M., 1973. Tidal current asymmetries over the Norfolk Sandbanks.—Est. coast. mar. Sci. **1:** 89-99.

IMASATO, N., 1983. What is Tide-Induced Residual Current.—J. Phys. Oceanogr. **13:** 1307-1317.

——, 1987. Application Limit of Tide-Induced Residual Current Theory.—J. Oceanogr. Soc. Jap. **43:** 319-331.

LEENDERTSE, J.J., 1967. Aspects of a computational model for long period water wave propagation. Memorandum RM-5294-PR, Rand Corporation, Santa Monica, 1967.

MADDOCK, L.& R.D. PINGREE, 1978. Numerical simulation of the Portland Tidal Eddies.—Est. coast. mar. Sci. **6:** 353-363.

OEY, L.Y., G.L. MELLOR & R.I. HIRES, 1985. Tidal modelling of the Hudson Raritan Estuary.—Est. coast. Shelf Sci. **20:** 511-527.

OONISHI, Y., 1977. A numerical study on the tidal residual flow.—J. Oceanogr. Soc. Jap. **33:** 207-218.

PINGREE, R.D., 1978. The formation of the shambles and other banks by tidal stirring of the sea.—J. mar. biol. Ass. U.K. **58:** 211-226.

PINGREE, R.D. & L. MADDOCK, 1977. Tidal residuals in the English Channel.—J. mar. biol. Ass. U.K. **57:** 339-354.

——, 1979. The tidal physics of headland flows and offshore tidal bank formation.—Mar. Geol. **32:** 269-289.

——, 1980. The effects of bottom friction and earth's rotation on an island's wake.—J. mar. biol. Ass. U.K. **60:** 499-508.

RIDDERINKHOF, H., 1988a. Tidal and residual flows in the Western Dutch Wadden Sea. I: Numerical model results.—Neth. J. Sea Res. **22:** 1-21.

——, 1988b. Tidal and residual flows in the Western Dutch Wadden Sea. II: An analytical model to study the constant flow between connected tidal basins.—Neth. J. Sea Res. **22:** 185-198.

RIEPMA, H.W., 1987. Topographically induced tidal vorticity in a shallow homogeneous sea area.—Oceanol. Acta. **10:** 393-401.

ROBINSON, I.S., 1981. Tidal vorticity and residual circulation.—Deep Sea Res. **28:** 195-212.

——, 1983. Tidally induced residual flow. In: B. JOHNS. Physical Oceanography of Coastal and Shelf Seas. 321-357.

STELLING, G.S., 1984. On the construction of computational methods for shallow water flow problems. Communications no. 35, Rijkswaterstaat, The Netherlands: 1-226.

SWART, H.E. DE & J.T.F. ZIMMERMAN, 1987. Tidal rectification in lateral viscous boundary layers of a semi-enclosed basin.—J. Fluid. Mech. **184:** 381-397.

TEE, K.T., 1976. Tide induced residual current, a 2-d non linear numerical tidal model.—J. Mar. Res. **34:** 603-628.

——, 1977. Tide induced residual current - verification of a numerical model.—J. Phys. Oceanogr. **7:** 396-402.

YANAGI, T., 1976. Fundamental study on the tidal residual circulation. I.—J. Ocenogr. Soc. Jap. **32:** 199-208.

——, 1978. Fundamental study on the tidal residual circulation. II.—J. Oceanogr. Soc. Jap. **34:** 67-72.

ZIMMERMAN, J.T.F., 1976. Mixing and flushing of tidal embayments in the western Dutch Wadden Sea. II: Analysis of mixing processes. —Neth. J. Sea Res. **10:** 397-439.

——, 1978. Topographic generation of residual circulation by oscillatory (tidal) currents.—Geophys. Astrophys. Fluid Dyn. **11:** 35-47.

——, 1980a. Vorticity transfer by tidal currents over an irregular topography.—J. Mar. Res. **38:** 601-630.

——, 1980b. Vorticity dynamics of tidal residual circulation. Proc. 17th Assembly of the ESC. Budapest, 1980: 661-664.

——, 1981. Dynamics, diffusion and geomorphological significance of tidal residual eddies.—Nature **290:** 549-555.

(received 28 September 1989; revised 14 June 1989)

TIDAL EXCHANGE BETWEEN THE NORTH SEA AND DUTCH WADDEN SEA AND MIXING TIME SCALES OF THE TIDAL BASINS*

H. RIDDERINKHOF[1], J.T.F. ZIMMERMAN[1, 2] and M.E. PHILIPPART[2]

[1]*Netherlands Institute for Sea Research, P.O. Box 59, 1790 AB Den Burg, Texel, The Netherlands*
[2]*Inst. Meteorology and Oceanography, Buys Ballot Laboratory, University Utrecht, The Netherlands*

ABSTRACT

Particle trajectories in a numerical model of the Western Dutch Wadden Sea and the adjacent North Sea are used to study the tidal exchange between the North Sea and the tidal basins. Tidal exchange of watermasses appears to depend strongly on the tidal phase at which the computation is started. In general the volume displaced by the large scale throughflow between connected tidal basins, is much smaller than the exchanged volume. For all inlets North Sea water mainly enters the Wadden Sea from the southern side of the inlet whereas basin water leaves the Wadden Sea mainly along the northern coast. Differences in exchanged volume between the inlets are caused by differences in bathymetry at the seaside of the different inlets. Schematizing each tidal basin as a single well-mixed box, in which an exchange coefficient parameterizes the exchange with the North Sea, allows a rough estimate of the turn-over time of a tidal basin. A salt balance for v a simple two-box schematisation of the Marsdiep and Vlie basin gives an independent estimate of the exchange coefficient between the Marsdiep basin and the North Sea. Its value appears to be larger than the tidally exchanged volume. The revised salt balance, in which the effect of the throughflow between the Marsdiep and Vlie basin is incorporated, is used to calculate the flushing time of fresh water in the western Dutch Wadden Sea which appears to be larger than previous estimates. The tidally exchanged volume through the inlets as calculated with the numerical model combined with the relation between the exchange coefficient and the tidally exchanged volume for the Marsdiep basin, are used to give a rough estimate of the turn-over time of all Dutch Wadden Sea basins. For the Eierlandse Gat and the Borndiep the exchanged volume is calculated by means of our hydrodynamical model. For the other basins it is assumed that its value is a fixed percentage of the tidal prism entering a basin.

1. INTRODUCTION

The Dutch Wadden Sea is a shallow, well-mixed tidal area that consists of some more or less seperated tidal basins. The shape of these tidal basins is roughly identical to a broad system of tidal channels connected to the adjacent North Sea by a relatively narrow and deep tidal inlet between the islands. The easternmost basin, the Ems-Dollart, differs in that, compared with the other basins, its shape is more elongated. Horizontal mixing has been studied in those basins which have a substantial fresh waterinput, *viz.* the Ems-Dollart (DORRESTEIN & OTTO, 1960; HELDER & RUARDY, 1982) the Marsdiep basin (POSTMA, 1954) and the connected system of the Marsdiep and Vlie basin (ZIMMERMAN, 1976a, 1976b). In these studies the fresh water content of a basin during stationary periods is used to calculate the flushing time of fresh water. In order to calculate other time scales, like the turn-over time of a basin or the flushing time of sea water, the basins are subdivided in a number of boxes. Then a tidally averaged advection-diffusion equation is used to describe the transport of an arbitrary constituent between these boxes. This approach in which 'gradient type' fluxes are accepted, has also been applied, among others, to the Eastern Scheldt (DRONKERS *et al.*, 1981) and the Bay of Fundy (HOLLOWAY, 1981). In these one- dimensional tidally averaged box models the advective horizontal velocity is induced by the fresh water input. The horizontal dispersion coefficient is either derived from equating salt exchange (dispersion) and residual salt transport (advection) during stationary periods (DORRESTEIN & OTTO, 1960; HELDER & RUARDY, 1982; ZIMMERMAN, 1976a; DRONKERS *et al.*, 1981; VAN DE KREEKE, 1990) or the formulation of this coefficient is chosen such that observed and computed salinity distributions agree reasonably (HOLLOWAY, 1981). The dispersion coefficient in these models can be interpreted as a bulk parameter. Its value lies in the range of 50-500 $m^2 s^{-1}$.

For the open sea the physical mechanism responsible for these relatively large effective dispersion coefficients is often assumed to be a cascade of shear dispersion processes (YOUNG *et al.*, 1982 and ZIMMERMAN, 1986). In the classical shear dispersion concept, dispersion due to turbulence proper is increased by the interaction of turbulence with vertical and/or horizontal shear in the velocity field. This concept was originally developed for steady turbulent flows (TAYLOR, 1954) and later extended to time-periodic turbulent flows (OKUBO, 1967). An important

Publication no. 3 of the project 'Applied Scientific Research Netherlands Institute for Sea Research'.

aspect of this concept is that random motions at small time- or length scales have to be present for an effective dispersion of watermasses to occur.

In tidal areas with a more complex bathymetry, like the Wadden Sea, this concept fails because of the inhomogeneity of the current field at length scales smaller than the tidal excursion length. Tidal trapping and pumping (FISCHER *et al.*, 1979) is one of the consequences of such longitudinal velocity variations. These longitudinal and lateral velocity variations are assumed to be the most important mechanism for dispersion, or exchange of water between different regions (ZIMMERMAN, 1976b; RIDDERINKHOF & ZIMMERMAN, 1990b). In such systems chaotic trajectories of fluid parcels may be the result of the nonlinear character of the Lagrangean particle trajectories, when expressed in the Eulerian velocity field, as has been shown by PASMANTER (1988). Anyhow, the overall effect of a spatially varying current velocity field is that water can be exchanged between different regions without the intermediate presence of small scale turbulence.

Experiments with a numerical model of the Seto Sea in Japan (IMASATO *et al.*, 1980; IMASATO, 1983; AWAJI, 1982) confirm that mixing of watermasses occurs in spatially complicated Eulerian velocity fields even if the latter does not contain any random motions. They used a Lagrangean approach by simulating the track of free flowing particles in the neighbourhood of straits and showed that the resulting mixing or exchange across the strait after one tidal period does not change significantly by adding small scale turbulence to their simulation.

In the first part of the present study we apply the Lagrangean approach to examine the tidal exchange process through the inlets of the western Dutch Wadden Sea. Particle trajectories are determined on the basis of the deterministic velocity field of our detailed two-dimensional hydrodynamical model. After a short description of the model and the applied method, we discuss first the tidal exchange between the four tidal basins and the adjacent North Sea. This tidal exchange can be interpreted as the overall effect of the horizontal mixing in the inlet region and is of great importance for the exchange of materials between the Wadden Sea and the North Sea.

In the second part a simple method is applied to estimate mixing time scales of the tidal basins. For this each tidal basin is schematized as a single well-mixed box. A salt balance during stationary periods is used for an independent estimate of the exchange coefficient between the Marsdiep basin and the North Sea. Compared with previous studies (ZIMMERMAN, 1976a) this salt balance differs in that the effect of a tidally driven throughflow is considered which influences the determination of the flushing time of freshwater from the IJsselmeer. In order to estimate the turn-over time of all tidal basins use is made of the calculations on the tidal exchange process through the inlets.

Acknowledgements.—We are much indebted to Rijkswaterstaat, Dienst Informatie Verwerking, for the use of their computer and the support in employing their extended system of computerprograms for simulating two dimensional tidal flows (WAQUA system).

2. NUMERICAL MODEL

In order to study Lagrangian trajectories in the Western Dutch Wadden Sea we use a detailed two-dimensional numerical model of the tidal flows. Fig. 1 gives the boundaries and some isobaths of this model which covers four tidal basins and a part of the adjacent North Sea in which the open boundaries are located. An ADI-method (LEENDERTSE, 1967; STELLING, 1984) is used to solve the shallow water equations:

$$\frac{\partial u}{\partial t}+u\frac{\partial u}{\partial x}+v\frac{\partial u}{\partial y}-fv=-g\frac{\partial \zeta}{\partial x}-g\frac{u\sqrt{(u^2+v^2)}}{C^2(H+\zeta)}+\nu\left(\frac{\partial^2 u}{\partial x^2}+\frac{\partial^2 u}{\partial y^2}\right) \tag{1}$$

$$\frac{\partial v}{\partial t}+u\frac{\partial v}{\partial x}+v\frac{\partial v}{\partial y}+fu=-g\frac{\partial \zeta}{\partial y}-g\frac{v\sqrt{(u^2+v^2)}}{C^2(H+\zeta)}+\nu\left(\frac{\partial^2 v}{\partial x^2}+\frac{\partial^2 v}{\partial y^2}\right) \tag{2}$$

$$\frac{\partial \zeta}{\partial t}+\frac{\partial (H+\zeta)\,u}{\partial x}+\frac{\partial (H+\zeta)\,v}{\partial y}=0 \tag{3}$$

in which:

u, v = vertically averaged velocity components
ζ = water elevation relative to a reference plane
H = depth relative to a reference plane
f = coriolis parameter
g = acceleration of gravity
ν = horizontal eddy viscosity coefficient
C = bottom friction coefficient (Chezy coefficient)

The grid size of our model is 500 m and the time step is 150 s. In the present study the trajectories of free flowing particles are computed. For this, each time step the velocity of a particle is bilinearly interpolated from the velocities in the surrounding grid points. For the integration scheme a second order midpoint rule is employed. The numerical error introduced by this method has a random character (HEEMINK, 1989; HEEMINK & VAN STIJN, 1989). For the present application this error is discussed in section 3.2.

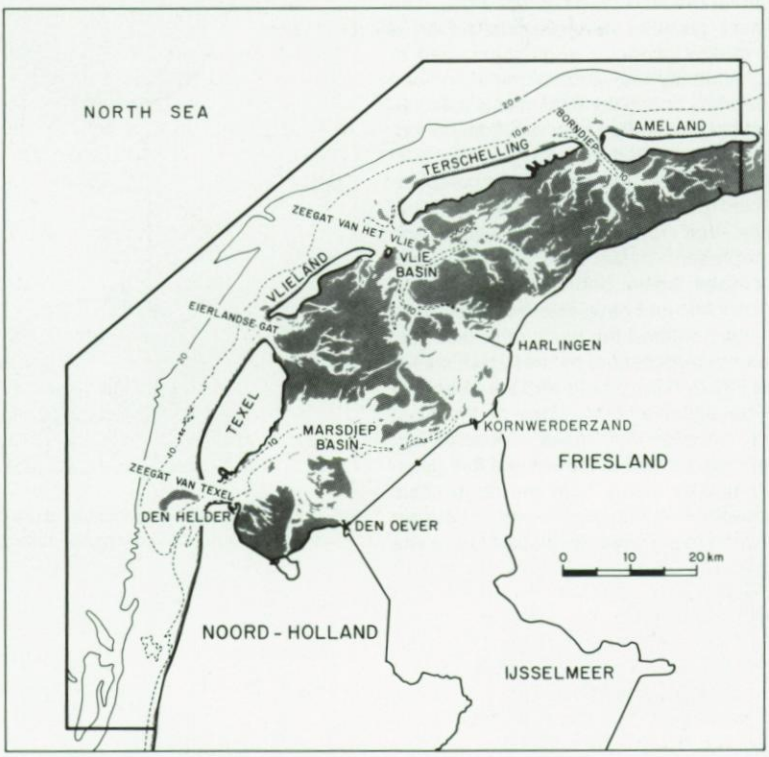

Fig. 1. Boundaries and some isobaths (10 m, 20 m) of the hydrodnamical model. Shaded areas represent tidal flats.

Results concerning the computed tidal and residual water levels and velocity field have been discussed extensively by RIDDERINKHOF (1988a, 1988b, 1989) and are summarized by RIDDERINKHOF & ZIMMERMAN (1990a). Here we only give some characteristics of the velocity field that are of interest for the present study. A characteristic value of the amplitude of the periodic tidal currents is about 1.25 ms^{-1} in the tidal inlets and about 1 ms^{-1} in the centre of the main channels. The Eulerian residual flow field can be interpreted as a composition of a small scale part, the residual eddies, and a large scale part, the throughgoing flow. In most regions residual velocities associated with the small scale part are an order of magnitude ($O(10^{-1}ms^{-1})$ larger than the velocities associated with the large scale flow ($O(10^{-2}ms^{-1})$.

3. TIDAL EXCHANGE THROUGH THE INLETS

3.1. METHOD

To determine the tidally exchanged volume through the inlets we follow the method applied by IMASATO *et al.* (1980) in which the position of labeled particles after one tidal period is used to calculate the exchanged volume. At the start of a computation the area surrounding a tidal inlet is covered with labeled particles. Each particle is located in the centre of a computational grid unit. The watervolume represented by a specific particle depends on the grid size and the local waterdepth at the start of the computation:

$$V_i = \Delta x \Delta y \, (H + \zeta) \qquad (4)$$

in which V_i is the volume represented by particle i, Δx and Δy are the grid size (500 m) and $(H+\zeta)$ is the local waterdepth at the start of the computation. The trajectory of these particles during a tidal period is calculated by means of the method mentioned in section 2. Subsequently the watervolume displaced over a fixed boundary line in the tidal inlet is calculated from the particle distribution after one tidal period. Fig. 2 shows schematically how the process of tidal exchange is quantified. At the start of the computation, t_0, the fixed boundary line discriminates between particles that represent 'sea' water and particles that represent 'basin' water. As a result of exchange processes 'basin' particles have crossed the fixed boundary line and have entered the sea and 'sea' particles have entered the basin after one tidal period. The volume represented by these particles is called V_{EX}, see Fig. 2. For a single enclosed tidal basin V_{EX} must be equal at both sides of the fixed boundary line because of mass conservation. However, in our model a part of the volume that passes this fixed boundary stems from the large scale throughflow between the tidal basins and causes an imbalance between basin water displaced to the sea

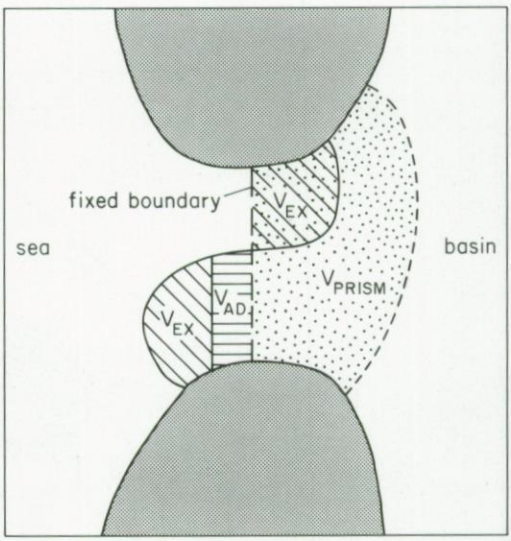

Fig. 2. Schematical representation of the quantities used in computing the tidal exchange through the inlets.

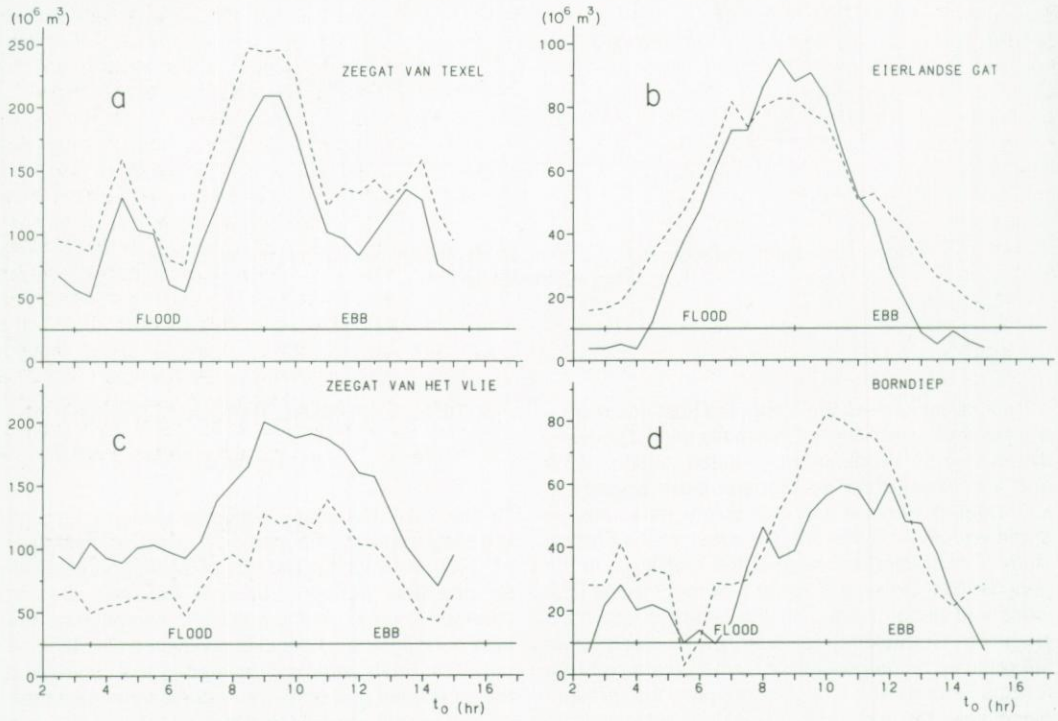

Fig. 3. Displaced volume over a fixed boundary line in the tidal inlets after one tidal period, as a function of the tidal phase at which the computation is started, t_0 (hr). Dashed lines represent the volume displaced from a Wadden Sea basin towards the North Sea and solid lines represent the volume displaced from the North Sea towards the Wadden Sea basin.

and sea water displaced to the basin. The volume associated with this large scale throughflow is known from the Eulerian computations (RIDDERINKHOF, 1988a). This part of the displaced volume is interpreted as advection and the volume involved is called V_{AD}. To have a relative measure for the tidal exchange we relate the exchanged volume to the tidal prism entering the basin during a flood period:

$$E_v = \frac{V_{EX}(t_0)}{V_p} \tag{5}$$

where E_v is called the volume exchange ratio, V_{EX} is the exchanged volume after one tidal period dependent on the time of release of the particles (t_0) and V_p the volume of the tidal prism entering the basin during a flood period. For a single inlet-basin system, the exchange ratio E_v represents the fraction of new water entering on the flood.

3.2. RESULTS

Fig. 3 shows the watervolume exchanged through the four different tidal inlets (indicated in Fig. 1) dependent on t_0, the tidal phase at which the computation is started. Solid lines give the computed volume of North Sea water that remains in a Wadden Sea basin after a tidal period and dashed lines give the volume of Wadden Sea water remaining in the North Sea. Table 1 gives the mean value of these exchanged volumes, the volume displaced by the large scale residual transport in which a positive (negative) number corresponds with a residual flow towards the North Sea (Wadden Sea), and values for the numerical error, as discussed below. The difference between both exchanged volumes should be equal to V_{AD} which is known from the Eulerian computations. This enables us to quantify the numerical error, E, that arises in the Euler-Lagrange transformation. The mean value as well as the mean absolute value of E is listed in the last columns of Table 1. The mean value is calculated over the computations with a different initial phase. For the two most important inlets draining the largest tidal basins, the Zeegat van Texel and the Zeegat van het Vlie, this error is smaller than for the inlets draining relatively small tidal basins, the Borndiep and the Eierlandse Gat. The errors seem nonetheless small enough in order to be neglected in the rest of this section.

Most striking of Fig. 3 is that the exchanged volume depends strongly on the tidal phase at which the particles are released. The maximum value of the exchanged volume is 4 to 5 times larger than the minimum value. For all inlets the exchanged volume appears to have its maximum value when the particles are released around slack tide before ebb which is approximately 1 hour after high water in the inlet. In general the water volume associated with the large scale through flow, V_{AD}, is smaller than the volume associated with the exchange processes.

For each tidal inlet Fig. 4 shows the distortion of the boundary between 'basin' and 'sea' water during a tidal period. The computation starts at slack tide before ebb for which the exchanged volume reaches its maximum value (see Fig. 3). The first picture of each series also gives the local isobaths in the area of interest. The distance between the particles marking this line is .0025 grid unit (= 1.25 m) at t_0. The position of the labeled particles is shown with an interval of 0.2 tidal period (= 9000s). In Fig. 4 we see that during the outflow (t = 0, t = 0.2T, t = 0.4T) this particle line is stretched by the spreading of the basin water in the adjacent North Sea. During this period deviations from a regular shaped boundary stem from irregularities in the bathymetry such as the shoals in front of the Zeegat van Texel, the Zeegat van het Vlie and the Borndiep. These shoals divide the watermass leaving the tidal basins in two more or less seperate watermasses. This is most clearly visible in the displacement of the boundary in the Zeegat van Texel where the shoal is emersed during the complete tidal cycle. For all inlets the southward directed ebb currents in the North Sea deflect the outflow in a southward direction. During the subsequent

TABLE 1

Mean values of the volumes displaced across a fixed boundary in the inlets and magnitude of the numerical error. V_{AD} is the volume displaced by the large scale throughflow. V_{EX}(W-N) and V_{EX}(N-W) are the volumes displaced from Wadden Sea to North Sea or from North Sea to Wadden Sea respectively. The error, E, is defined as: $E=(V_{EX}(W\text{-}N)-V_{EX}(N\text{-}W))-V_{AD}$

Inlet	V_{AD} ($10^6 m^3$)	V_{EX} (N-W) ($10^6 m^3$)	V_{EX} (W-N) ($10^6 m^3$)	$\bar{E}$ ($10^6 m^3$)	$\lvert\bar{E}\rvert$ ($10^6 m^3$)
Zeegat van Texel	36.9	113.9	147.1	3.7	11.1
Eierlandse Gat	12.1	41.2	49.3	4.0	5.2
Zeegat van het Vlie	−51.5	130.5	82.6	3.6	14.1
Borndiep	2.5	33.2	42.2	6.5	11.6

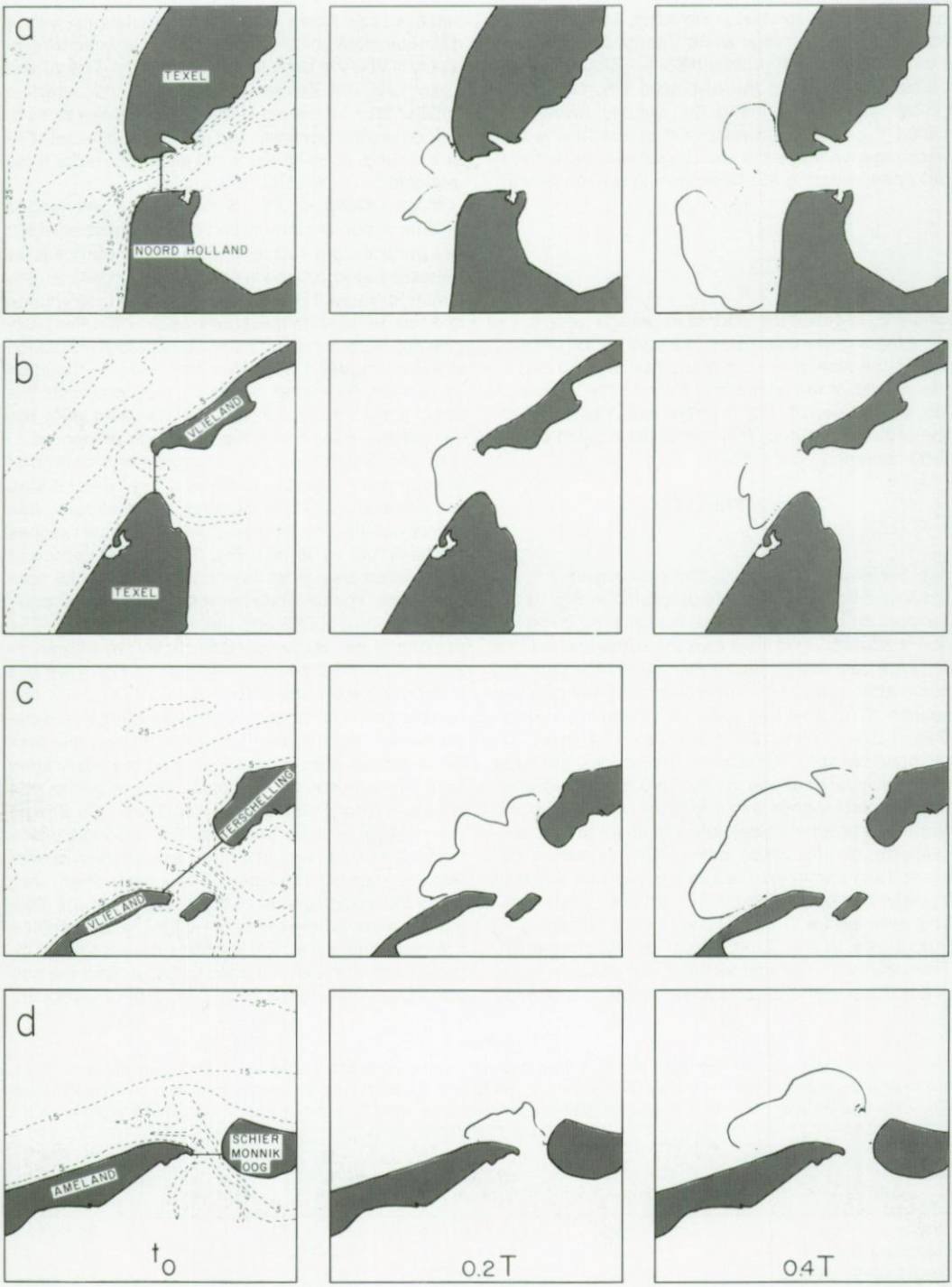

Fig. 4. Distortion of the boundary between the tidal basins and the adjacent North Sea within a tidal period. Each row gives the deformation near a specific inlet. The interval between successive pictures in a row is 0.2 tidal period. Dashed lines

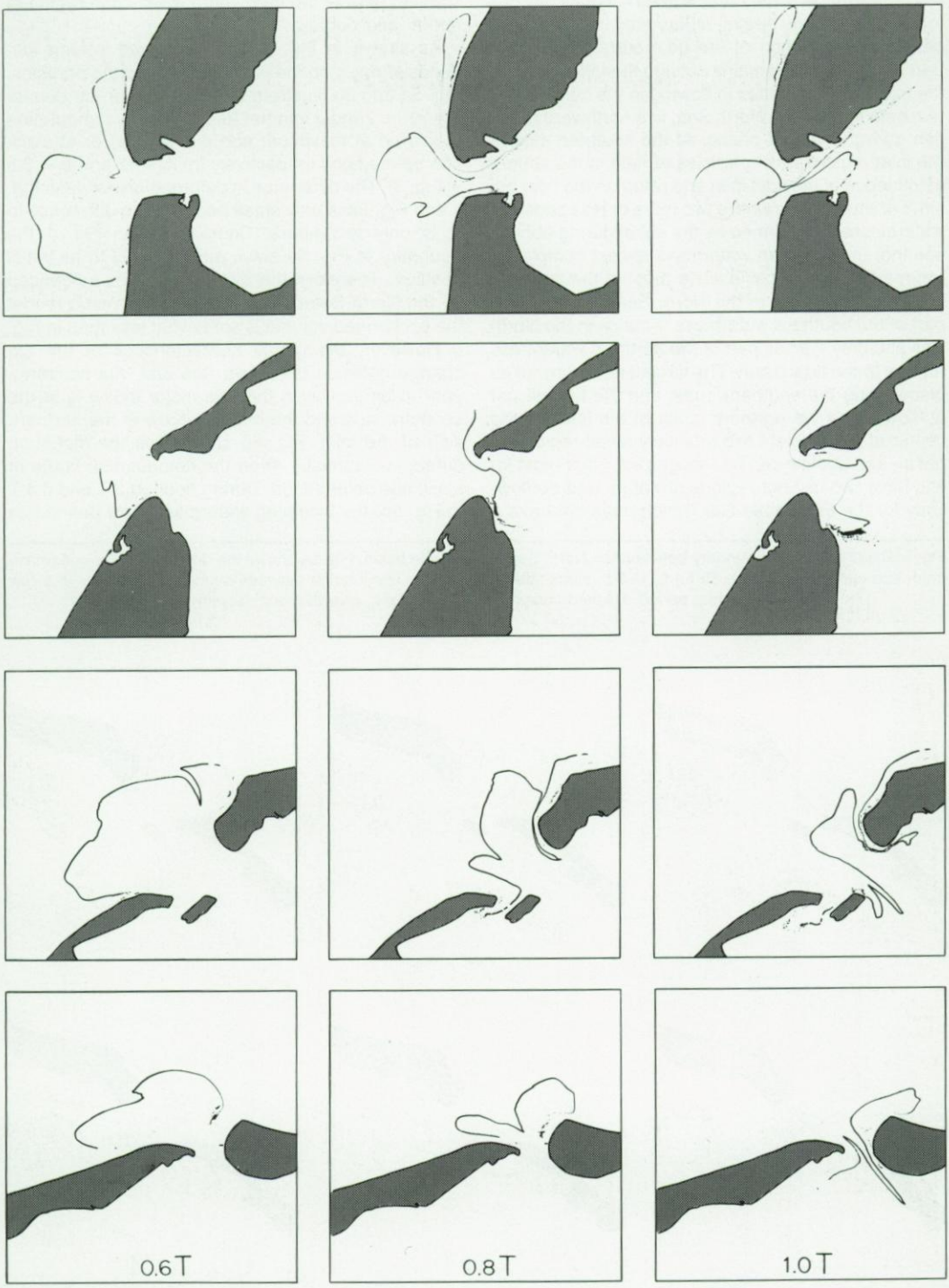

in the first column give the local isobaths (5, 15 and 25 m). Fig. a) gives the distortion in the Zeegat van Texel, b) in the Eierlandse Gat, c) in the Zeegat van het Vlie and d) in the Borndiep.

inflow the shape of the particle lines is drastically distorted due to large spatial differences in phase, amplitude and direction of the tidal currents. A small part of the volume remains outside the inflow area of the inlets and continues in flowing in the current system belonging to the North Sea, in a northward direction during this tidal phase. At the southern side of the inlet regions most particles remain in the sphere of influence of the tidal inlet and return to the tidal basin. For those inlets where two more or less seperate watermasses are formed by the shoal during ebb we see that the southern watermass almost completely returns to the tidal basin while most of the northern watermass remains in the North Sea. Only a small part of the southern watermass remains in the North Sea and only a small part of the northern watermass returns to the tidal basin. The largest net inflow takes place along the southern coast and the largest net outflow along the northern coast of the inlet. In the center of these inlets two relatively small regions of net in- and outflow can be recognized. Thus most inlets have two distinct regions of net in- and outflow. Only for the Eierlandse Gat, which does not have a shoal in front of the inlet, there is only one region of net in- and outflow.

As shown in Fig. 3 the exchanged volume depends strongly on the time of release of the particles. Fig. 5a and 5b illustrate the distortion of the boundary in the Zeegat van het Vlie when the computation is started at maximum ebb currents (a) or at slack tide before flood respectively (b) ($t_0 = 12$ and $t_0 = 3.5$ in Fig. 3). The difference in deformation between Fig. 4 and Fig. 5a is only small because the difference in t_0 is only two hours. Compared with Fig. 4 the boundary in Fig. 5a stays more closely to its initial position. Therefore the distortion is less influenced by the North Sea current system. The result is that the exchanged volume is somewhat less than in Fig. 4 However, the global characteristics of the exchange between the North Sea and Vlie basin appear to be similar in that the major inflow is at the southern side and the major outflow at the northern side of the inlet. Fig. 5b shows that the distortion differs substantially when the computation starts at slack tide before flood. During flood (0.2 T and 0.4 T in Fig. 5b) the incoming watermass, now defined as

Fig. 5. Distortion of the boundary between the North Sea and the Vlie basin. Fig. 5a shows the distortion for $t_0 = 6$ (maximum ebb currents) and Fig. 5b for $t_0 = 3.5$ (slack tide before flood) The interval between successive pictures in a row is 0.2 tidal period. Dashed lines in the picture for t_0 give the local isobaths.

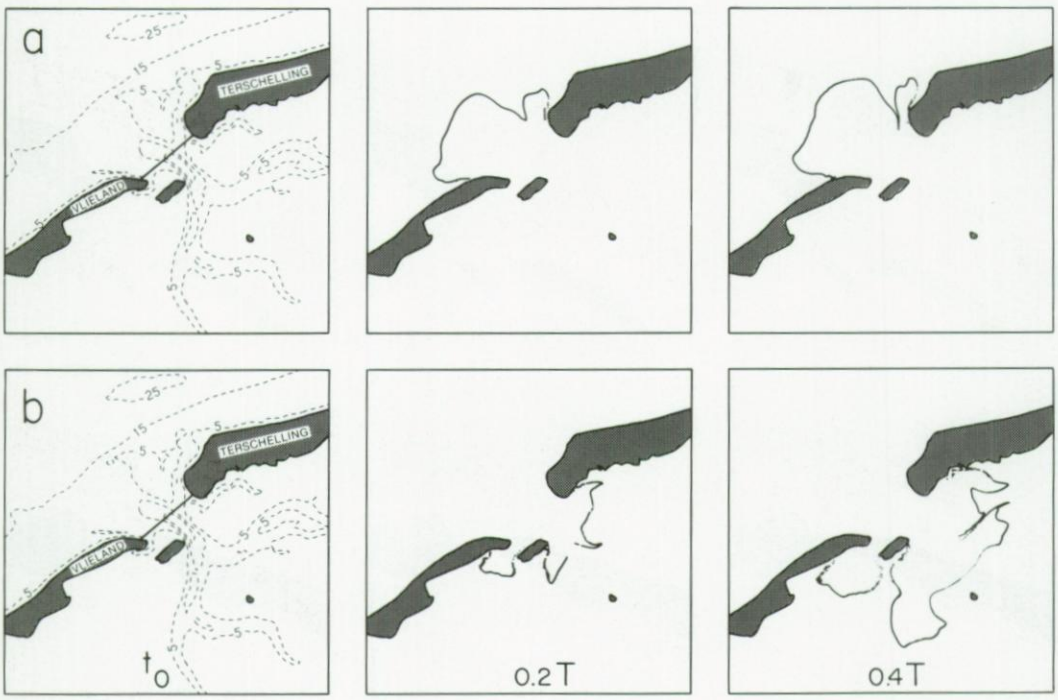

'sea' water, enters the basin mainly through two relatively large tidal channels in the centre of the basin and two relatively small channels near both islands. The shear in the velocity field in these channels makes that the boundary of each separate watermass is strongly stretched. After the reversal of the tide (0.6 T and 0.8 T in Fig. 5b) spatial phase and amplitude differences of the currents in each channel and phase differences between current systems of different channels result in a further distortion. The irregularity of the velocity field at the basin side of the inlet makes that it is hard to reconstruct the shape of the boundary after a full tidal period. However, despite the more complex shape of this boundary, the exchanged volume is less than the exchanged volume in Fig. 5a and Fig. 4. The bathymetry at the basin side is such that, compared with the seaside of the inlet, the tidal prism entering and leaving the basin is less spread out and more compressed in a channel system resulting in a smaller exchanged volume.

In summary, the deformation of the boundary between the Wadden Sea and the North Sea and consequently the exchanged volume through the inlet, depends on the velocity field through which this boundary travels. A comparison of the bathymetry at both sides of the inlet makes clear that the difference in bathymetry mainly causes the differences in velocity field at both sides. Another contribution to this difference is formed by the interaction of two different current systems at the seaside of the inlet where the velocity pattern is influenced by the in- and outflow of the tidal basin as well as by the current system in the adjacent North Sea as discussed by DRONKERS (1982) for exchange processes in an idealised inlet region. This enlarges the exchange if the particles travel primarily through this region.

This raises the question as to which value of the exchanged volume has to be used when the interest lies in the average flux of constituents from or towards a tidal basin due to tidal exchange. In fact the initial phase of these computations defines what is called 'basin' water and what is called 'sea' water. Common practice is to give the concentration distribution of a constituent for the midtide position of basin water, which is assumed to be representative for the tidally averaged concentration distribution of the mean basin volume. The midtide position of basin water corresponds approximately with the moment of maximum ebb or flood transport rate in the inlets. Therefore the value of the exchanged volume for these initial phases, when the volume of basin water

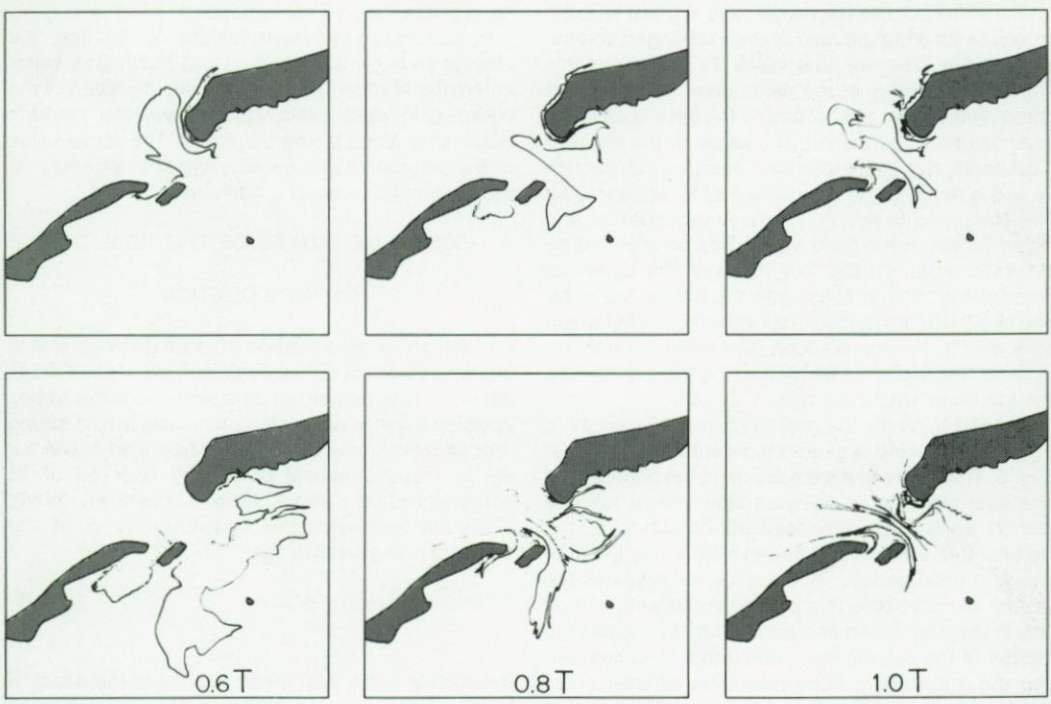

TABLE 2

Tidal prism V_p, exchanged volume, V_{EX} and volume exchange ratio, E_v.

Inlet	V_P	V_{EX} ($10^6 m^3$)			E_v (%)		
		midtide		mean	midtide		mean
	($10^6 m^3$)	flood	ebb		flood	ebb	
Zeegat van Texel	1140	113	97	112	9.9	8.5	9.8
Eierlandse Gat	195	40	45	39	20.5	23.1	20.0
Zeegat van het Vlie	1060	62	108	81	5.8	10.2	7.6
Borndiep	475	33	59	37	6.9	12.4	7.7

is approximately equal to the mean basin volume, has to be used. These values are listed in the second and third column of Table 2. For a specific inlet both values can differ substantially. Although the boundary between both watermasses travels through the same region for both initial phases, the asymmetrical bathymetry at both sides of the inlets makes that the deformation of this boundary depends on whether it travels first through the basin side or through the sea side of the inlet. No general conclusions can be drawn from these figures, *e.g.* for the Zeegat van Texel the exchanged volume is larger when the computation starts at maximum flood whereas for the Zeegat van het Vlie the exchanged volume is larger when the computation starts at maximum ebb. In the following sections the mean value of both numbers is used.

The water volume exchange ratio, E_v, is a suitable measure for a comparison of the exchanged volume through the different tidal inlets. Table 2 gives this ratio and the value of the parameters used. For the three relatively large tidal basins the difference in exchange ratio is only small. The value for the smallest tidal basin, the Eierlandse Gat, deviates substantially and is much larger. The values of E_v appear to be low compared to the values for Akashi, Naruto and Kitan Straits in the Seto Inland Sea as reported by IMASATO *et al.* (1980). For these straits E_v varies from about 20% to 60%, with the largest value for the strait with the highest tidal velocity amplitude (up to 5 ms^{-1}). For the Wadden Sea inlets the tidal regime is less vigorous which may be the explanation for the lower exchange ratio.

In order to clarify the reason for the differences in E_v for different inlets of our model we have to look at Fig. 6. This figure gives the shape of the boundary of the tidal prism at its seaward side after a full ebb period as well as the seaward boundary of the volume that enters the Wadden Sea during the subsequent flood period. Thus the former indicates the border of the volume that passes the fixed boundary line in the inlet during ebb and the latter indicates the border of the volume that passes this fixed line during the subsequent flood tide. The difference between both volumes indicates the watermasses that are involved with the net exchange. It confirms the mentioned large scale features of the tidal exchange in that fresh North Sea water mainly enters the Wadden Sea from the south and basin water leaves the Wadden Sea along the northern side of the inlet. This is most clear for the Eierlandse Gat where, compared with the other inlets, the flow pattern is less disturbed by the local bathymetry. For the other inlets the major part of the outflow during ebb is deflected towards the south by a shoal at the northern side of the inlet region. By this, the region of influence of the tidal inlet during flood differs less from the region of influence during ebb, resulting in a smaller exchange ratio. This figure also shows that each inlet with a shoal in front has two distinct zones of in- and outflow. For both zones the southward shift of the tidal prism, comparing the ebb prism with the flood prism, can be recognized.

In summary, the main feature of the tidal exchange through the inlets is that North Sea water enters the Wadden Sea from the southern part of the inlet region while basin water leaves the Wadden Sea mainly along the northern part. The actual value of the volume exchange ratio depends strongly on the bathymetry around a tidal inlet.

4. MIXING TIME SCALES OF THE TIDAL BASINS

4.1. INTRODUCTION

A rough and simple method to estimate integral mixing time scales of a tidal basin can be applied if a tidal basin is schematized as a single well-mixed box in which the internal mixing processes are so strong that effectively any substance introduced in the basin is instantaneously distributed over all of its volume (VAN DE KREEKE, 1984; ZIMMERMAN, 1988). Then the basin-averaged concentration, c, of any substance is governed by:

$$V \frac{dc}{dt} = K(c(0) - c) + F_i \qquad (6)$$

in which V is the tidal mean volume of the basin, K the exchange coefficient for the water exchange with

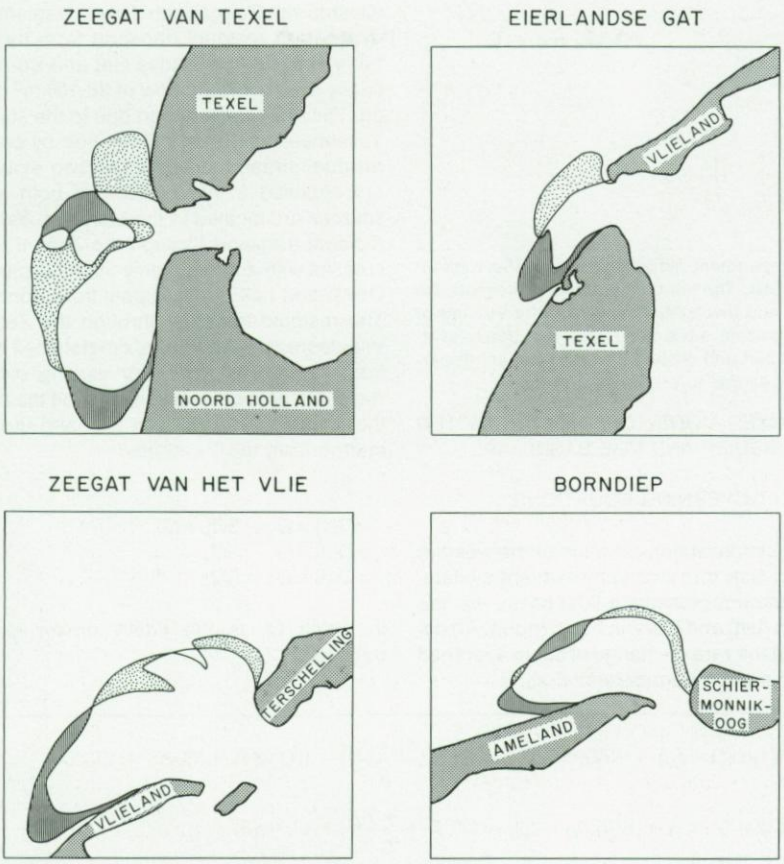

Fig. 6. Sea boundary of the tidal prism that has left the Wadden Sea during a full ebb tide (solid lines) and sea boundary of the tidal prism that enters the Wadden Sea during the subsequent flood tide (dashed lines). Dotted areas remain in the North Sea after a full tidal period and hatched areas enter the Wadden Sea.

the open sea, c(0) the concentration in the open sea and F_i the flux from an internal source.

Such a simple schematisation allows a rough estimate of the turn-over time of basin water, τ_e, defined as the time interval necessary to reduce the mass originally present in the basin to a fraction e^{-1} of the original mass:

$$\tau_e = \frac{V}{K} \tag{7}$$

Eq. (7) suggests that the turn-over time of the four tidal basins for which the tidally exchanged volume has been calculated can be estimated if we assume that K equals V_{EX} for the midtide position of basin water. Such an assumption can be tested for the Marsdiep basin. For this basin, which has a substantial fresh water input, salinity distributions during stationary periods have been measured in previous studies (POSTMA, 1954; ZIMMERMAN, 1976a). In section 4.2 these measurements are used for an independent estimate of K for the exchange between the Marsdiep basin and the North Sea. A new aspect in section 4.2 as compared with previous studies is that the effect of the large scale throughflow from the Vlie basin towards the Marsdiep basin is considered. This throughflow influences the determination of the fresh water flushing time as discussed in section 4.2.3. Finally, in section 4.3 the turn-over time of all Dutch Wadden Sea basins is estimated.

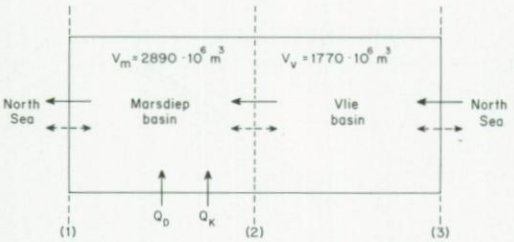

Fig. 7. Two compartment schematization of the western Dutch Wadden Sea. The left compartment represents the Marsdiep basin and the right comparment the Vlie basin. Solid arrows represent advective fluxes due tidally averaged mass transport and dashed arrows represent dispersive fluxes due to exchange processes.

4.2. A TWO-BOXES MODEL OF THE CONNECTED MARSDIEP AND VLIE BASIN

4.2.1. GOVERNING EQUATIONS

Fig. 7 shows a simple schematisation of the western Dutch Wadden Sea in a two compartment system. Each compartment represents a tidal basin, *viz.* the Marsdiep basin (left) and the Vlie basin (right). Analogously to eq. (6) the rate of change of basin averaged concentrations can be parameterized as:

$$V_M \frac{dc_M}{dt} = K(1)(c(1) - c_M) + K(2)(c_V - c_M) + Q(2)\left(\frac{c_V + c_M}{2}\right) - Q(1)c(1) + Q_D c_D + Q_K c_K$$

$$V_V \frac{dc_V}{dt} = K(3)(c(3) - c_V) + K(2)(c_M - c_V) - Q(2)\left(\frac{c_V + c_M}{2}\right) + Q(3)c(3) \qquad (8)$$

in which V_M and V_v are the tidal mean volumes of the Marsdiep and Vlie basin respectively, c_M and c_v the corresponding basin averaged concentrations, K(i) the exchange coefficient for boundary (i) and Q_K,Q_D and c_K,c_D the discharge and concentration from the sluice at Kornwerderzand and den Oever respectively. The difference with a single box schematization is that this two-box model allows a flux of constituents across the boundary between the Marsdiep and Vlie basin. Fluxes due to the residual mass transport (terms including Q(i)) are referred to as advective fluxes and fluxes due to exchange processes (terms including K(i)) as dispersive fluxes.

With respect to the advective fluxes we only consider the residual transport caused by the tide and by the discharge from both sluices. The internally tidally driven residual transport has been determined with our detailed hydrodynamical model (RIDDERINKHOF, 1988a) From the residual streamfunction (fig. 14 in RIDDERINKHOF, 1988a) it is clear that the major throughflow is directed from the Zeegat van het Vlie towards the Zeegat van Texel. Neglecting the relatively small residual transport from the Zeegat van het Vlie to the Eierlandse Gat and Borndiep gives a tidally driven throughflow of $36 \cdot 10^6$ m^3 per tidal period. The residual transport due to the supply from the Ysselmeer has been determined by calculating the residual streamfunction when two external sources are imposed at the position of both sluices. Both sources are located in the Marsdiep basin. Then the residual transport through the Zeegat van Texel increases with approximately the total supply from den Oever and half of the supply from Kornwerderzand. The residual transport through the Zeegat van het Vlie decreases with approximately half of the supply from Kornwerderzand. For varying discharges the residual transport is assumed to be the summation of the constant tidally driven part and the varying discharge from the Ysselmeer:

$$\begin{aligned} Q(1) &= Q_T + .5Q_K + Q_D \\ Q(2) &= Q_T - .5Q_K \\ Q(3) &= Q_T - .5Q_K \end{aligned} \qquad (9)$$

in which Q_T is the tidally driven residual mass transport.

4.2.2. SALT FLUXES DURING STATIONARY PERIODS

Table 3 gives the supply from the Ysselmeer, the basin averaged salinities, and the observed salinities at the sea boundary of both basins for three periods which have a more or less stationary salinity distribution (ZIMMERMAN, 1976a). Period 1 is representative for a period of low supply, period 2 for an average supply and period 3 for a high supply. The general characteristics of the longitudinal salinity distribution along the main axes connecting the Marsdiep and Vlie basin during these periods are schematized in Fig. 8 (deduced from fig. 7 in ZIMMERMAN,1976a).

The first three columns of Table 4 give the advective salt fluxes during these periods, F_{AD}, which have been determined by applying:

$$F_{AD}(i) = Q(i)s(i) \qquad (10)$$

TABLE 3

Parameters derived from Zimmerman's observations (1976a) which are used in the salt balance calculations (see Fig. 7.). S(1) and s(3) are the tidally averaged salinity at the sea boundary of the Marsdiep and Vlie basin and s_M and s_V are the basin averaged salinity of the Marsdiep and Vlie basin.

Period	Q_D ($10^6 m^3 T^{-1}$)	Q_k ($10^6 m^3 T^{-1}$)	*s(1)* (ppt)	*s(3)* (ppt)	s_M (ppt)	s_V (ppt)
1	12.0	0	30.5	32.5	28.7	32.3
2	11.9	8.8	30.5	30.8	26.7	29.5
3	25.3	18.5	25.0	28.5	18.4	25.7

in which s(i) is the salinity at boundary (i). For the salinity at boundary (2) the value $s(2) = (s_M + s_V)/2$ has been taken (analogously to eq. 7.).

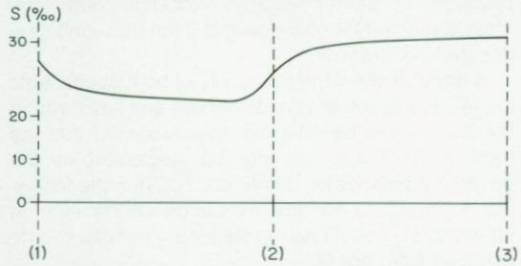

Fig. 8. Schematized longitudinal salinity distribution in the main channels of the connected Marsdiep and Vlie basin during stationary periods.

The assumption of stationarity makes that the difference in advective fluxes towards a tidal basin must be balanced by a net dispersive flux across the boundaries. Fig. 8 shows that there exists an obvious increase of the salinity gradient near the Zeegat van Texel as compared with gradients further in the basin. The opposite can be remarked about the Vlie basin, *viz.* a strong decrease of the salinity gradient near the tidal inlet as compared with gradients further in the Vlie basin. Thus Fig. 8 suggests that the dispersive salt flux across the inlet of the Vlie basin can be neglected during stationary periods. Introducing this assumption, which makes sense only for stationary situations, implies that during each period the dispersive salt flux across the other boundaries must be equal to the difference between the advective flux through the Zeegat van het Vlie and the advective flux across the boundary considered. Thus the dispersive salt flux across boundary (1) and (2), F_D, can be calculated independently from the exchange coefficients at these boundaries

$$F_D(i) = F_{AD}(3) - F_{AD}(i), \quad i = 1,2 \qquad (11)$$

The last two columns of Table 4 give the dispersive salt fluxes for the different periods.

4.2.3. EXCHANGE COEFFICIENTS

Substituting the values from Table 3 and 4 in the parameterizations for the dispersive fluxes in eq. (7) gives the exchange coefficients listed in Table 5.

TABLE 4

Advective and dispersive salt fluxes across the boundaries during stationary periods. A positive flux is directed southwards (from rigth to left in Fig. 7).

	boundary				
	F_{AD} ($\cdot 10^6 m^3 T^{-1} ppt$)			F_D ($\cdot 10^6 m^3 T^{-1} ppt$)	
period	*(1)*	*(2)*	*(3)*	*(1)*	*(2)*
1	1464	1098	1170	−294	72
2	1595	888	973	−622	85
3	1764	591	762	−1002	171

For the Zeegat van Texel the exchange coefficients are nearly equal which suggests that the ever present tidal exchange is the most dominant process for the exchange between the Wadden Sea and the North Sea. However, its value is about 1.5 times larger than the mean value of V_{EX} for the midtide position of basin water. This may be due to the fact that V_{EX} has been computed on the basis of a two-dimensional tidal current field whereas in reality three dimensional aspects, wind *etc.* may also play a role so that the exchanged volume in reality is larger. The exchange coefficients across the boundary between both basins appear to be much smaller than the exchange coefficient across the inlet. In this area the amplitude of the tidal currents is small resulting in relatively weak mixing.

TABLE 5

Exchange coefficients for boundary (1) and (2).

	$K(\cdot 10^6 m^3 T^{-1})$	
Period	*(1)*	*(2)*
1	163	20
2	164	30
3	152	23

The exchange coefficients K(1) and K(2) depend on the way of parametrizing the dispersive salt flux in the form given in (7). Its calculated value depends on [1]) the magnitude and direction of the throughflow and [2]) on the assumption of zero dispersive flux through the Zeegat van het Vlie.

The magnitude of the throughflow used to calculate the advective fluxes is questionable mainly because in reality density differences and/or wind may influence this flow. Therefore the sensitivity of the calculated exchange coefficients to the magnitude of Q_T is discussed. From eq. (7) the following expression can be deduced for the exchange coefficient at both boundaries:

$$K(1) = \frac{Q_T(s(1)-s(3)) + .5Q_K(s(1)+s(3)) + Q_D s(1)}{s(1)-s_m}$$

$$K(2) = \frac{Q_T(s(3)-s(2)) + .5Q_K(s(3)-s(2))}{s_v-s_m} \qquad (12)$$

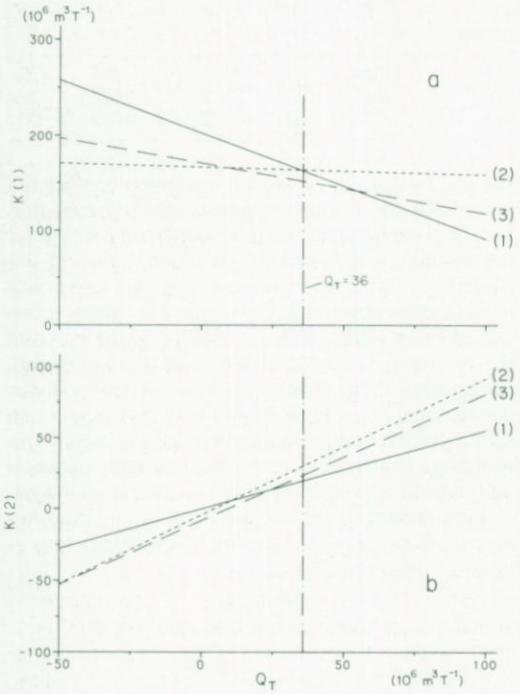

Fig. 9. The exchange coefficient at boundary (1), K (1) in Fig. 9, and at boundary (2), K(2) in Fig. 9, for three different stationary periods as a function of the magnitude of the tidally driven throughflow, Q, see eq. (12).

The dependence of both K values on the throughflow, Q_T, is shown in Fig. 9a and 9b. The salinity difference between both sea boundaries determines the influence of the throughflow on K(1), the exchange coefficient between the Marsdiep basin and the adjacent sea. Therefore the dependence of K(1) on Q_T is relatively large during period 2 and relatively small during period 3. Fig. 9a clearly shows that the magnitude of the throughflow as calculated with our hydrodynamical model ($Q_T = 36 \cdot 10^6 m^3 T^{-1}$) corresponds with a zone of minimum differences between values for K(1) for the different observation periods. Fig. 9b shows that for all 4 periods a northward throughflow (Q_T negative) would require a physically unrealistic negative exchange coefficient. Thus stationarity is only possible if the throughflow is directed southwards.

In order to show the sensitivity of both coefficients to the assumption of zero dispersive salt flux through the Zeegat van het Vlie it is now assumed that the term $K(3)(s(3)-s_v)$ can not be neglected in the governing balance equation (eq. 7). Then the following expressions for the exchange coefficients at boundary (1) and (2) during stationary periods can be decuced from eq. (7):

$$K(1) = \frac{Q_T(s(1)-s(3)) + .5Q_K(s(1) + s(3)) + Q_D s(1)}{s(1)-s_m}$$

$$- \frac{K(3)(s(3) - s_V)}{s(1)-s_m} \qquad (13)$$

$$K(2) = \frac{Q_T(s(3)-s(2)) - .5Q_K(s(3)-s(2)) + K(3)(s(3)-s_V)}{s_v-s_m}$$

Fig. 10a and 10b show the values of K(1) and K(2) respectively as a function of the value of K(3). Both figures show that with increasing dispersive salt flux through the Zeegat van het Vlie, the exchange coefficients required to preserve stationarity diverge for the different periods. Thus a zero dispersive flux corresponds with a minimum in difference between K values for different observation periods.

In summary, both Fig. 9 and Fig 10 show that the observed salinity distributions make it plausible that there exists a southward throughflow through the system during these periods and that the dispersive salt flux through the Zeegat van het Vlie can be neglected during stationary periods.

4.2.4. FLUSHING TIME OF YSSELMEERWATER

The flushing time of fresh water, τ_f, is given by:

$$\tau_f = \frac{V_f}{Q_f} \qquad (14)$$

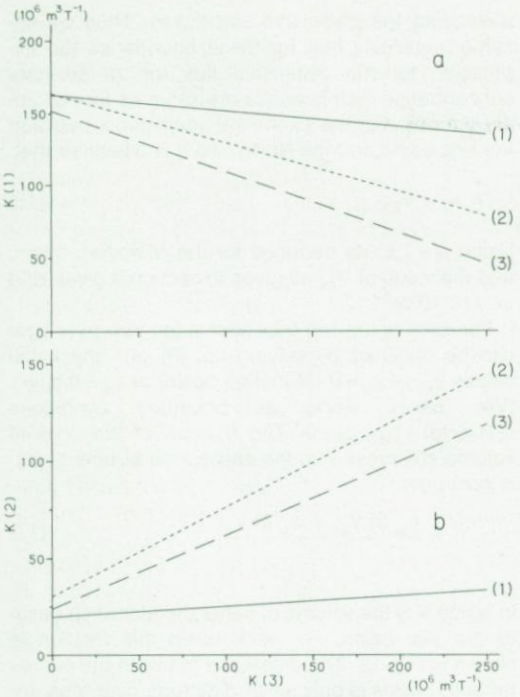

Fig. 10. The exchange coefficient at boundary (1), K (1) in Fig. 10 and at boundary (2), K(2) in Fig. 10 for three different stationary periods as a function of the magnitude of the salt flux through the Zeegat van het Vlie, see eq. (13).

in which V_f is the fresh water content and Q_f is the fresh water discharge to the basin. The fresh water content of a single basin can be determined from the difference between the basin averaged salinity and the sea water salinity at the sea boundary. In our two-box model we need to know the volume of the sea water originating from the Zeegat van het Vlie and from the Zeegat van Texel because the salinity of both 'sea water fractions' differs. In general the salinity at the inlet of the Vlie basin is higher (Table 3).

From eq. (7) the following expressions can be deduced for the basin averaged concentration of an arbitrary constituent that is distributed like salt during stationary periods:

$$c_M = \frac{(K(1) - Q(1))c(1) + Q(3)c(3) + Q_K c_K + Q_D c_D}{K(1)}$$

$$c_V = \frac{(K(2) - .5Q(2))c_M + Q(3)c(3)}{K(2) + .5Q(2)} \qquad (15)$$

TABLE 6

Volume fraction from different sources present in a tidal basin during period 2.

	Volume fraction	
source	*Marsdiep basin*	*Vlie basin*
den Oever	7.4	0.4
Zeegat Texel	70.6	3.7
Zeegat van het Vlie	22.1	95.9

The volume fractions in the Marsdiep and Vlie basin that originate from a specific source or boundary can now be calculated by substituting c = 1 for the source required and c = 0 for the other sources or boundaries. Results for period 2 with only discharge near den Oever are presented in Table 6. Abouth 20 percent of the water present in the Marsdiep basin appears to originate from the Zeegat van het Vlie whereas only a few percent of the Vlie basin water originates from the Zeegat van Texel. Multiplying the volume fraction originating from den Oever with the basin volumes gives the fresh water fraction present in the area. Now the flushing time of fresh water discharged near den Oever can be calculated by applying eq. (12) resulting in τ_D = 18T. This value appears to be larger than the values reported by POSTMA (1954) and ZIMMERMAN (1976a) (τ_D = 13T and τ_D = 15T respectively) although the same observed salinities are used as in the latter study. Compared with their model a larger amount of sea water originating from the Zeegat van het Vlie is present in the area due to the southward directed throughflow. The salinity of this fraction (32.5 ppt) is substantially larger than the salinity of the fraction from the Zeegat van Texel (30.5 ppt). This increases the average 'sea' water salinity which has to be used to determine the fresh water content. Consequently the fresh water content and flushing time increase.

In order to calculate the flushing time of the discharge near Kornwerderzand for period 3 and 4 two methods can be applied. In the first method it is assumed that the flushing time of the discharge near den Oever for period 3 and 4 is the same as the value for period 2, *viz.* τ_D = 18T. Multiplying this flushing time with the discharge at den Oever during period 3 and 4 gives the fresh water fractions originating from this source during these periods. Subtracting this amount from the total fresh water content gives the content of fresh water originating from Kornwerderzand. The flushing time from the latter is then again obtained by applying eq. (18). The result is τ_k = 25T for period 3 and τ_k = 27T for period 4. ZIMMERMAN (1976a) applied this method and found a mean value of τ_k = 30T. The smaller value of the present calculation is mainly caused by the increased flushing time of fresh water discharged near

den Oever which, compared with Zimmerman's calculation, increases the fresh water fraction from den Oever during period (3) and (4).

In the second method the volume fractions from both sources during period 3 and 4 are determined by applying eq. (19) for these periods. Then the resulting flushing times are τ_D = 21T, τ_k = 21T for period 3 and τ_D = 22T, τ_k = 22T for period 4. The higher flushing time of fresh water from den Oever in the latter method is caused by the decreased advective flow between both basins, Q(2), during period 3 and 4. This makes that a larger percentage fresh water from this source is present in the Vlie basin which gives a higher flushing time. Taking the mean value of both methods gives τ_D = 20T and τ_k = 24T.

In summary, the main consequence of the throughflow through the area is that the Marsdiep basin consists of water originating from the Zeegat van Texel, the Zeegat van het Vlie and the Ysselmeer. Thus in order to calculate the fresh water content in the Marsdiep basin the salinity of the sea water from the Zeegat van het Vlie has to be taken into account, resulting in a larger fresh water content compared with previous estimates.

4.3. TURN-OVER TIME OF TIDAL BASINS

4.3.1. MARSDIEP AND VLIE BASIN

The turn-over time is defined as the time interval necessary to reduce the mass present in a basin to a fraction e^{-1} of the original mass. Thus, in contradiction with the previous calculations for stationary situations, this time scale is calculated from the rate of change of basin averaged concentrations before reaching stationarity. Before reaching stationarity the dispersive flux through the Zeegat van het Vlie cannot be neglected. Thus to calculate the turn-over time we have to apply eq. (8) which includes the dispersive flux through the Zeegat van het Vlie. The values of the parameters used are listed in Table 7.

TABLE 7

Parameters used in the two compartment model to calculate turn-over time scales.

boundary	$Q(\cdot 10^6 m^3 T^{-1})$	$K(\cdot 10^6 m^3 T^{-1})$
1	50	160
2	33	24
3	33	140

The residual mass transport follows from eq. (9) using the annual mean values for Q_D ($11 \cdot 10^6 m^3 T^{-1}$) and Q_k ($6 \cdot 10^6 m^3 T^{-1}$). The exchange coefficients at the boundary (1) and (2) are the mean values of the coefficients for period 1, 2 and 3 as used in parameterizing the dispersive salt fluxes. Thus we assume implicitely that for these boundaries the expression for the dispersive flux for an arbitrary concentration distribution is the same as for stationary periods. For the exchange coefficients between the Vlie basin and the North Sea it is assumed that:

$$K = \alpha V_{EX} \tag{16}$$

Using $\alpha = 1.5$, as deduced for the Marsdiep basin, and the value of V_{EX} as given in section 3 gives K(3) = $140 \cdot 10^6 m^3 T^{-1}$.

For each of the two tidal basins the turn-over time can be obtained by solving eq. (8) with the initial values $c_M = 1, c_V = 0$ (Marsdiep basin) or $c_D = 0, c_V = 1$ (Vlie basin) using as boundary conditions $c(1) = c(3) = c_D = c_k = 0$. The fraction of the original volume still present in the entire area at time t, $\gamma(t)$, is given by:

$$\gamma(t) = \frac{c_M(t)\, V_M + c_V(t)\, V_V}{V} \tag{17}$$

in which V is the volume of either the Marsdiep basin or the Vlie basin. For each basin this fraction is shown in Fig. 11. The difference between the curves for both basins is only small. The turn- over time appears to be 17.4 T for the Marsdiep basin and 12.7 T for the Vlie basin. Neglecting the throughflow (Q = 0) gives 17.1 T and 12.5 T for the Marsdiep and Vlie basin respectively. Thus the influence of the throughflow on this time scale can be neglected.

The value for the exchange coefficients used in our model are about 25 percent smaller than the values used by POSTMA (1954) and ZIMMERMAN (1976) resulting in a larger turn-over time of both basins as compared with their estimates.

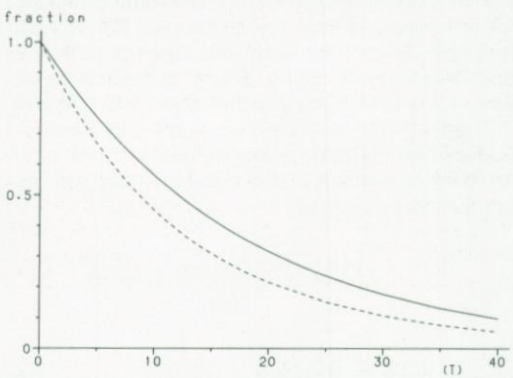

Fig. 11. Volume of basin water still present in the western Dutch Wadden Sea at time t as a fraction of the original volume which is either the volume of the Marsdiep basin (solid line) or the volume of the Vlie basin (dashed line).

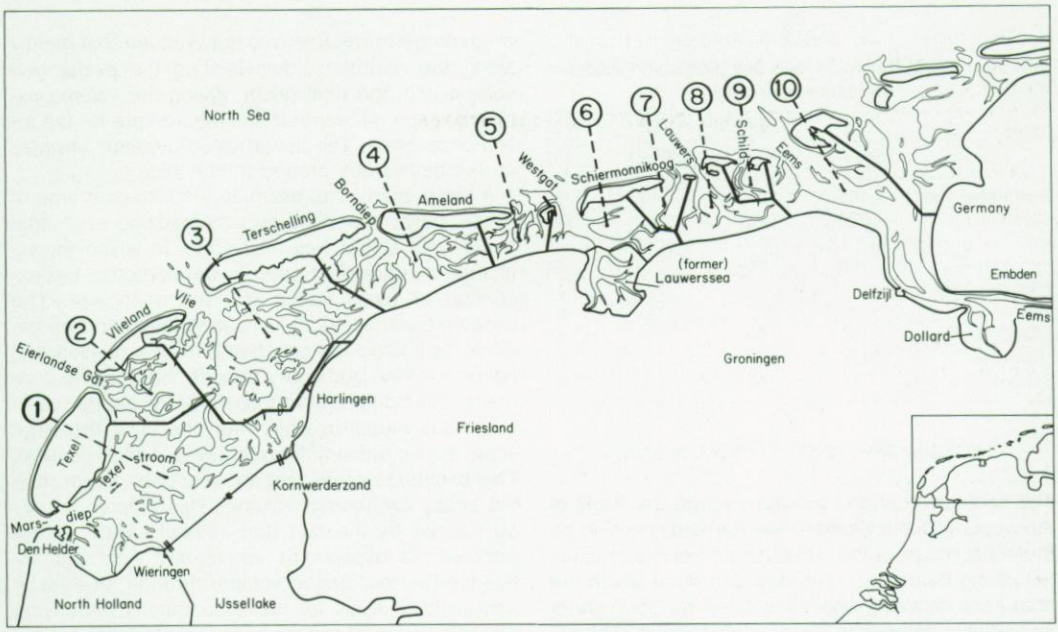

Fig. 12. Map of the tidal basins in the Dutch Wadden Sea. Thick solid lines indicate the area drained by a tidal inlet. 1 – Marsdiep, 2 – Eierelandse Gat, 3 – Vlie, 4 – Borndiep, 5 – Pinkegat, 6 – Friesche Zeegat, 7 – Eilanderbalg, 8 – Lauwers, 9 – Schild, 10 – Ems-Dollart.

4.3.2. OTHER TIDAL BASINS

A map of the tidal basins in the entire Dutch Wadden Sea is shown in Fig. 12. The shape of these tidal basins is roughly identical to the shape of the Vlie basin. A relatively narrow and deep tidal inlet connects a broad system of branched tidal channels with the North Sea. Although their shape is roughly the same, the volume of these basins can differ substantially. Most basins are separated from each other by a tidal watershed that emerses during a large part of the tidal cycle. The supply of fresh water to these basins, if present, is negligible. Only the Ems Dollart differs in that its shape is more elongated and that this basin has fresh water sources of importance. Mixing time scales for this basin have been calculated by DORRESTEIN & OTTO (1960) and HELDER & RUARDIJ (1982). A rough estimate of the turn-over time scale is obtained by applying eq. (7) together with eq. (14):

$$\tau_e = \frac{V}{\alpha V_{EX}}, \quad \alpha = 1.5 \tag{18}$$

The exchanged volume through the inlets of the Eierlandse Gat and Borndiep has been calculated with our hydrodynamical model (Table 2). For the midtide position of basin water as initial value in the calculation of the trajectories the mean values are $43 \cdot 10^6 m^3 T^{-1}$ and $46 \cdot 10^6 m^3 T^{-1}$ for the Eierlandse Gat and Borndiep respectively. For the other tidal basins it is assumed that the exchanged volume through the inlets is a fixed percentage of the tidal prism entering a basin. For four western Wadden Sea basins this percentage has been calculated by means of our hydrodynamical model. For an arbitrary inlet in the eastern part of the Dutch Wadden Sea it is assumed that the exchanged volume is 8 percent of the tidal prism which is the mean percentage for the Zeegat van Texel, Zeegat van het Vlie and the Borndiep, giving:

$$\tau_e = \frac{V}{0.12 V_p} \tag{19}$$

Thus it is assumed that the relatively high exchange through the Eierlands Gat is exceptional and not representative for the other Wadden Sea basins.

Table 8 gives the tidal mean volume, the tidal prism and the resulting estimates of the turn-over time of each tidal basin. Compared with the Marsdiep and Vlie basin the turn-over time of most basins is shorter which mainly stems from the smaller dimensions of these tidal basins.

TABLE 8

Turn-over time of Dutch Wadden Sea basins and values of the parameters used.

basin	V_B ($10^6 m^3$)	V_P ($10^6 m^3$)	V_{EX} ($10^6 m^3 T^{-1}$)	τ_P (T)
Eierlandse Gat	185	195	46	3
Borndiep	670	475	43	10
Pinkegat	80	95		7
Friesche Zeegat	225	200		9
Eilanderbalg	50	80		5
Lauwers	175	190		8
Schild	45	45		8

5. SUMMARY AND CONCLUSIONS

The tidally exchanged volume through the inlets of the western Dutch Wadden Sea depends strongly on the initial phase of the computation because the initial phase determines the region through which the boundary between what is defined as 'sea' water and what is defined as 'basin' water travels. The exchanged volume to be used in calculating the average exchange of constituents is the value for the midtide position of basin water. An important feature is that for all inlets North Sea water mainly enters the Wadden Sea from the southern side of the inlet whereas basin water leaves the Wadden Sea mainly along the northern side. Relating the exchanged volume with the tidal prism, giving the volume exchange ratio, shows that this ratio differs for the inlets considered. The actual value depends strongly on the bathymetry around a tidal inlet.

A rough method to estimate the turn-over time of a tidal basin is applied by schematizing each tidal basin as a single well mixed box in which an exchange coefficient is used to parameterize the exchange of basin water with the open sea. The exchange coefficient to be used for the Marsdiep basin is estimated independently from a revised salt balance during stationary periods. For this the connected Marsdiep and Vlie basin are schematized in a two-box model in which the effects of the large scale tidally driven throughflow are incorporated. This exchange coefficient appears to be larger than the tidally exchanged volume. This difference may be caused by the fact that in reality wind, three-dimensional aspects of the current field etc. influence the exchanged volume through an inlet. A sensitivity analysis for the assumptions underlying the calculation of the exchange coefficients for the Marsdiep basin indirectly supports the existence of a southward directed throughflow from the Vlie basin towards the Marsdiep basin. A consequence of this throughflow is that, compared with previous estimates, more 'sea' water originating from the Zeegat

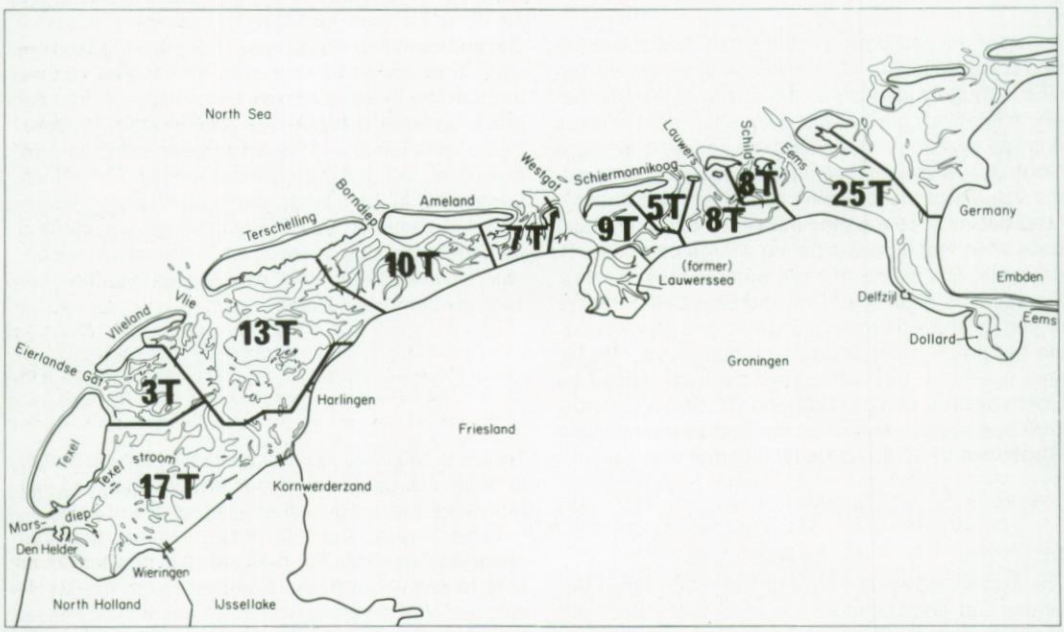

Fig. 13. Estimated mean turn-over time of tidal basins in the Dutch Wadden Sea.

van het Vlie and less 'sea' water originating from the Zeegat van Texel is present in the western Dutch Wadden Sea. In general the former fraction has a higher salinity than the latter. The increased average salinity of what is defined as 'sea' water results in an increased fresh water content which in turn gives an increased flushing time of water discharged near den Oever. The mean value appears to be 20 tidal periods for this source and 24 tidal periods for fresh water discharged near Kornwerderzand. This implies a smaller mixing intensity compared to former estimates. Consequently the turn-over time of the Marsdiep and Vlie basin increases compared with former estimates.

For the other basins of the Dutch Wadden Sea it is assumed that the exchange coefficient to be used in a single box-schematization can be deduced from the tidally exchanged volume by multiplying this value with a factor 1.5, as deduced for the Marsdiep basin. Then the tidally exchanged volume through the inlets combined with the mean tidal volume of a basin can be used to give a rough estimate of the turn-over time. For the Eierlandse Gat and Borndiep the exchanged volume is known from calculations with our hydrodynamical model whereas for the remaining tidal basins a fixed percentage of the tidal prism is used. For all basins the mean value of the resulting turn-over time is presented in Fig. 13. The value for the Ems Dollart estuary in this map has been adopted from HELDER & RUARDY (1982).

6. REFERENCES

AWAJI, T., 1982. Water mixing in a tidal current and the effect of turbulence on tidal exchange through a strait.—J. Phys. Oceanogr. **12:** 501-514.

DORRESTEIN, R. & L. OTTO, 1960. On the mixing and flushing of the water in the Ems-estuary.—Verh. K. ned. geol.-mijnb. Genoot. **19:** 83-102.

DRONKERS, J., 1982. Inshore/offshore water exchange in shallow coastal systems. In: B.O. JANSON. Coastal-offshore ecosystem interactions. Lecture notes on coastal and estuarine studies, vol. 22. Springer-Verlag, Berlin: 3-39.

DRONKERS, J., A.G. VAN OS & J.J. LEENDERTSE, 1981. Predictive salinity modelling of the Oosterschelde with hydraulic and mathematical models. In: H.B. FISCHER. Transport models for inland and coastal water. Acad. Press, New York: 451-482.

DRONKERS, J. & J.T.F. ZIMMERMAN, 1982. Some principles of mixing in tidal lagoons. Oceanol. Acta SP: 107-117.

FISCHER, H.B., E.J. LIST, R.C.Y. KOH, J. IMBERGER & N.H. BROOKS, 1979. Mixing in inland and coastal waters. Acad. Press, New York: 1-483.

HEEMINK, A.W., 1989. Stochastic modelling of dispersion in shallow water. Stochastic Hydrology and Hydraulics (submitted).

HEEMINK, A.W. & TH.L. VAN STIJN,1989. Numerical and stochastic modelling of advection and diffusion of water pollutants. To appear in Proc. VIth Int. Conf. on Numerical Methods in Laminar and Turbulent Flow. C. TAYLOR, 1989.

HELDER, W. & P. RUARDIJ, 1982. A one-dimensional mixing and flushing model of the Ems-Dollard estuary: Calculation of time scales at different river discharges.—Neth. J. Sea Res. **15:** 293-312.

HOLLOWAY, P.E., 1981. Longitudinal mixing in the upper reaches of the Bay of Fundy.—Est. Coast. Shelf Sci. **13:** 495-515.

IMASATO, N., 1983. A numerical experiment on water and salt exchange through the Akashi and Naruto Straits.—J. Phys. Oceanogr. **13:** 1526-1533.

IMASATO, N., T. AWAJI & H. KUNISHI, 1980. Tidal exchange through Naruto, Akashi and Kitan Straits.—J. Oceanogr. Soc. Japan **36:** 151-162.

KREEKE, J. VAN DE, 1984. Residence time: Application to small boat basins. Journal of Waterway, Port, Coastal and Ocean Engineering, Vol. 109, No. 4, 416-428

——, 1990. Longitudinal dispersion of salt in the Volkerak estuary. Accepted for publication in: CHENG. Lecture Notes on Coastal and Estuarine Studies. Springer Verlag.

LEENDERTSE, J.J., 1967. Aspects of a computational model for long period water wave propagation. Memorandum RM-5294-PR, Rand Corporation, Santa Monica, 1967.

OKUBO, A., 1967. The effect of shear in an oscillatory current on horizontal diffusion from an instantancous source.—Int. J. Oceanol. Limnol. **1:** 194-204.

PASMANTER, R., 1988. Deterministic diffusion, effective shear and patchiness in shallow tidal flows. In: J. DRONKERS & W. VAN LEUSSEN. Physical processes in estuaries. Springer-Verlag, New-York: 42-52.

POSTMA, H., 1954. Hydrography of the Dutch Wadden Sea.—Archs. Néerl. Zool. **10:** 405-511.

RIDDERINKHOF, H., 1988a. Tidal and residual flows in the Western Dutch Wadden Sea, I: Numerical model results.—Neth. J. Sea Res. **22:** 1-22.

——, 1988b. Tidal and residual flows in the Western Dutch Wadden Sea, II: An analytic model to study the constant flow between connected tidal basins.—Neth. J. Sea Res. **22:** 185-198.

——, 1989. Tidal and residual flows in the Western Dutch Wadden Sea, III: Vorticity balances.—Neth. J. Sea Res. **24:** 9-26.

RIDDERINKHOF, H. & J.T.F. ZIMMERMAN, 1990a. Residual currents in the Western Dutch Wadden Sea. Accepted for publication in: CHENG. Lecture Notes on Coastal and Estuarine Studies. Springer-Verlag.

——, 1990b. Mixing processes in a numerical model of the western Dutch Wadden Sea. Accepted for publication in: CHENG. Lecture Notes on Coastal and Estuarine Studies. Springer-Verlag.

STELLING, G.S., 1984. On the construction of computational methods for shallow water flow problems. Communications no. 35. Rijkswaterstaat, The Netherlands: 1-226

TAYLOR, G.I., 1954. The dispersal of matter in turbulent flow through a pipe.—Proc. Roy. Soc. (A) **223:** 446-468.

YOUNG, W.R., P.B. RHINES & C.J.R. GARRET, 1982. Shear flow dispersion, internal waves and horizontal mixing in the ocean.—J. Phys. Oceanogr. **12:** 515-527.

ZIMMERMAN, J.T.F., 1976a. Mixing and flushing of tidal embayments in the western Dutch Wadden Sea, **I:** Distribution of salinity and calculation of mixing time scales.—Neth. J. Sea Res. **10:** 149-191.

——, 1976b. Mixing and flushing of tidal embayments in the western Dutch Wadden Sea, II: Analysis of mixing processes.—Neth. J. Sea Res. **10:** 397-439.

——, 1986. The tidal whirlpool: A review of horizontal dispersion by tidal and residual currents.—Neth. J. Sea Res. **20:** 133-154.

——, 1988. Estuarine residence times. In: B. KJERFVE. 'Hydrodynamics of estuaries', vol I, CRC Press, 75-84.

CHAPTER 6

MIXING PROCESSES IN A NUMERICAL MODEL OF THE WESTERN DUTCH WADDEN SEA*

H. RIDDERINKHOF [1] and J.T.F. ZIMMERMAN [1, 2]

[1]) *Netherlands Institute for Sea Research, P.O. Box 59, 1790 AB Den Burg, Texel, The Netherlands*

[2]) *Institute for Meteorology and Oceanography, Buys Ballot Laboratory, University Utrecht, The Netherlands*

ABSTRACT

Particle trajectories in a numerical model of the Western Dutch Wadden Sea are used to study the horizontal mixing processes in this area. The Lagrangean displacement of watermasses appears to be very sensitive to the time of release, the initial position and the initial volume of the watermass considered. The advective component of this displacement only agrees with the Eulerian residual currents on relatively large scales. In a Lagrangean sense the small scale Eulerian residual currents have no physical meaning. With respect to tidal dispersion our results are in conflict with the classical shear dispersion concept in that dispersion occurs without the presence of random motions (turbulence). In our model dispersion is caused by the interaction of longitudinal and lateral velocity variations. These spatial variations are caused by the complexity of the bathymetry that varies over a length short compared with the tidal excursion length. Regarding the tidal distortion in more detail, similarities with results from studies on the chaotic aspects of fluid mixing can be recognized, *e.g.* the extremely fast growth of the perimeter of a watermass and the strong sensitivity of the Lagrangean trajectory of a particle to its initial position.

1. INTRODUCTION

The Western Dutch Wadden Sea is a typical shallow tidal area that consists of some more or less separated tidal basins. In previous studies (POSTMA, 1954 and ZIMMERMAN, 1976) one dimensional tidally averaged advection-diffusion models were used to describe observed salinity distributions in this part of the Wadden Sea. This approach, which uses 'gradient type' fluxes for salt transport, has also been applied to the Ems Dollart estuary (HELDER & RUARDY, 1982), the Eastern Scheldt (DRONKERS *et al.*, 1981) and the Bay of Fundy (HOLLOWAY, 1981). In these one-dimensional tidally averaged box models the advective horizontal velocity is induced by the fresh water input. The horizontal dispersion coefficient is either derived from equating salt exchange (dispersion) and residual salt transport (advection) during stationary periods or is chosen such that observed and computed salinity distributions agree reasonably well. In two dimensional transport models for the North Sea (PRANDLE, 1984 and DE RUYTER *et al.*, 1987) basically the same concept has been applied. The advective horizontal velocity results from locally averaging the time dependent velocity vector, and the parametrisation of the horizontal dispersion coefficient is chosen such that the outcome of the model agrees reasonably with tracer observations. The dispersion coefficient can be interpreted as a bulk parameter in these models. Its value lies in the range of 50 - 500 m^2s^{-1}. The physical mechanism responsible for these relatively large effective dispersion coefficients is often assumed to be a cascade of shear dispersion processes (YOUNG *et al.*, 1982 and ZIMMERMAN, 1986). In estuaries tidal trapping and pumping (FISCHER *et al.*, 1979) can also play an important role. In the classical shear dispersion concept (TAYLOR, 1954), dispersion due to turbulence proper is increased by the interaction of turbulence with vertical and/or horizontal shear in the velocity field. This concept was originally developed for steady turbulent flows (TAYLOR, 1954) and later extended to periodic turbulent flows by OKUBO (1967). An important aspect of this concept is that random motions need to be present for an effective dispersion of watermasses.

However, experiments with a numerical model of the Seto Sea in Japan (IMASATO *et al.*, 1980; IMASATO, 1983 and AWAJI, 1982) have shown that mixing of watermasses can also occur if random motions are absent. They used a Lagrangean approach by simulating the track of free flowing particles in the neighbourhood of straits and showed that the resulting mixing or dispersion after a tidal period does not change significantly by adding small scale turbulence to their simulation. These results are in conflict with the shear dispersion concept in that the

* *Publication no. 34 of the project 'Ecological Research of the North Sea and Wadden Sea'.*

horizontal dispersion after a tidal period does not seem to rely on the presence of turbulence.

More recently, studies on the chaotic aspects of mixing of fluids in two dimensional time-periodic flows have been presented (*e.g.* AREF, 1984; OTTINO *et al.*, 1988 and PASMANTER, 1988). These laboratory and numerical studies indicate that relatively simple periodic flow fields can give rise to spatially complicated particle behavior. This complex behavior, in which, on relatively small distances apart, so called islands with practically no mixing are surrounded by areas with very strong mixing, is ascribed to the nonlinear aspects of the Euler-Lagrange transformation. Anyhow, these theoretical studies result in Lagrangean dispersion without the presence of random components in the underlying velocity field.

In the present study we also apply the Lagrangean approach to examine tidal dispersion. Particle trajectories in a detailed two-dimensional hydrodynamical model of the western Dutch Wadden Sea are determined on the basis of the deterministic velocity field in which we do not incorporate the effect of random motions. After a short description of our model and the method applied, we shall treat separately the advective and dispersive component of the Lagrangean displacement of watermasses.

With respect to the advective component the discussion will be focussed on the relation between Eulerian and Lagrangean residual velocities. For the dispersive component most attention is paid to the basic mechanisms responsible for tidal dispersion in our model.

Acknowledgements.—We are much indebted to Rijkswaterstaat, Dienst Informatie Verwerking, for the use of their computer and the support in employing their extended system of computerprograms for simulating two dimensional tidal flows (WAQUA system).

2. NUMERICAL MODEL AND METHOD OF CALCULATION

To compute trajectories of free flowing particles we use a detailed two dimensional vertically averaged numerical model of the tidal flows in the Western Dutch Wadden Sea. The model covers four tidal basins and the open boundaries are located in the adjacent North Sea. The grid size is 500 m and the time step in a numerical simulation is 150 s. Results concerning the computed tidal and residual water levels and velocity field have been discussed extensively by RIDDERINKHOF (1988, 1989) and have been summarized in a companion paper (RIDDERINKHOF & ZIMMERMAN, 1989). Here we only give some characteristics of the velocity field that are of interest for the present study. A characteristic value of the amplitude of the periodic tidal currents is about 1.25 ms^{-1} in the tidal inlets and about 1 ms^{-1} in the center of the main channels. The Eulerian residual flow field can be interpreted as a composition of a small scale part, the residual eddies, and a large scale part, the throughgoing flow. In most regions residual velocities associated with the small scale part are an order of magnitude ($O(10^{-1}ms^{-1})$) larger than the velocities associated with the large scale flow ($O(10^{-2}ms^{-1})$).

For the present study at each time step the Lagrangean velocity of a particle is bilinearly interpolated from the velocities in the surrounding gridpoints. For the integration scheme a second order midpoint rule is employed (HEEMINK, 1988; HEEMINK

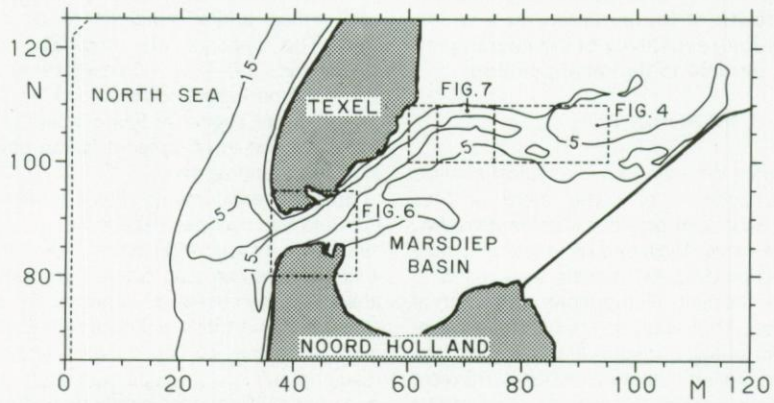

Fig. 1. Isobaths in a representative area of the two dimensional numerical model for the western Dutch Wadden Sea that is used for particle computations. Grid numbers are indicated on the m- and n-axes. Open boundaries are located in the adjacent North Sea. Dashed lines mark sub regions as used in Fig. 4, 6 and 7.

& VAN STIJN, 1989). It is assumed that the numerical error introduced by this method, which has a random character, can be ignored.

In our vertically averaged model each particle can be interpreted as representative for a water column equal to the local waterdepth at the time of release (H). The center of mass of a particle group is defined as:

$$(X_c,\ Y_c)=\left(\frac{\sum_{i=1}^{n} X_i H_i}{\sum_{i=1}^{n} H_i},\ \frac{\sum_{i=1}^{n} Y_i H_i}{\sum_{i=1}^{n} H_i}\right) \quad (1)$$

in which (X_c,Y_c) is the position of the center of mass, (X_i,Y_i) the position and H_i the waterdepth at the time of release of particle i and n the number of particles in a specific group. The displacement of this center of mass is used to examine the advective component of the transport.

The distortion of a particle group can be described by the displacement covariance tensor (σ). The components of this tensor define the mean square distances about the center of mass:

$$\sigma^2_{xx}=\frac{\sum_{i=1}^{n} (X_i-X_c)^2 H_i}{\sum_{i=1}^{n} H_i},\quad \sigma^2_{yy}=\frac{\sum_{i=1}^{n} (Y_i-Y_c)^2 H_i}{\sum_{i=1}^{n} H_i}$$

$$\sigma_{xy}=\frac{\sum_{i=1}^{n} (X_i-X_c)(Y_i-Y_c) H_i}{\sum_{i=1}^{n} H_i} \quad (2)$$

The Lagrangean dispersion coefficient is calculated from the distortion after one tidal period (T):

$$D_{xx}=\frac{\sigma^2_{xx}|_{t_0+T}-\sigma^2_{xx}|_{t_0}}{2T},\quad D_{yy}=\frac{\sigma^2_{yy}|_{t_0+T}-\sigma^2_{yy}|_{t_0}}{2T}$$

$$D_{xy}=\frac{\sigma_{xy}|_{t_0+T}-\sigma_{xy}|_{t_0}}{2T} \quad (3)$$

Tensor transformation rules can subsequently be used to determine the orientation of the dominant axes of distortion (along these dominant axes the cross terms in eq. (2) and (3) equal zero).

The above defined measures are discussed for particle displacements in a part of our numerical model. Fig. 1 displays isobaths in this representative area which covers the tidal inlet region and the inner part of the Marsdiep basin.

3. LAGRANGEAN DISPLACEMENT OF WATERMASSES

3.1. ADVECTION

In this section we will treat the advective component of particle spreading by regarding the displacement of the center of mass of groups of particles after a tidal period. This Lagrangean residual displacement appears to be a function of the time of release (initial tidal phase), the initial position and of the initial dimensions of the water mass considered.

The dependence on the initial phase is shown in Fig. 2. This figure gives the final positions of the center of mass of 16 particles which are initially released inside the three marked grid units. The 12 different final positions stem from successive computations in which the time of release was varied with an interval of 1 hour. It clearly shows that the Lagrangean residual displacement is strongly dependent on the time of release. This initial phase dependence stems from the relatively large spatial variations in the velocity field of our numerical model. The time of release determines the velocity field in which a particle group travels and the Lagrangean

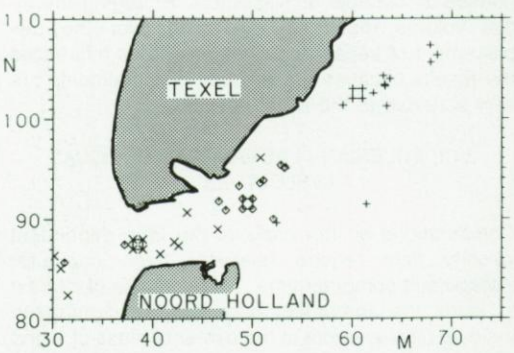

Fig. 2. Positions of the center of mass after one tidal period of particle groups initially released inside the dashed grid units. The 12 different final positions for each particle group depend on the time of release which was varied with an interval of 1 hour. Marks at the final position correspond with marks that indicate the initial angular points of a particle group.

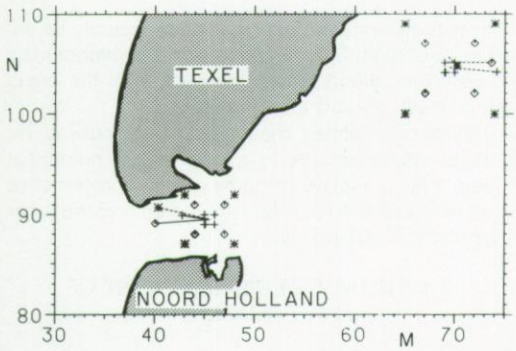

Fig. 3. Displacement of the center of mass after one tidal period depending on the initial dimensions of the square considered. Corresponding marks indicate the initial angular points of these squares as well as the final position of the center of mass after one tidal period.

residual displacement is a result of the velocity field experienced. Thus the initial phase strongly influences the residual displacement.

The dependence of the displacement of the center of mass on the initial position is also clear from Fig. 2. The initial position also determines the velocity field in which a watermass travels. Thus the same arguments as for the phase dependence can be used to explain the dependence on the initial position.

The influence of the initial dimensions of a water mass on its residual displacement is shown in Fig. 3. This figure gives for two different regions the residual displacement of the center of mass depending on the volume represented by the particles at the time of release, during ebb tide. From this figure it is clear that the initial dimensions of a watermass strongly influence its residual displacement. Enlarging the initial volume results in averaging over the displacement of separate subvolumes. This influences the results because the residual displacements are very sensitive to the initial position.

3.1.1. EULERIAN - LAGRANGEAN RESIDUAL VELOCITIES

Computations on the basis of the time dependent velocity field require relatively large computer storage and computer time. Therefore it is of interest to study the agreement between the Lagrangean residual displacement of the center of mass of a grid unit and the Eulerian residual velocities. If both agree, the advective component of spreading can be computed relatively simply on the basis of the Eulerian residual velocity field.

The Eulerian residual velocity field can be computed by time averaging the computed time dependent velocity in each specific grid unit:

$$\overline{\underline{u}}_E = \frac{1}{T} \int_0^T \underline{u}(t)\, dt \tag{4}$$

Averaging the vertically integrated mass transport gives the so called residual transport velocity:

$$\overline{\underline{u}}_T = \frac{1}{T} \frac{\int_0^T u(t)\,(H + \zeta(t))\, dt}{\int_0^T (H + \zeta(t))\, dt} \tag{5}$$

It should be noted that both, the residual velocity as well as the residual transport velocity, are Eulerian quantities.

The Lagrangean residual velocity is defined as:

$$\overline{\underline{u}}_L = \frac{X(T) - X(0)}{T} \tag{6}$$

in which X(0) and X(T) are the position of the center of mass of a watermass at the start of the computation and after one tidal period respectively. In the figures shown the Lagrangean residual velocity is attributed to the starting point X(0).

Fig. 4 shows the three different quantities for a representative region (see Fig. 1) in the inner part of the Marsdiep basin. Fig. 4a and 4b show the Eulerian residual velocity field ($\underline{u}_E$) and the Eulerian residual transport velocity field ($\underline{u}_T$) respectively. The difference between both velocity fields is only small. Both show the dominant presence of tidal residual eddies in this area. However, Fig. 4c shows that Lagrangean residual velocities ($\underline{u}_L$) differ appreciably from the Eulerian residual velocity field. For these Lagrangean computations each grid unit was represented by 16 particles, evenly distributed over the grid unit at the time of release, at maximum ebb tide. As discussed before the initial tidal phase strongly influences the Lagrangean residual velocity. Although not shown here, averaging the results from computations in which the initial phase is varied gives the same conclusion that Lagrangean residual velocities differ substantially from the Eulerian residual velocity field. Thus the detailed Eulerian residual velocity field cannot be used to predict the advective component of the transport of mass in our numerical model.

3.2. DISPERSION

The dispersive component of the displacement of a watermass can be described by the displacement covariance tensor (defined in section 2). Fig. 5 marks

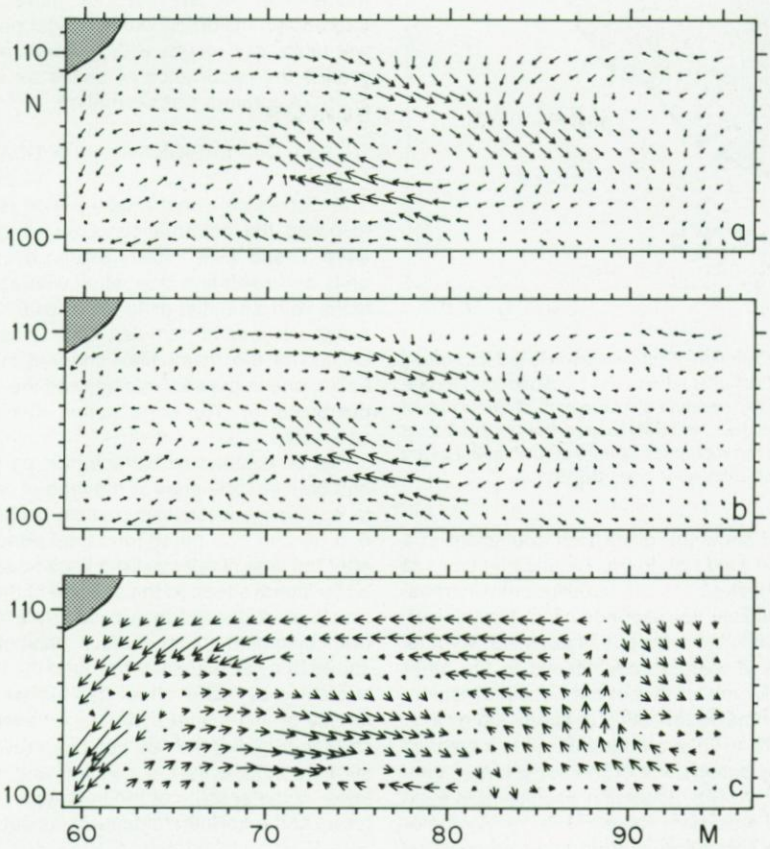

Fig. 4. Eulerian and Lagrangian residual velocities in a representative region of the Marsdiep basin (see Fig. 1). a) Eulerian residual velocity field ($\underline{u}_E$); b) Eulerian residual transport velocity field ($\underline{u}_T$); c) Lagrangian residual velocity field ($\underline{u}_L$). One grid unit corresponds with 0.10 ms^{-1}. See text for a definition of these velocities.

some grid units in which 16 particles were released at maximum ebb tide and gives the residual displacement of the center of mass and the dimensions and orientation of the principal axes of the distortion tensor after one tidal period. Again, most striking are the large differences between the various particle groups. Some particle groups remain relatively close together while others show a remarkable distortion and growth. The distortion is anisotropic with the main axes tending to be oriented in the dominant current direction, parallel to the local isobaths. The length of the axis perpendicular to the dominant current direction remains only small. In general the direction of the residual displacement of the center of mass does not agree with the main axis of the covariance tensor. Thus a decomposition of the Lagrangian motion in an advective and dispersive component would require the introduction of cross terms in the dispersion tensor to be able to describe the dispersive component correctly.

Fig. 5 only shows the influence of the initial position on particle dispersion. Although not shown, the dispersion is also strongly dependent on the initial tidal phase. The same arguments as in section 3.1. can be used to explain these dependencies.

As described before the distortion can be used to compute the dispersion coefficient. Fig. 6 gives isopleths for this coefficient along the dominant axes of distortion for the region near the Zeegat van Texel. Particle computations were started during ebb tide with 16 particles evenly distributed over each grid unit. In this region the dispersion coefficient reaches values up to 700 m^2s^{-1}. Dispersion coefficients perpendicular to this main axis are much smaller.

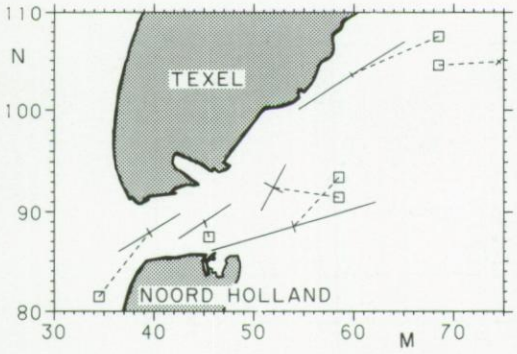

Fig. 5. The tidal distortion of different particle groups initially released inside the dashed squares. Dashed lines represent the Lagrangian residual displacement of the center of mass. Solid lines give the orientation of the principal axes of distortion and the root-mean square displacement along these axes after one tidal period.

Fig. 7a to 7d show the dispersion coefficient in a part of the inner basin when the initial dimensions of each separate watermass are subsequently increased. Fig. 7a, which corresponds with Fig. 6 with respect to the initial dimensions of each sub volume, shows that the dispersion coefficients in the inner basin are much smaller that in the tidal inlet region. In this area the maximum value is about 100 m^2s^{-1}. However, Fig. 7b to 7d show that this value increases with increasing dimensions of the subvolumes considered. In Fig. 7d the dispersion coefficient is even larger than the maximum value in Fig. 7a. A greater part of particle spreading is attributed to dispersion instead of advection if a larger water mass is used to make a distinction between the advective and dispersive component. Thus also the ratio between advection and dispersion strongly depends on the initial dimensions of a particle group. In general this ratio decreases with increasing initial dimensions.

3.3. BASIC MECHANISMS

Previous examples of particle behavior have clearly shown that a particle does not return to its initial position after one tidal period. Furthermore the position after one tidal period is very sensitive to the initial phase of release and the initial position of the particle considered. As a consequence a watermass, marked by a lot of particles, is displaced and distorted by the flow field in our numerical model. The fact that distortion occurs in our model is in contrast with the theoretical shear-dispersion concept for oscillating flow in which, without the presence of random motion, a particle would return to its original position. This makes it interesting to examine which mechanism causes distortion in our numerical model. For this we first look more closely to the Lagrangian distortion within a tidal period. Then we will relate our results with (theoretical) studies that predict the occurrence of chaos as a result of the Euler - Lagrange transformation.

3.3.1. DISPERSION WITHIN A TIDAL PERIOD

The dispersion within a tidal period is discussed by following the deformation of two originally straight lines. These lines initially extend over about 6 grid units and each line is labelled with about 2500 particles with an initial distance of 0.0025 grid unit between successive particles. Both lines cover a cross section of the major tidal channel in the southern basin, one in the tidal inlet (a) and the other in the inner basin (b). The computation was started during ebb tide.

Fig. 8a displays isobaths in this part of our model and both particle lines at the time of release. Fig. 8b to 8g display successive particle positions after 2, 4, 6, 8, 10 and 12.5 hours (one tidal period). Two hours after the time of release both lines have been stretched by lateral shear. At the seaside of the inlet the particle line is divided in two separate groups by the branching of the main channel. Next picture (Fig. 8c) shows that two hours later, around the turn of the tide, stretching by lateral shear has further increased the length of both lines. Six hours after the time of release (Fig. 8d) the tide has been reversed and this strongly influences the position and shape of both lines. At the seaside of the inlet a part of the particle group at the northern side remains outside the inflow

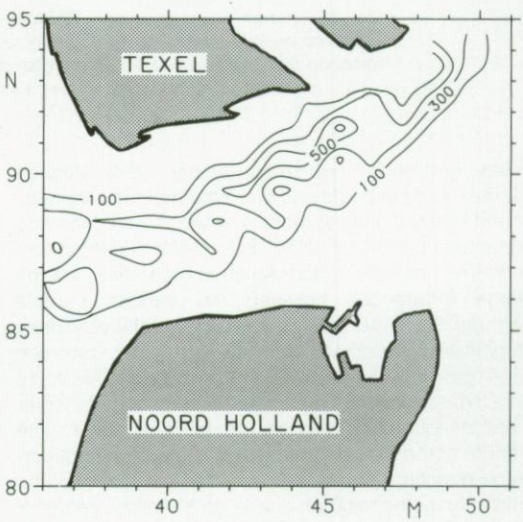

Fig. 6. Isopleths of the dispersion coefficient (m^2s^{-1}) along the dominant axis of dispersion in the tidal inlet region.

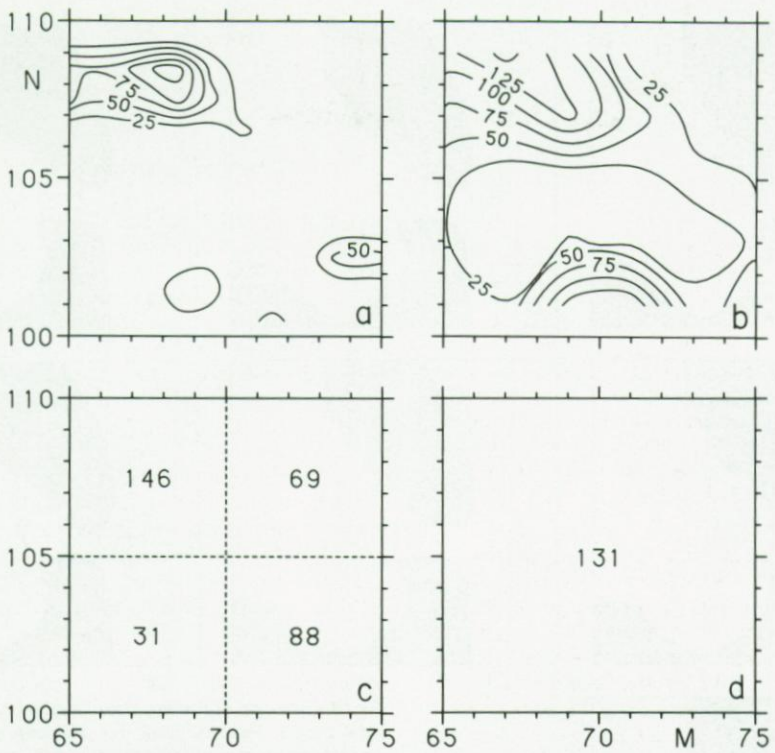

Fig. 7. Dispersion coefficients (m^2s^{-1}) along the dominant axis of distortion in a part of the inner basin (see Fig. 1) dependent on the initial dimensions of each watermass considered. The dimension of each watermass is 1, 4, 25 and 100 grid units in Fig. 7a to d respectively.

area of the tidal inlet and continues to flow in a northward direction, even after the reversal of the tide. This illustrates that a part of the outflowing watermass is influenced by two different current systems which enlarges the stretching. At the southern side of the inlet region, most of the particles remain in the sphere of influence of the tidal inlet. The relatively regular shape of this particle group during ebb has been distorted by lateral phase and amplitude differences. The most striking of the shape of the other line at this tidal phase is that after the reversal of the tide an important part of this line has not travelled along the center of the main channel but follows a more southward route. Besides this, lateral phase differences in the main channel, in which slack tide in the shallower parts preceeds slack tide in the deeper parts, causes an increased stretching of this line. Lateral shear in the velocity field further stretches both lines during the flood period, see Fig. 8e and 8f. A small part of the particles that left the inlet at the southern side during ebb appears to travel around the emersed sandbank at the seaside of the inlet during flood. However, most particles from the southern part of the inlet return to the inner basin during flood. In the northern part most particles remain in the adjacent sea. In the inner basin a part of the line of particles appears to branch off to another tidal channel where it is stretched further by lateral shear. The final positions after one tidal period (and one more slack tide) are shown in Fig. 8g. It is hard to reconstruct the shape of the originally straigth line in the tidal inlet. Although somewhat less pronounced the same can be said about the shape of the line in the inner basin.

From these particle distributions dispersion coefficients can be derived. Decomposed along and perpendicular to the main axis of deformation these coefficients are 340 m^2s^{-1} and 100 m^2s^{-1} respectively for the line in the inlet region and 185 m^2s^{-1} and 0 m^2s^{-1} for the line in the inner basin.

From this sequence of figures it is clear that dispersion results from the spatial variations in amplitude, direction and phase of the oscillatory currents. At the seaside of the inlet the spatial variations in dominant current directions and tidal phase of the

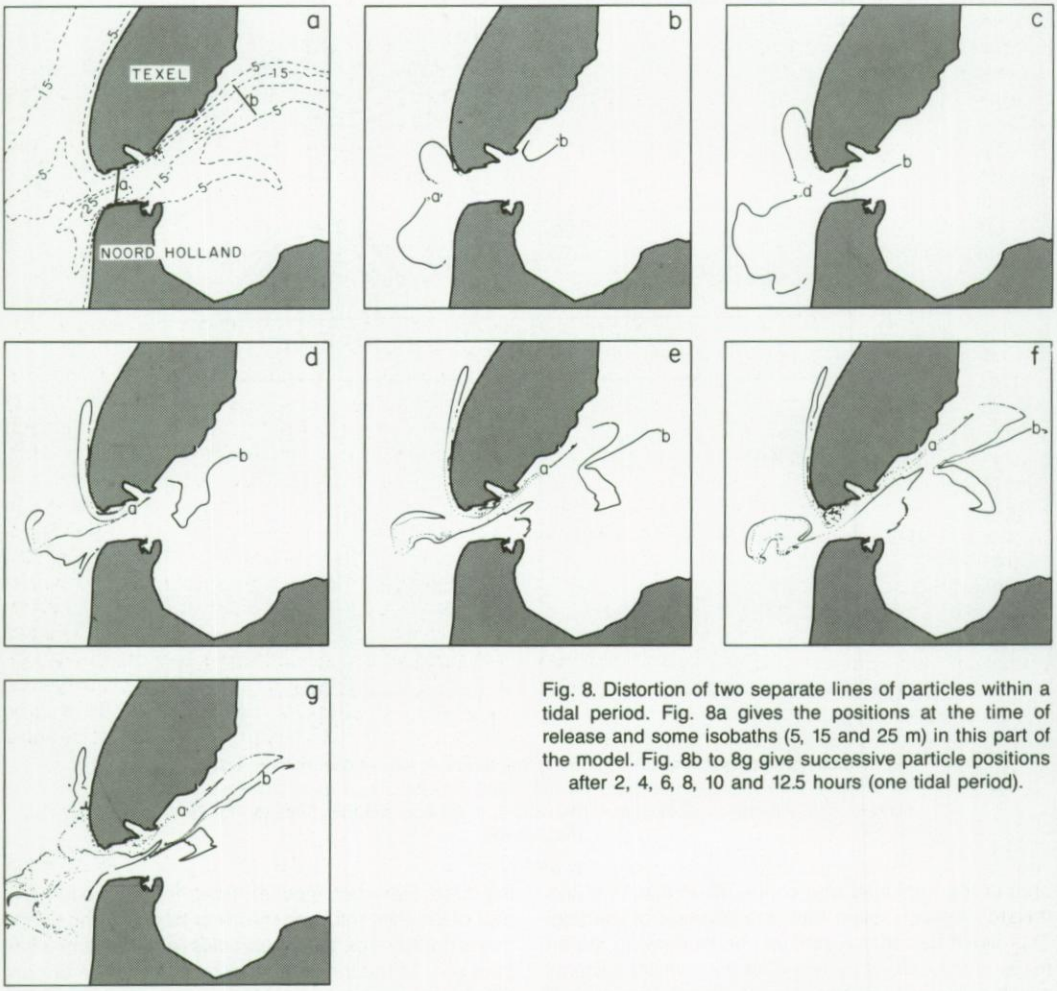

Fig. 8. Distortion of two separate lines of particles within a tidal period. Fig. 8a gives the positions at the time of release and some isobaths (5, 15 and 25 m) in this part of the model. Fig. 8b to 8g give successive particle positions after 2, 4, 6, 8, 10 and 12.5 hours (one tidal period).

currents are extremely large. This is the transition zone of two current regimes, one belonging to the tidal basin and the other to the adjacent open sea. A watermass travelling through both regimes is therefore strongly deformed. In the tidal basin itself the interaction between the complicated bottom topography and the tidal wave creates large spatial variations in amplitude, phase and direction of the oscillatory currents. Here the most important cause for Lagrangean dispersion appears to be that the bottom topography varies over a length short compared to the tidal excursion length. Thus a watermass meets substantially different velocity fields during its tidal excursion.

A more detailed study of the particle distribution after one tidal period shows that the stretching within both lines is rather irregular. There appear to be large differences in the growth of segments of both lines. This strong variability in line stretching has also been recognized in studies of the chaotic aspects of fluid mixing. In the next section we will relate the particle behavior in our numerical model to these studies.

3.3.2. LAGRANGEAN CHAOS?

Some recent publications on mixing in periodic velocity fields (AREF, 1984 and OTTINO *et al.*, 1988) have shown the possibility of chaotic particle behavior in that particle positions may become random functions of time even if the underlying velocity field does not contain a stochastic component. Laboratory studies of flows with very low Reynold numbers as well as numerical studies with relatively simple periodic velocity fields have shown such

Lagrangean chaotic behavior. Most fascinating is that these velocity fields, which are very simple in an Eulerian sense, can cause very complicated Lagrangean trajectories. The velocity field used by PASMANTER (1986) comes close to the velocity field in our numerical model of the Wadden Sea. He shows that depending on the initial positions particles can stick together, like patchiness, as well as that the distance between particles can grow exponentially in the same velocity field. This kind of particle behavior is demonstrated by showing maps of particle positions after relatively many (tidal) periods. Thus particles remain in a specific velocity field over a relatively long period. In our numerical model we cannot simulate particle trajectories over long periods in the same velocity field. Most particles of a specific group would have left such a velocity field within a few tidal periods. Even if we regard the velocity field in a complete tidal basin as our velocity field of interest only a few tidal periods can be used if we do not want our results to be influenced by the closed boundaries of the basin or by substantially different flow fields, belonging to the tidal inlet region or the adjacent sea.

However, some general features of this anomalous particle behavior can also be recognized in our numerical model. To demonstrate this we show the deformation of a water column initially released in the middle of the southern basin. On the perimeter of this column we labelled 200 particles per grid, equivalent to an initial distance of 2.5 m between subsequent particles. Fig. 9 shows the position of these particles at the start of the computation and after 1, 2, 3, 4 and 5 tidal periods successively. From these maps we see that the watermass considered deforms strongly and that its perimeter grows extremely fast. Already after one tidal period the perimeter is strongly stretched and the deformation is so strong that it is hard to recognize the shape of the perimeter in the following pictures.

A characteristic feature of chaotic behavior is that the distance between particles that are initially close to each other, grows exponentially in time. Thus the length of the perimeter of the watermass should grow exponentially in a chaotic regime. Fig. 10a shows the length of the perimeter as a function of time. Although only five tidal periods have been shown it is clear that the growth is stronger than linear. The computed length should be interpreted as a minimum value, because in comparison with this computation decreasing the initial distance between successive particles would, after a few tidal periods, certainly give an increased length.

In some parts of the maps in Fig. 9 one can recognize that there is a large difference in stretching of different segments of this perimeter. This phenomenon has much in common with the joint occurrence of patchiness as well as chaos, depending on the initial positions of the particles considered, in Pasmanter's study. This strong spatial variability of line stretching is illustrated in Fig. 10b and Fig. 10c, which give the length of a segment of 20 particles as a function of time for two different segments initially being about one grid unit apart. In spite of the small initial distance between these segments the growth of their length extremely differs (note the large difference in vertical scale in both figures). Thus large variations of line stretching, and mixing, can occur on relatively small distances apart.

4. DISCUSSION AND CONCLUSIONS

With respect to the advective part of water mass displacement our results confirm previous studies (ZIMMERMAN, 1979; CHENG & CASULI, 1982) in that the small scale Eulerian residual velocity field or

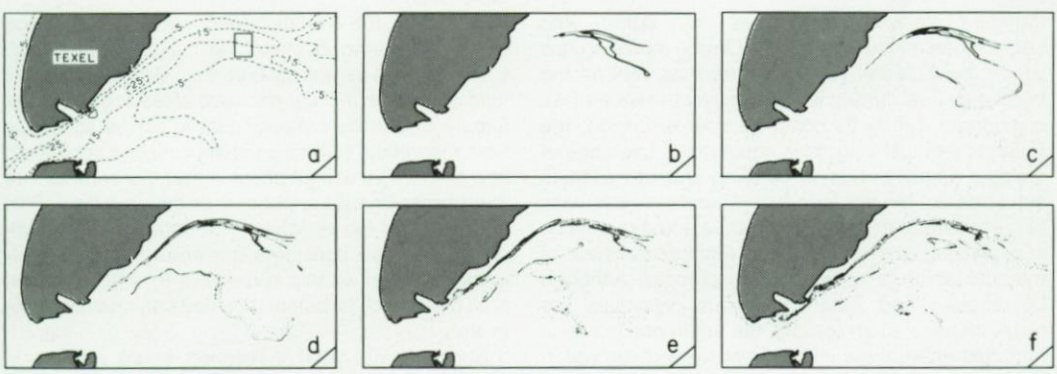

Fig. 9. Tidal deformation of a watercolumn initially released in the middle of the Marsdiep basin. Fig. 9a gives particle positions at the time of release and some isobaths. Fig. 9b to 9f give the particle positions after 1, 2, 3, 4 and 5 tidal periods.

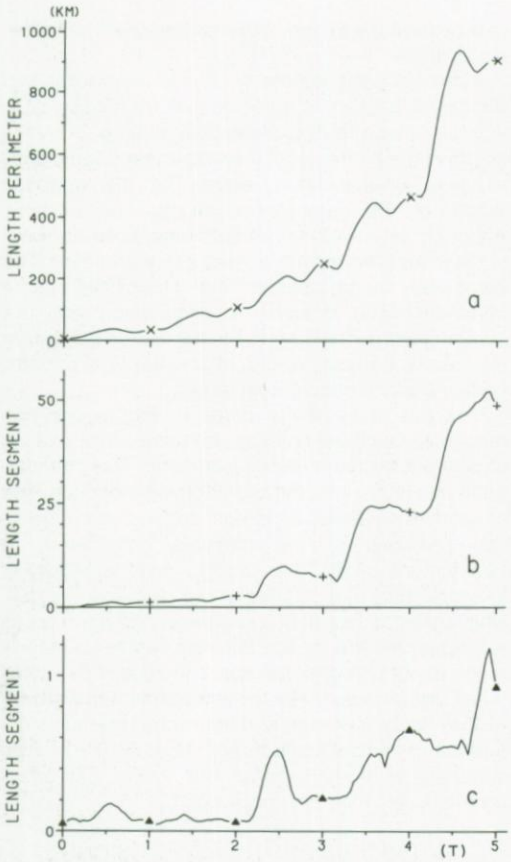

Fig. 10. a) Length of the perimeter of a watermass (see Fig. 9) as a function of tidal period. b) and c) Length of two segments of 20 particles as a function of tidal period. Initially both segments are one grid unit apart. Note the different scales of the vertical axes.

transport velocity field does not agree with Lagrangean residual velocities. Only in those regions where the Eulerian residual current as well as the oscillatory tidal current is uniform over the watermass considered during its complete tidal excursion, the Eulerian residual velocity is equal to the Lagrangean residual velocity. This is certainly not the case in estuaries like the Wadden Sea. Therefore we have to be very careful in using Eulerian residual quantities in explaining or even predicting residual transport of material which is a Lagrangean process. Although Lagrangean and Eulerian residual velocities are never identical in an estuary, the difference between both decreases if the initial dimensions of the watermass are large. This can be explained from a decomposition of the Eulerian residual flow field in a large scale part, the throughgoing flow, and a small scale part, the residual eddies. If the dimensions of a water mass are such that it covers the cross section of the estuary (or tidal channel) and that its length exceeds the length scale of the residual eddies, spatial averaging results in the relatively uniform large scale residual velocity. Then the Lagrangean residual velocity equals approximately the Eulerian residual velocity. Thus, only if the inital volume covers the cross section of a channel and its length exceeds the tidal excursion length the difference between its Lagrangean and Eulerian residual velocity will be small.

With respect to the dispersive part of watermass displacement our results show that in a complex bathymetry like the western Wadden Sea relatively large horizontal dispersion coefficients stem from spatial variations in the periodic tidal current. Thus dispersion does not depend exclusively on the presence of random motion. In the classical shear dispersion concept the effective dispersion coefficient is a function of lateral variations in velocity amplitude and of the magnitude of turbulence. Applying this concept to tidal flow basically gives the same results. The only difference is that the time scale ratio between the tidal period and the cross-sectional (turbulent) mixing time scale now enters the expression for the effective horizontal dispersion coefficient. In essence turbulence is indispensible for horizontal dispersion in this concept. Our particle computations show that in an estuary like the Wadden Sea longitudinal variations in the velocity field play an important role in particle spreading. Due to these longitudinal variations a particle does not return to its initial position and, considering the displacement of a watermass, horizontal dispersion is the result. Thus horizontal dispersion stems from the strong spatial variability of the oscillatory currents and the effective horizontal dispersion strongly depends on the combined effect of longitudinal and lateral velocity variations.

Regarding the tidal distortion in more detail, large spatial variations in stretching can be recognized. Extremely fast as well as extremely slow stretching of fluid segments initially released close together, is a feature of particle behavior that is similar to results from theoretical studies on chaotic mixing in periodic flow fields. The overall effect is that the perimeter of a watermass grows stronger than linear in time. This fast growth of the perimeter of a water mass is of importance if one considers the mixing with the surrounding water as this is decisive for the interfacial area over which turbulent diffusion can operate effectively.

Summarizing, tidal dispersion in an estuary is mainly caused by the irregularity of the flow field which stems from the interaction of the tidal flow with the complex bathymetry. The tidal excursion length

far exceeds the length over which the bathymetry and associated velocity field varies. Thus the non-uniformity of the flow field in a longitudinal direction can be seen as the essential mechanism for tidal dispersion. The actual value of the dispersion coefficient primarily depends on the complexity of the bathymetry.

5. REFERENCES

AREF, H., 1984. Stirring by chaotic advection.—J. Fluid. Mech. **143:** 1-21.

AWAJI, T., 1982. Water mixing in a tidal current and the effect of turbulence on tidal exchange through a strait.—J. Phys. Oceanogr. **12:** 501-514.

CHENG, R.T. & V. CASULLI, 1982. On Lagrangian residual currents with applications in South San Francisco Bay, California.—Wat. Res. Res. **18:** 1652-1662.

DRONKERS, J., A.G. VAN OS & J.J. LEENDERTSE, 1981. Predictive salinity modelling of the Oosterschelde with hydraulic and mathematical models. In: H.B. FISCHER. Transport models for inland and coastal water. Acad. Press, New York: 451-482.

FISCHER, H.B., E.J. LIST, R.C.Y. KOH, J. IMBERGER & N.H. BROOKS, 1979. Mixing in inland and coastal waters. Acad. Press, New York: 1-483.

HEEMINK, A.W., 1988. Stochastic modelling of dispersion in shallow water. Stochastic Hydrology and Hydraulics (submitted).

HEEMINK, A.W. & TH.L. VAN STIJN, 1989. Numerical and stochastic modelling of advection and diffusion of water pollutants. To appear in Proc. VIth Int. Conf. on Numerical Methods in Laminar and Turbulent Flow. C. TAYLOR (ed.), 1989.

HELDER, W. & P. RUARDIJ, 1982. A one-dimensional mixing and flushing model of the Ems-Dollard estuary: Calculation of time scales at different river discharges.—Neth. J. Sea Res. **15:** 293-312.

HOLLOWAY, P.E., 1981. Longitudinal mixing in the upper reaches of the Bay of Fundy.—Est. Coast. Shelf Sci. **13:** 495-515.

IMASATO, N., 1983. A numerical experiment on water and salt exchange through the Akashi and Naruto Straits.—J. Phys. Oceanogr. **13:** 1526-1533.

IMASATO, N., T. AWAJI & H. KUNISHI, 1980. Tidal exchange through Naruto, Akashi and Kitan Straits.—J. Oceanogr. Soc. Japan **36:** 151-162.

OKUBO, A., 1967. The effect of shear in an oscillatory current on horizontal diffusion from an instantancous source.—Int. J. Oceanol. Limnol. **1:** 194-204.

OTTINO, J.M., C.W. LEONG, H. RISING & P.D. SWANSON, 1988. Morphological structures produced by mixing in chaotic flows.—Nature **333:** 419-425.

PASMANTER, R., 1986. Dynamical systems, deterministic chaos and dispersion in shallow tidal flow. Preprint.

POSTMA, H., 1954. Hydrography of the Dutch Wadden Sea.—Archs Néerl. Zool. **10:** 405-511.

PRANDLE, D., 1984. A modelling study of the mixing of Cs^{137} in the seas of the European continental shelf.—Phil. Trans. R. Soc. (A) **310:** 407-436.

RIDDERINKHOF, H., 1988. Tidal and residual flows in the Western Dutch Wadden Sea, I: Numerical model results.—Neth. J. Sea Res. **22:** 1-22.

——, 1989. Tidal and residual flows in the Western Dutch Wadden Sea, III: Vorticity balances.—Neth. J. Sea Res. **24:** 9-26.

RIDDERINKHOF, H. & J.T.F. ZIMMERMAN, 1990. Residual currents in the Western Dutch Wadden Sea. Accepted for publication in: R.T. CHENG. Residual currents and long term processes in Estuaries and Bays. Lecture Notes on Coastal and Estuarine Studies. Springer Verlag, Berlin.

RUIJTER, W.P.M. DE, L. POSTMA & J.M. DE KOK, 1987. Transport Atlas of the Southern North Sea. Mooren, Nijmegen: 1-33.

TAYLOR, G.I., 1954. The dispersal of matter in turbulent flow through a pipe.—Proc. Roy. Soc. (A) **223:** 446-468.

YOUNG, W.R., P.B. RHONES & C.J.R. GARRET, 1982. Shear flow dispersion, internal waves and horizontal mixing in the ocean.—J. Phys. Oceanogr. **12:** 515-527.

ZIMMERMAN, J.T.F., 1976. Mixing and flushing of tidal embayments in the western Dutch Wadden Sea, I: Distribution of salinity and calculation of mixing time scales.—Neth. J. Sea Res. **10:** 149-191.

——, 1979. On the Euler-Lagrange transformation and the Stokes drift in the presence of oscillatory and residual currents.—Deep Sea Res. **26:** 505-520.

——, 1986. The tidal whirlpool: A review of horizontal dispersion by tidal and residual currents.—Neth. J. Sea Res. **20:** 133-154.

CURRICULUM VITAE

Herman Ridderinkhof is geboren op 6 februari 1959 te Zwartsluis. Vanaf 1971 volgde hij het voorbereidend wetenschappelijk onderwijs aan het Carolus Clusius College te Zwolle, en behaalde in 1977 het Gymnasium β diploma. Vervolgens studeerde hij Civiele Techniek aan de Technische Hogeschool Delft. Het kandidaatsexamen werd behaald in 1983 en het ingenieursdiploma in de afstudeerrichting Waterbouwkunde en Hydrologie in juni 1984. Van november 1984 tot april 1985 is hij (vrijwillig) werkzaam geweest bij de voormalige Deltadienst van Rijkswaterstaat. In de periode april 1985 - december 1987 was hij bij het Nederlands Instituut voor Onderzoek der Zee (NIOZ) in tijdelijk dienstverband aangesteld bij de projektgroep Ecologisch Onderzoek Waddenzee en Noordzee (EON). Vanaf januari 1988 is hij als wetenschappelijk medewerker werkzaam bij het NIOZ, aangesteld bij de projektgroep Beleidsgericht Wetenschappelijk Onderzoek Noordzee (BEWON).